

# Marine Geology

## Neogene to Quaternary evolution of carbonate and mixed carbonate-siliciclastic systems along New Caledonia's eastern margin (SW Pacific)

	<p>Charles Kerans University of Texas at Austin ckerans@jsg.utexas.edu</p>
	<p>Frederique Leclerc Universite de Nice Sophia Antipolis leclerc@geoazur.unice.fr</p>
	<p>Jody Webster University of Sydney School of Geosciences jody.webster@sydney.edu.au</p>
	<p>Gilbert Camoin CEREGE: Centre Europeen de Recherche et d'Enseignement des Geosciences de l'Environnement camoin@cerege.fr</p>
	<p>Eberhard Gischler University of Frankfurt: Goethe-Universitat Frankfurt am Main, Germany gischler@em.uni-frankfurt.de</p>
	<p>Colin Woodroffe University of Wollongong Faculty, New South Wales, Australia colin@uow.edu.au</p>
	<p>Mark J.F Lawrence GNS, New Zealand m.lawrence@gns.cri.nz</p>
	<p>Thomas Lüdmann Universitat Hamburg, Germany thomas.luedmann@uni-hamburg.de</p>
<b>Response to Reviewers:</b>	

*Powered by Editorial Manager® and ProduXion Manager® from Aries Systems Corporation*

## REPLY TO REVIEWERS' COMMENTS

Authors' replies are in blue

### Reviewer #1:

Dear Editor,

I went through the revised manuscript by Tournadour et al. Most of the comments regarding the initial submission have been addressed, and in my opinion the manuscript now is almost ready for publication.

I do, however, have some minor comments:

- Line 18: tilt of which margin?

➤ Eastern margin (“eastern” added).

- I would avoid e.g. when referring to work from other people, it may give an impression of superficiality

➤ “e.g.” has been removed when referring to other studies, except in the data and methods section of the manuscript (lines 219-223), where we only give a few references of the tens of cruises that acquired bathymetric data in our study area, notably those conducted within the ZoNéCo research program.

- Lines 52: not sure why cool-water carbonates are discussed here?

➤ This was a suggestion from R2 to add the Brachert et al. study on mixed cool water carbonate platforms to highlight that the reciprocal sedimentation concept is not always applicable.

- Line 68: siliciclastic

➤ Spelling corrected.

- Fig. 1. Not sure if there is a vertical exaggeration in Fig. 1C? In any case the cross section only differentiates the green color of the peridotite. Difficult to assess, but there should be further colors in there? See map in Fig. 1B.

➤ Fig. 1C is a schematic geological cross-section of Grande Terre that is not to scale. It is thus not possible to specify a vertical exaggeration. This cross-section illustrates the

structure of the ophiolite relatively to autochthonous units. We voluntarily represented the ophiolite as a single unit that comprises both the mantle peridotites and oceanic crust nappes of Fig. 1B. However, we agree that the green colour chosen for the ophiolite was misleading as it was the same color as the peridotites of 1B. We have thus changed this colour to grey and made Fig 1C a grey-shaded figure.

- Line 95: could not find Ponérihouen and Antigonía in Fig. 1.

➤ “Pn” and “A” in Fig. 1 respectively stand for “Ponérihouen” and “Antigonía Seamount”, as mentioned in the figure caption.

- Figure caption Fig. 3: Not sure what is meant by "restricted" deltas (I think you can delete the word terrigenous...).

➤ The term “restricted deltas” is mentioned in the manuscript to describe small deltas restricted to the coastal domain that are interpreted to result from low terrigenous sedimentation rates (see lines 655-657). Terrigenous has been removed from the figure caption.

- Fig. 4. I am not sure if I understand what is meant with the hatched area where erosion is evoked? Is it eroding now, has there be some erosion? What is the evidence that differential subsidence has acted or acts?

➤ This hatched area corresponds to the elevation difference between bathymetrical profiles from the southern (profile E-01) and central (E-02) parts of the eastern margin (see Fig. 2 for profile locations). This difference is due to the fact that in the central part of the margin, the Mio-Pliocene unit (“eastern terrace” on Fig. 3) is almost entirely lacking, and is likely eroded by slope canyons that reach the external barrier reef. The timing of this erosion is yet poorly constrained. For clarity, we have specified this in the figurecaption.

- Lines 531. A strong statement here about the controlling factor, which is, however, not really supported by data presented in the manuscript. What would be the subsidence rate in the region? Is the dip of surface S1 due to tilting, or is this just the drowning unconformity tracing the depositional relief = paleoseafloor?

➤ We agree that the dip of surface S1 could be partly depositional. However, this surface caps a Mio-Pliocene shallow water succession that presently lies at 300-600m water depth and, considering maximum amplitudes of RSL fluctuations during the Neogene-Quaternary, tectonic subsidence must be involved. This subsidence is likely due to Neogene extensional tectonics, as supported by a wealth of studies (Lagabrielle et al., 2005; Chardon & Chevillotte, 2006, Lagabrielle & Chauvet, 2008; Collot et al., 2017; Moretti & Turcotte, 1985, Chardon et al., 2008, Patriat et al., 2018).

I still think that the written English would benefit from the support by a native speaker, as the sentences in many cases are very difficult to follow.

➤ The manuscript has been checked by all co-authors (including native English speakers) and also benefited from a very careful editing from R2 during this second review round. We thus believe that it is now written in proper scientific English.

**Reviewer #2:**

Dear editor,

The authors have adequately addressed all issues raised in the earlier review. Some minor things left to do that can be addressed without any problem; no new review needed.

Stay safe.

Kind regards,  
John Reijmer

-----  
MARGO-D-20-00350\_R1  
Tournadour et al.

General

1. All review remarks are addressed adequately.

Text edits

2. Some suggestions for text edits marked in the text. See PDF.

➤ We went through all these suggestions and accepted almost all of them.

Regarding the comment on line 707 “carbonate platform/ramp/shelf?”; unfortunately we do not think that we have sufficient data to characterise the type of carbonate platforms that cap lowstands prims.

Note that we are grateful to the reviewer for his careful editing of the written English.

532: Please do introduce first that you interpret the submerged bank to be drowned. Subsidence does not equal drowning.

➤ We agree that drowning is inappropriate since we do not show that the bank was drowned. We therefore prefer the term subsidence. “This important **drowning** cannot be explained...” is changed to “This important **subsidence** cannot be explained...”.

578: References needed to support the statement.

➤ References are provided in the two following sentences (Ehrenberg et al., 2008; McCaffrey et al., 2020; Tcherepanov et al., 2008), lines 587-593.

634 ... with aggrading to retrograding shallow water carbonate transgressive sequences? Do you intend to say: ... aggrading and retrograding carbonate sequences that developed during a transgression?

➤ Yes this is exactly what we meant. The sentence has been modified accordingly.

651: Why not cite earlier studies instead of a study that is on-line since March 2021?

Tcherepanov, E.N., Droxler, A.W., Lapointe, P., Dickens, G.R., Bentley, S.J., Beaufort, L., Peterson, L.C., Daniell, J. and Opdyke, B.N. (2008) Neogene evolution of the mixed carbonate-siliciclastic system in the Gulf of Papua, Papua New Guinea. *Journal of Geophysical Research: Earth Surface*, 113, F01S21.

Tcherepanov, E.N., Droxler, A.W., Lapointe, P. and Mohn, K. (2008) Carbonate seismic stratigraphy of the Gulf of Papua mixed depositional system: Neogene stratigraphic signature and eustatic control. *Basin Research*, 20, 185-209.

Tcherepanov, E.N., Droxler, A.W., Lapointe, P., Mohn, K. and Larsen, O.A. (2010) Siliciclastic influx and burial of the Cenozoic carbonate system in the Gulf of Papua. *Marine and Petroleum Geology*, 27, 533-554.

➤ [References added.](#)

JR 21.04.30

## HIGHLIGHTS

- An extensive Miocene-Pliocene shallow water carbonate bank currently lies at 300 to 600 m water depths around the main island of New Caledonia.
- This Mio-Pliocene bank evolved into Quaternary rimmed platforms following regional subsidence and/or a carbonate producers change.
- Coeval terrigenous inputs with carbonate production are evidenced as early as the Serravalian.
- The architectures of mixed carbonate-siliciclastic systems vary widely alongshore, from north to south.
- Terrigenous inputs, paleo-drainage network or by-pass transport influenced the mixed system architectures.

# 1 Neogene to Quaternary evolution of carbonate and mixed 2 carbonate-siliciclastic systems along New Caledonia's eastern 3 margin (SW Pacific)

4 E. Tournadour<sup>1,2</sup>, S.J. Jorry<sup>1</sup>, S. Etienne<sup>2</sup>, J. Collot<sup>2</sup>, M. Patriat<sup>1</sup>, M.K. BouDagher-Fadel<sup>3</sup>, F.  
5 Fournier<sup>4</sup>, B. Pelletier<sup>5</sup>, P. Le Roy<sup>6</sup>, G. Jouet<sup>1</sup>, P. Maurizot<sup>2</sup>

6 *1. IFREMER, Unité Géosciences Marines, 29280 Plouzané, France*

7 *2. Service Géologique de la Nouvelle-Calédonie, DIMENC, B.P. 465, 98845 Nouméa, New Caledonia*

8 *3. University College London, Earth Science, 2 Taviton St, London WC1H 0BT, UK*

9 *4. Aix Marseille Univ, CNRS, IRD, INRAE, Coll France, CEREGE, case 67, 3, Place Victor Hugo 13331 Marseille  
10 cedex 03, France*

11 *5. Géosciences Azur (UMR 6526), IRD, 101 Promenade R. Laroque, BP A5, 98800 Nouméa, New Caledonia*

12 *6. Université Européenne de Bretagne Occidentale, UMR-6538 Domaines Océaniques, IUEM/CNRS, Place  
13 Copernic, 29280 Plouzané, France.*

14

## 15 **ABSTRACT**

16 Neogene and Quaternary shallow-water carbonate records surrounding New Caledonia  
17 main island, Grande Terre, provide a good example for understanding the stratigraphic  
18 architecture of tropical mixed carbonate-siliciclastic systems. Due to a southeastern tilt of the  
19 eastern margin, the eastern shelf of Grande Terre has been better preserved from erosion than  
20 the western part, favouring the development and preservation of shallow-water carbonates.  
21 Based on the integration of bathymetric and seismic data, along with paleoenvironmental and  
22 biostratigraphic constraints derived from dredged carbonate rocks, a comprehensive  
23 geomorphological and architectural characterization of the offshore eastern margin of Grande  
24 Terre has been made. During the Mio-Pliocene, a wide, up to 750 m-thick carbonate build-up  
25 developed and extended over at least 350 km from north to south. This Mio-Pliocene build-up,  
26 currently lying at 300 to 600 m water depths, is overlain by a Pleistocene-Holocene barrier reef-  
27 lagoon complex and associated slope deposits. The switch from aggrading Neogene carbonate  
28 banks to backstepping Quaternary platforms likely reflects an increase in accommodation due to  
29 a high subsidence rate or to relative sea-level rise, and/or results from a switch in carbonate

30 producers associated with global environmental changes. The internal architecture of the  
31 Quaternary barrier reef-lagoon complex is highlighted, especially the development of lowstand  
32 siliciclastic prisms alternating with transgressive shallow-water carbonate sequences. This  
33 pattern agrees with the reciprocal sedimentation model typically invoked for mixed sedimentary  
34 systems. This stratigraphic pattern is well developed in front of the Cap Bayes inlet in the north  
35 of our study area, yet it is not observed southward along the eastern margin. This difference  
36 suggests that other factors than relative sea-level variations directed the architecture of the  
37 margin, such as low terrigenous inputs, lagoon paleo-drainage networks or sediment by-pass  
38 towards deep basins.

39

40 **Keywords:** mixed carbonate-siliciclastic system, reciprocal sedimentation, tropical carbonates,  
41 terrigenous inputs, New Caledonia, SW Pacific.

## 42 1. INTRODUCTION

43 Mixed carbonate-siliciclastic depositional systems are characterized by a high variability in  
44 facies and architectures resulting from several factors, such as relative sea-level change, tectonic  
45 motions, carbonate production, terrigenous inputs, sediment transfer and hydrodynamic  
46 conditions, complicating the sequence stratigraphy interpretation (Droxler and Jorry, 2013;  
47 Zeller et al., 2015). According to the classical “reciprocal sedimentation” model (Wilson, 1967),  
48 mixed systems in the tropical realm have been commonly subdivided into alternating temporal  
49 phases where siliciclastic deposits would prevail during low sea-level periods whereas  
50 carbonates would dominate during transgressions and highstands. This reciprocal concept is yet  
51 relevant for several ancient and some modern cases studies (Kerans & Tinker, 1999; Toomey et  
52 al., 2016), but has been shown to be inadequate in describing several others examples. This  
53 model appears not applicable for some mixed cool-water carbonate platforms, where  
54 sandstones can be deposited when wave abrasion depth rises above the seafloor during  
55 transgressions, whereas shell-beds formed during lowstands (Brachert et al., 2003). Another  
56 example is the Great Barrier Reef, where siliciclastic deposits are released to the slope and basin  
57 during late transgression, possibly due to the reworking of significant amounts of fine-grained  
58 terrigenous sediment stored on the shelf during lowstand (Wallace et al., 2002; Dunbar and  
59 Dickens, 2003; Mitchell et al., 2007; Harper et al., 2015). In addition, wave and/or current  
60 energy might prevent the infill of the lagoon during highstands, during which carbonate  
61 production is thought to be maximal, inducing, thus, an “empty bucket” pattern (Schlager, 1989;  
62 Purdy and Gischler, 2005; Zinke et al., 2001; Weij et al., 2019). This variability in the  
63 sedimentological response of mixed systems to relative sea-level changes demonstrates that  
64 other controlling parameters should also be considered in order to improve the prediction of  
65 their complex depositional architectures.

66 Around the main island of New Caledonia, “Grande Terre”, Neogene to Quaternary shallow-  
67 water carbonate systems occur coeval with high terrigenous fluxes derived from the erosion of

68 rugged mountain ranges located all across the island and primarily composed of obduction-  
69 related thrust sheets. The oldest known Neogene shallow-water carbonates on Grande Terre are  
70 lower Miocene mixed carbonate-siliciclastic series cropping out in the Népoui area, on the  
71 western part of the island, close to the present day coastline (Fig. 1). These outcrops were  
72 interpreted as reflecting sediment deposition on Aquitanian and Burdigalian ramps where  
73 seagrass-related and scleractinian carbonate production occurred simultaneously to strong  
74 fluvio-deltaic terrigenous inputs (Maurizot et al., 2016; Tournadour et al., 2020). However, the  
75 offshore extent of this Miocene mixed system remains unknown.

76 At the present day, Grande Terre is surrounded by one of the largest modern barrier reef in  
77 the world. This barrier reef has been drilled on the western margin and past studies (Coudray,  
78 1975; Cabioch et al., 2008b ; Montaggioni et al., 2011) showed that it initiated at 400 cal kyr B.P.  
79 or Marine Isotope Stage 11 (MIS 11), over non-reefal shallow water carbonates that were  
80 deposited as of *ca.* 1.2 Ma ago on a carbonate ramp or non-rimmed platform (Montaggioni et al.,  
81 2011). The inner lagoon, in turn, started its infill only since 200 cal kyr, B.P. or Marine Isotope  
82 Stage 7 (MIS7) (Le Roy et al., 2008). This points to the fact that the southwestern shelf of New  
83 Caledonia does not follow a classic reciprocal sedimentation pattern but constitutes a unique  
84 mixed carbonate-siliciclastic tropical system with a strong temporal and spatial partitioning  
85 between the outer coral plateau and the inner lagoon depression where terrigenous clastic  
86 sediments prevail (Le Roy et al., 2019).

87 In contrast, the Neogene to Quaternary shallow-water mixed systems of the eastern margin  
88 of Grande Terre are much less documented than their western counterparts, largely because of a  
89 lack of boreholes, rare outcrops onshore and few acoustic data offshore. However, this margin is  
90 thought to have a very different tectonic history than the western margin, probably a higher  
91 subsidence that would have resulted in a better preservation of shallow-water systems on the  
92 shelf, thus allowing to improve our understanding of the onset of Neogene carbonate systems  
93 and the transition to Quaternary barrier reef lagoon in the regional tectonic context. In addition,  
94 those sedimentary records allow to discuss the potential controlling factors determining the

95 stratigraphic architectures along the margin, such as terrigenous inputs or paleo-drainage  
96 networks. With that aim, we have compiled both existing and newly acquired geophysical data  
97 and dredged carbonate rock samples from Ponérihouen to Antigonía seamount (Fig. 1) to  
98 perform a comprehensive analysis of slope morphologies and to reconstruct the depositional  
99 environments and ages of the main terraces and seismic units observed along the eastern  
100 margin.

## 101 **2. GENERAL SETTINGS**

### 102 **2.1. Geography**

103 New Caledonia is a remote archipelago located in the South West Pacific (Fig.1). Its main  
104 island, Grande Terre, is a 50 to 80 km wide and approximately 400 km long land stripe  
105 oriented in a N140° direction. Highest summits are *ca.* 1600 m high. Because of dominant  
106 southeastward trade winds (N110-120°) its eastern margin is positioned on the windward side,  
107 whereas the western margin is the leeward side. Its eastern part is typified by steep reliefs,  
108 deeply incised valleys and short coastal plains, whereas the western part has more extended  
109 valleys, wider alluvial lowlands and large coastal plains. This landform dissymmetry impacts the  
110 spatial distribution of rainfall, with the eastern windward coast receiving twice as much  
111 precipitation than the western leeward coast. Such differences induce a one-and-a-half-time  
112 higher river discharge along the eastern coast compared to the western coast (Terry & Wolting,  
113 2011).

### 114 **2.2. Tectonics**

115 Grande Terre marks the northeastern tip of Zealandia (Mortimer et al., 2017), a mostly  
116 submerged fragment of continental crust isolated from Gondwana during the Late Cretaceous to  
117 Paleocene due to regional rifting followed by seafloor spreading in the Tasman Sea (Hayes &  
118 Ringis, 1973; Gaina et al., 1998). During the Eocene Grande Terre underwent a convergence

119 phase that led to the NE-SW emplacement of several tectonic nappes and finally, in the late  
120 Eocene-early Oligocene, to the obduction of a prominent kilometres-thick ophiolite mostly  
121 constituted of serpentinized peridotites (Paris, 1981; Maurizot et al., 2020). Once obduction  
122 terminated, extensional tectonics prevailed all over Grande Terre (Lagabrielle et al., 2005;  
123 Chardon & Chevillotte, 2006; Lagabrielle & Chauvet, 2008). During this post-obduction  
124 extensional phase, that may still be active today, widespread normal faulting affected both island  
125 margins. The asymmetric morphology of Grande Terre is likely the result of these obduction and  
126 post-obduction tectonics. Drivers of the extension are either attributed to a plate tectonic  
127 divergent phase (i.e. far-field stresses related to initiation of east-verging subduction of the  
128 Australian plate beneath the Pacific Plate, Chardon & Chevillotte, 2006) and/or to post-orogenic  
129 collapse, dismantling and combined isostatic rebound (Lagabrielle et al. 2005, Lagabrielle &  
130 Chauvet, 2008; Moretti & Turcotte 1985; Collot et al., 2017). In this second hypothesis, unroofing  
131 the ridge of dense allochthonous mantle material and loading the adjacent basins resulted in  
132 subsidence of the basins and uplift of the ridge. The latter uplift is thus interpreted as being at  
133 the origin of the steepening of both the western and eastern margins of Grande Terre. The deep  
134 structure of the eastern margin has not been imaged by seismic data but is interpreted to be  
135 structured by a series of normal faults (see simplified geological cross-section of Fig. 1 and Collot  
136 et al. (1987)). Timing and amplitudes of these extensional events and vertical motions over the  
137 post-obduction period are not constrained as no continuous Oligocene to present day geological  
138 records exist. The Neogene to Quaternary carbonates that are the focus of this paper have  
139 developed on these structures. Offshore, towards the south, major listric normal faults bordering  
140 the obducted mantle sheets are imaged by seismic data along Pines Ridge (Chardon &  
141 Chevillotte, 2006; Flamand, 2006; Chardon et al., 2008; Patriat et al., 2018) (Fig.1). Apart from  
142 post-obduction extension, since the late Miocene, the southern part of Grande Terre and the  
143 Loyalty Islands are the foreland area of the Vanuatu Subduction Zone where the Australian Plate  
144 subducts beneath the Pacific Plate. A lithospheric flexure associated to this process is observed  
145 and results in the uplifts of the Loyalty Islands, the southern tip of Grande Terre and the Isles of

146 Pines. As a result, Quaternary 125 ka fringing reefs around Yaté and Isle of Pines are uplifted and  
147 now are positioned 10 to 20 m above present-day sea level (Cabioch et al., 1996).

### 148 **2.3. Miocene mixed carbonate siliciclastic systems**

149 On land, the post-obduction geology is characterized by an Oligocene sedimentary hiatus  
150 and the oldest known marine sediments that overlie allochthonous units are Miocene mixed  
151 carbonate-siliciclastic sedimentary rocks only cropping out in a restricted nearshore area  
152 located west of Grande Terre, in the region of Népoui (Coudray, 1975; Maurizot et al., 2016;  
153 Tournadour et al., 2020). These successions have been interpreted to reflect deposition of an  
154 Aquitanian carbonate ramp dominated by seagrass-related carbonate production, overlain by  
155 Burdigalian fan delta deposits that laterally evolve towards a carbonate ramp dominated by  
156 seagrass meadows and small-sized coral bioconstructions (Tournadour et al., 2020).

157 Offshore, despite a lack of drill core data, a few dredged carbonate samples were  
158 recovered from the outer slope of the eastern margin of Grande Terre (Chardon et al., 2008;  
159 Yamano et al., 2015) and close to *Munida* and *Crypthelia* seamounts (Daniel et al., 1976; Bitoun  
160 and Recy, 1982) (Fig. 2). These samples, collected between 400 m and 800 m water depths, are  
161 the only evidences of Miocene shallow-water carbonate deposits along the eastern margin of  
162 Grande Terre and Pines Ridge. Based on the interpretation of seismic profiles along Grande  
163 Terre's southeastern margin, Chardon et al. (2008) identified several normal faults that they  
164 interpret as being related to Late Miocene extensional tectonics. These authors also interpreted  
165 two planar surfaces as post-obduction erosional lateritic land surfaces resulting from  
166 weathering processes overlain by shallow-water carbonate deposits.

### 167 **2.4. Quaternary carbonate systems**

168 Our knowledge on the nature, structure and chronology of the New Caledonian  
169 Quaternary carbonate systems primarily comes from coring investigations carried out through  
170 the western parts of the New Caledonian barrier system (Coudray, 1976, Cabioch et al., 2008b;

171 Montaggioni et al., 2011). Four cores, 120 to 226 m-long, reached the upper Cretaceous and  
172 Eocene bedrock and allowed to characterize the Quaternary development history of the western  
173 carbonate shelf margin. The recovered carbonate sequences result from stacking of about ten  
174 sedimentary carbonate units that were deposited during successive transgressive and high sea-  
175 level stands corresponding to interglacial periods (Cabioch et al., 2008b). These units are  
176 separated from each other by unconformities formed during sea-level drops in glacial periods.  
177 The succession of depositional events was reconstructed using lithostratigraphy,  
178 magnetostratigraphy, uranium-series dating and nannofossil stratigraphy (Cabioch et al., 2008b;  
179 Montaggioni et al., 2011). Carbonate sediment production was initiated prior to 1.2 Ma within an  
180 open shallow-water shelf margin, which acted as a carbonate ramp system until 0.48 Ma.  
181 Corresponding deposits forming the lower units recovered in boreholes (red dots on Fig. 1)  
182 include grainstone, packstone and wackstone rich in corals, coralline algae, encrusting  
183 foraminifera with locally thick rodoliths accumulations (Montaggioni et al., 2011). The ramp  
184 system is assumed to have evolved into a rimmed, reef platform as of 0.40 Ma. The initiation of  
185 coral reef tracts and the associated reef-rimmed platform are thus considered to have begun  
186 after MIS 11 (Montaggioni et al., 2011), i.e. the Mid-Brunhes Event. Corresponding sedimentary  
187 units are made up of stacked *poritid*-rich framework beds correlated to reef-flat environments  
188 with moderate to lower-water energy, and corallgal frameworks partly including arborescent  
189 acroporids suggesting deposition in a protected reef-flat setting (Montaggioni et al., 2011).  
190 Complementary studies of the Quaternary evolution of the south-west lagoon obtained seismic,  
191 bathymetric and coring data (Le Roy et al., 2008; Le Roy et al., 2019). Results showed that infill  
192 is composed of two or three 100 ka sedimentary sequences with a first significant flooding of the  
193 lagoon assumed to have started during MIS7, at 220 cal kyr B.P. The disparate ages of the lagoon  
194 and reefs can be reconciled with the fact that the first reefs were probably initially fringing  
195 structures without a significant lagoon that has expanded later in response to subsidence of the  
196 margin and reef growth (Le Roy et al., 2018). Offshore, the outer barrier reef slopes of Grande  
197 Terre are marked by five marine terraces located between ca. 20 and ca. 120 m water depths

198 that Flamand (2006) tentatively correlated to the five reefal lithological sequences cored on the  
199 western barrier reef and interpreted as the morphological expressions of Quaternary  
200 interglacials. However, a younger, last deglacial origin for these terraces located above 120 m  
201 water depth cannot be ruled out. Note that these Quaternary marine terraces are located in the  
202 area indicated by the blue arrow on bathymetrical and seismic data (Figs. 5 to 8).

### 203 **2.5. Quaternary subsidence rates**

204 Based on cores of the Quaternary barrier reef of the western margin of Grande Terre, subsidence  
205 rates are estimated to range between 0.03 to 0.20 mm.yr<sup>-1</sup> since the last 400 ka (Coudray, 1975;  
206 Cabioch et al., 1996; Flamand, 2006; Frank et al., 2006) and display mean rates of  $\leq 0.08$  mm.yr<sup>-1</sup>  
207 over the past 1 Ma (Montaggioni et al., 2011). Such values possibly reflect a long-term  
208 subsidence of the western margin of Grande Terre suggesting that post-obduction extensional  
209 tectonics are still active and allowing sufficient accommodation space to record most Quaternary  
210 sea-level highstands. Unfortunately, the lack of core data on the eastern margin does not allow  
211 reconstructing any Neogene to Quaternary vertical motions.

## 212 **3. DATA AND METHODS**

213 Our morphological and stratigraphic analyses are based on the integration of existing and  
214 newly acquired bathymetrical and 2D seismic reflection data supplemented by dredged rock  
215 samples (Fig. 2). Existing bathymetrical data are derived from four datasets. The former covers  
216 the lagoon of Grande Terre and was essentially acquired during hydrographic surveys of the  
217 French Navy (SHOM), compiled by the New Caledonia Government within a 25 m resolution  
218 grid. The second dataset corresponds to data acquired between 2002 and 2006 onboard RV *Alis*  
219 (EM1002 multibeam echosounder) along all the outer slopes of Grande Terre and Loyalty  
220 islands, as well as on seamounts of the Pines Ridges (down to *ca.* 1000 m of water depth), in the  
221 framework of the ZoNéCo program (*e.g.* Pelletier et al., 2002, 2004, 2012; Perrier et al., 2004a,  
222 2004b, 2004c, 2005) and IRD research projects (*e.g.* Cabioch et al., 2002a, 2002b). The third

223 dataset consists of data acquired in the 90's and 2000's in deeper waters (>1000 m of water  
224 depth), such as in the South Loyalty Basin, onboard RV *L'Atalante* (EM12D multibeam  
225 echosounder), again through ZoNéCo (*eg.* ZoNéCo-1, Pautot et al., 1993; ZoNéCo-2, Lafoy et al.,  
226 1994; and ZoNéCo-3; Missègue et al., 1996). These two multibeam datasets were compiled in  
227 2009 in 25 m (EM1002) and 100 m (EM12D) resolution grids by New Caledonia Government  
228 (Juffroy, 2009) and included in the 2012 atlas of New Caledonia (Pelletier et al., 2012). The  
229 fourth dataset is the global seafloor topography derived from satellite altimetry and ship depth  
230 soundings (Smith and Sandwell, 1997). Newly acquired bathymetrical data corresponds to those  
231 gathered by the KANACONO cruise onboard R/V *Alis* (Puillandre & Samadi, 2016).

232 The seismic dataset mainly consists of published multichannel seismic reflection profiles  
233 located on the upper slope of the eastern margin of Grande Terre, acquired onboard R/V *Alis*  
234 during the NEOMARGES cruise (Chardon et al., 2007), using a 24 channel streamer and a 20  
235 cubic-inch air gun source. The high-resolution images have a maximum penetration of 0.25 s two  
236 way time (twt) (Table 1) and were reinterpreted in this study through detailed line drawings.  
237 Seismic profiles 206-04 (Lafoy et al. 1998) and AUS-104 (Bitoun & Recy et al. 1982), which are  
238 publicly available in the *Tasman Frontier seismic database* (Sutherland et al., 2012), were also  
239 interpreted. These profiles were acquired using lower frequency seismic devices (see Table 1)  
240 and hence have a lower resolution but a higher penetration, reaching 3 s twt in the offshore  
241 basins. Seismic stratigraphic analysis was performed on these profiles including identification of  
242 seismic facies, unconformities and sequences following Mitchum et al. (1977). To estimate the  
243 thickness of the carbonate units on the Pines Ridge, we assumed that they are composed of  
244 shallow-water carbonates with a low-porosity, affected by early compaction and dissolution, for  
245 which we attributed a mean velocity of 3000 m.s<sup>-1</sup> (Anselmetti & Eberli, 2001).

246 Sedimentary facies determinations were made on 17 carbonate rock samples dredged  
247 during the DR-2005-NC and KANACONO cruises onboard R/V *Alis* (Pelletier et al., 2006;  
248 Puillandre & Samadi, 2016; respectively) in water depths between 250 and 900 m (Table 2).  
249 Samples were described from large thin sections in order to identify textures and main

250 components and ultimately reconstruct depositional environments. Biostratigraphic datings and  
251 paleoenvironmental reconstructions were based on the interpretation of foraminiferal  
252 assemblages (larger benthic and planktonic foraminifera). In our definitions of stratigraphic  
253 ranges, the planktonic foraminiferal zonal scheme of BouDagher-Fadel (2015, 2018a) is used.  
254 This scheme is tied to the time scale of Gradstein et al. (2012) and the revision by Cohen et al.  
255 (2017).

## 256 **4. PHYSIOGRAPHY, STRUCTURE AND STRATIGRAPHY OF THE**

### 257 **EASTERN MARGIN**

#### 258 **4.1. Lagoon**

259 The eastern lagoon, extending from the shoreline to the external barrier reef, is 10-15  
260 km wide between Poindimié and Yaté with an average water depth of 40 m, whereas the  
261 western lagoon does not exceed a width of 5-10 km with an average water depth of 20 m, except  
262 in its southern part where it is deeper and wider (Le Roy et al., 2008, 2019). Another difference  
263 with the western lagoon, which is bounded by continuous barrier reefs, is that the eastern  
264 lagoon is typified by a discontinuous external barrier reef with drowned segments in its  
265 southern part, off Yaté (Cabioch et al., 1996; Andrefouet et al., 2009) (Fig. 2). The eastern lagoon  
266 can be divided into three morphological domains: (1) the shallow-water coastal zone, (2) the  
267 median lagoon and (3) the external barrier reef (Fig. 3B).

268 The shallow-water coastal zone is particularly well-developed between Ponérihouen to  
269 Thio, where coastal bays are shallow and have gentle slopes, due to terrigenous deltas located at  
270 river and estuarine mouths (Fig.3). The deltaic deposits extend for 2.5 to 7 km and can reach the  
271 central part of the lagoon. Between Côte Oubliée and Yaté, deltas are very restricted and do not  
272 exceed 2 km in length (Fig.3A). Previous studies on unconsolidated seafloor sediments revealed  
273 that these deltas are mainly composed of terrigenous sediments (Chevillon, 1997).

274 The deeper median lagoon, is relatively flat in its central part and contains isolated patch reefs  
275 as well as sandy islets aligned parallel to the coastline (Fig.3A). Southeast of the East Ngoé Pass,  
276 the median lagoon deepens (with an average water depth of 60-70 m) and contains a  
277 meandering channel that runs parallel to the coastline (Fig. 3A). This channel extends over 30  
278 km, incises the lagoon up to 40 m deep and is connected to the Kouakoué Pass, where it runs  
279 perpendicular to the coastline thanks to a *ca.* 90° bend (Fig.3A).

280 The barrier reef domain comprises the reef crest, close to sea level, as well as a back-reef  
281 and reef flats within a 5 km-wide shallow-water area (20 to 40 m water depths). The latter is  
282 dominated by carbonate sediments of heterogeneous grain size, ranging from fine-grained sands  
283 to gravels (Chevillon, 1997). The barrier reef domain is interrupted by numerous passes (ie.  
284 inlets) connected to lagoonal channels that cross-cut the back-reef domain and are oriented  
285 roughly perpendicular to the coastline and the reef crest (Fig.3).

## 286 **4.2. Outer slope**

### 287 **4.2.1 Overall slope profile**

288 The outer slope morphologies of Grande Terre were previously described by Bitoun and  
289 Récy (1982), Rigolot (1989), Flamand (2006) and Pelletier et al. (2012). The outer slope of the  
290 western margin is very steep with values up to 20° between 0 to 2000 m water depths. This  
291 margin is very abrupt as the upper part of the slope is also very steep (see W-01 and W-02  
292 profiles Fig.4). In comparison, the outer slope of the eastern margin, from Poindimié to Yaté, is  
293 smoother and extends over 15 to 20 km from the platform edge to the toe of slope at a water  
294 depth of approximately 2200 m (Fig. 4). It is composed of 3 domains: (1) the upper slope,  
295 characterized by a slope gradient lower than 3°, between 100 to approximately 500 m water  
296 depths and extending up to 20 km in areas preserved from the erosion (*e.g.* offshore Côte  
297 Oubliée and Yaté, see E-01 profile Fig.4). On the contrary, some areas are devoid of an upper  
298 slope domain and canyon heads are in direct contact with the external barrier reef (*e.g.* offshore

299 Houailou, see E-02 profile [Fig.4](#)); (2) the middle slope shows a slope gradient of up to 10°  
300 between 400-500 m to approximately 2200 m water depth; (3) the lower slope and toe-of-slope  
301 domain shows a gentle slope gradient ranging from 0.5 to 1°. This slope section starts  
302 approximately at 2200 m water depth, which corresponds with the transition to the Loyalty  
303 Basin floor. The slope section contains numerous erosional by-pass features such as submarine  
304 canyons that incise the slope up to a depth of 200 m. Backscatter imagery reveals depositional  
305 lobes at canyon mouths, offshore Thio and Yaté, as previously reported by Cotillon et al. (1989,  
306 1990). The cut off angles are intended to characterize the morphology of the slope and have no  
307 universal value. Even in the case of a Gaussian slope angle evolution (*sensu* Adams and Kenter,  
308 2013) angle values may vary between different carbonate systems.

#### 309 **4.2.2 Physiography of the upper slope**

310 The upper slope is delimited by a major scarp located at 300-400 m water depth close to  
311 the Cap Bayes Pass ([Fig. 5A](#)) and the Nakéti Pass ([Fig. 6A](#)), at 400-500 m water depth in front of  
312 Côte Oubliée ([Fig. 7A](#)) and at 500-600 m water depths close to the Yaté Pass. The low-angle  
313 upper slope is only 3 to 4 km wide close to Nakéti Pass and widens southward to reach a width  
314 of 20 km in the vicinity of Yaté ([Fig. 3A](#)). Arcuate scars occur along the scarp, suggesting slope  
315 failure processes along the upper slope ([Fig.5A](#) and [6A](#)). In front of Côte Oubliée, the 5-6 km  
316 wide upper slope is incised by low sinuosity, U-shaped, 40 to 80 m deep gullies ([Fig.7A](#)). Gullies  
317 are of variable extension along the upper slope, some start at 150 m water depth close to the  
318 outer reef slope, whereas others, shorter, gullies start at 300 m water depth, 3-4 km away from  
319 the shelf edge. The majority of gullies are located in front of Kouakoué Pass through which they  
320 are connected to the meandering lagoonal channel ([Fig.3A](#)).

#### 321 **4.2.3 Stratigraphy of the upper slope**

322 Seismic profiles covering the platform edge to the upper slope region reveal two main  
323 seismic units, U1 and U2 separated by unconformity S1 ([Fig. 5, 6 and 7](#)). These profiles also  
324 show that U1 is exposed on the seafloor along a major scarp (see red arrows on maps and

325 profiles of Fig. 5, 6 and 7). U1 comprises wavy reflections and is delimited at its top by erosional  
326 truncations and toplap terminations at bounding surface S1. The latter is overlain by unit 2 (U2)  
327 which shows well-layered reflections downlapping onto S1 (Figs. 5, 6 and 7). The maximal  
328 thickness of U2 varies between 0.1 to 0.25 s twt. In front of Côte Oubliée, on profile NM-13, at  
329 the mouth of the Kouakoué Pass, U2 is twice as thick than on profile NM-12b located 20 km  
330 further north at distance from any pass (Fig. 7).

331 Seismic profile NM1 at the mouth of the Cap Bayes Pass displays a well-developed unit  
332 U2 which forms a 0.2-0.25 s twt thick sedimentary prism (Fig. 5) composed of five stratigraphic  
333 sequences each composed of retrogradational sets (in pink on Fig. 5) overlain by progradational  
334 clinoform foresets (in beige on Fig. 5), noted 1 to 5. The slope break of the youngest (5<sup>th</sup>)  
335 clinoform foreset (annotated “Clinoform slope break” on Fig. 5) is located at 150 m water depth.  
336 Retrogradational sets contain low-amplitude, mound-shaped seismic reflections that are only  
337 observed in topsets. Progradational sets show high-amplitude sigmoidal oblique reflections that  
338 downlap onto the underlying unit and are mainly located in the distal part of the sedimentary  
339 prism.

### 340 **4.3. Pines Ridge**

341 The Pines Ridge corresponds to the structural extension of the eastern margin of Grande  
342 Terre towards the South (Fig. 2). It is a NNW-SSE trending structure extending from the Isle of  
343 Pines to the Cook Fracture Zone.

#### 344 **4.3.1 Basement structure and first-order seismic stratigraphy of the Pines** 345 **Ridge**

346 The Pines Ridge is a horst of peridotite bounded by normal faults (Bitoun & Recy, 1982;  
347 Patriat et al., 2018) and is the southern offshore extension of the Peridotite Nappe cropping out  
348 onland (Patriat et al., 2018). In this paper, we have studied the area comprised between the Isle  
349 of Pines and Antigonina seamount, where Pines Ridge is the shallowest (Fig. 8A). Seismic profile

350 AUS-104 (Fig. 8B) reveals that the Pines Ridge comprises at its top high-amplitude subparallel  
351 reflections between 0.7 and 0.9 s twt, which contrast with the transparent seismic character of  
352 the underlying acoustic basement. Along the eastern flank of the Pines Ridge, the acoustic  
353 basement crops out on the seafloor at 2000 m water depth and was sampled by dredge GEO-I-  
354 3D (Daniel et al., 1976; Bitoun & Recy, 1982) (Fig. 8). The samples comprised altered basalt  
355 pebbles within a carbonate mud matrix containing planktonic foraminifera from the late  
356 Oligocene – earliest Miocene (Daniel et al., 1976). At that location, the acoustic basement forms a  
357 slightly tilted plateau located between 2.5 and 2.7 s twt, interpreted as an erosional weathering  
358 surface on top of peridotites by Bitoun and Recy (1982). This peridotite platform constitutes the  
359 western edge of the South Loyalty Basin (Figs. 8B and 8C). The peridotite basement is covered  
360 by a seismic unit composed of discontinuous low-amplitude subparallel reflections that is about  
361 0.2 s twt thick at the crest of the ridge and up to 0.6 s twt-thick on its eastern flank. This unit is  
362 interpreted as a post-obduction sedimentary sequence (Bitoun & Recy, 1982 ; Patriat et al.,  
363 2018). The unit is incised by several submarine canyons along the eastern slope that extend  
364 from the Pines Ridge to the South Loyalty Basin (Fig. 8).

#### 365 ***4.3.2 Physiography of the Pines Ridge***

366 Along the northern part of the Pines Ridge, on the upper slope, the terrace identified on  
367 the eastern outer slopes of Grande Terre is continuously present between 300 to 600 m water  
368 depths (red arrows on Fig. 8A). East of the Isle of Pines, this terrace is affected by arcuate scarps  
369 most likely corresponding to submarine gravity collapses. Towards the Antigonía seamount, the  
370 top of the Pines Ridge is capped by this terrace (Fig. 2). Indeed, between the Banc de la Torche  
371 and Antigonía seamounts, the ridge's top remains positioned at 400-500 m water depth and its  
372 eastern slope is again characterized by a steep gradient and collapse features (red arrows on Fig.  
373 8A). In turn, the Banc de la Torche and Antigonía display flat tops in 30 m to 60 m water depths  
374 (blue arrows on Fig. 8A). These two submerged isolated banks are surrounded by two terraces  
375 at 80-90 m and 120 m water depth.

376           The isolated Crypthelia and Munida seamounts are delimited by a main scarp at 400-500  
377 m water depths (Figs.2 and 8). Their tops are located at 194 m and 93 m water depths,  
378 respectively. The Crypthelia seamount is 3 km wide and 12 km long elongated in a N160°  
379 direction (Fig. 9A and 9B). Three fault scarps located approximately in 250, 350 and 500 m  
380 water depth affect the seamount across its entire length. Fault scarp heights are comprised  
381 between 30 m and 100 m (see map and cross section of Fig. 9B). In the northern part, the  
382 eastern fault scarp is associated with a channel probably formed by bottom currents circulating  
383 along the footwall of the fault (Fig. 9A and 9B). The southern edge of the seamount is marked by  
384 two 2-3 km wide failure scars, evidenced by arcuate headscarps located between 350 to 600 m  
385 water depth. The Munida seamount, located further to the northeast, extends over 8 km wide  
386 and 18 km long with a N60° direction (Fig. 9C). Its edges are bordered by N60° and N160°  
387 oriented fractures. On its southern flank, a terrace (M1) bordered by fault scarps is identified  
388 between 400 m and 600 m water depth. Above 200 m water depth, the top of the seamount (M2)  
389 is relatively flat (Fig. 9C) but still shows terraces at 100 m and 120-130 m water depth.

### 390           **4.3.3 Stratigraphy of the Pines Ridge**

391           The internal architecture of the post-obduction sedimentary sequence overlying  
392 basement of Pines Ridge and Munida seamount are imaged by seismic profile 206-04 (Fig.10).  
393 Over the Pines Ridge, the capping sedimentary unit reaches up to 0.5 s twt thick, i.e.  
394 approximately 750 m thick considering a velocity of 3000 m.s<sup>-1</sup> for a 30% porosity limestones  
395 according to Geldart (2004). In details, this interval is composed of 3 units, UP1 to UP3 (Fig.10C  
396 and 10D). Unit UP1 mainly developed on the SW edge of the ridge and is composed of low-  
397 amplitude reflections northeastwardly downlapping on basement. Unit UP2 downlaps basement  
398 on the eastern edge of the ridge with very low-amplitude reflections that form mounded  
399 morphologies. To the west, the seismic character of UP2 laterally evolves into low-amplitude,  
400 wavy to horizontal parallel reflections onlapping onto UP1 towards the southwest. Unit UP3 is  
401 typified by low-amplitude, sub-parallel and nearly horizontal reflections with low relief,  
402 mounded morphologies on the eastern edge of the ridge. Because seismic line 206-04 runs along

403 the south-eastern slope of Munida Seamount (Fig. 9C), seismic imaging is poor due to 3D lateral  
404 effects. However, the profile intersects a part of the seamount with less slope that reveals that  
405 the sedimentary sequence has a minimum thickness of 0.4 s twt, i.e. approximately 600 m-thick  
406 (Fig.10A and 10B). It is composed of two distinct seismic units, UM1 and UM2 (Fig.10). Unit UM1  
407 overlies the basement and comprises low-amplitude subparallel mounded reflections with  
408 downlapping and onlapping terminations. Unit UM2 overlies UM1 and comprises high-  
409 amplitude subparallel reflections with downlapping terminations.

#### 410 **4.4. Lithologies and biostratigraphic ages**

##### 411 **4.4.1 Eastern margin of Grande Terre**

412 Seven carbonate rock samples have been collected along the upper slope of the eastern  
413 margin (Table 3, see location on Fig. 2). DR44 and DR45 were recovered on scarps located at  
414 400 m and 600 m water depths, at the seafloor exposure of seismic unit U1 (see location on Figs.  
415 6A and 6B). DR44 is a micritic packstone with recrystallised algae, large benthic foraminifera  
416 (LBF) of Serravallian age (PZ N12, Tf2, 13.82 Ma to 12.00 Ma) (see BouDagher-Fadel, 2018b)  
417 and corals. These elements are reworked within a pelagic mud dominated by planktonic  
418 foraminifera (Table 4) that comprise *Globigerinoides quadrilobatus* (Fig.11A, b.),  
419 *Dentoglobigerina altispira* (Fig.11B, b.), *Globorotalia menardii* (Fig.11B, c.), *Globigerinoides*  
420 *conglobatus* (Fig.11B, d.), *Globigerinoides ruber* (Fig.11B, e.), *Truncorotalia crassaformis*, *Orbulina*  
421 *universa*, *Globorotalia plesiotumida* (Fig.11C, a), *Sphaeroidinella dehiscens* of Early Pliocene age  
422 (N19-N20a, 5.3 Ma to 3.6 Ma). DR45 comprises ultramafic pebbles and gravels encrusted by  
423 algae incorporated in a micritic packstone similar to that of DR44 and also includes  
424 *Lepidocyclina* sp. (Fig. 11D) and *Alveolinella praequoyi*, with the same Serravallian age. DR46,  
425 DR47 and DR48 were collected on the edge of the terrace located between 200 to 400 m water  
426 depths near the Nakéti Pass (Figs. 6A and 6C). These three samples consist of micritic  
427 wackestone/packstones with patches of reworked pelagic micritic facies. DR46 assemblages are  
428 dominated by planktonic foraminifera such as *Truncorotalia crassaformis* (Fig. 11E, a.) *T.*

429 *truncatulinoides*, *Globorotalia inflata*, *Globorotalia menardii* and *Orbulina univesa* of Pleistocene  
430 age (N22, 1.8 Ma to 0.12 Ma). DR47 sample shows numerous terrigenous grains (quartz, altered  
431 serpentine and undifferentiated clasts). Planktonic foraminifera are common and include  
432 *Globoquadrina dehiscens* (Fig. 11F, a.), *Globigerinoides quadrilobatus*, *Globigerinoides trilobus*,  
433 *Globigerinoides ruber*, *Globorotalia tumida*, *Globigerinoides spp.*, and *Pulleniatina obliquiloculata*  
434 of Late Pliocene age (N20a, 3.8 Ma to 3.6 Ma). DR48 contains numerous recrystallized algae and  
435 reworked LBF, such as *Alveolinella praequoyi* (Fig. 12A, a.) of Serravallian age (see Adams, 1984;  
436 BouDagher-Fadel and Banner, 1999; BouDagher-Fadel, 2018b), planktonic foraminifera of  
437 Pleistocene in age (N22, 1.8 Ma to 0.12 Ma) such as *Pulleniatina obliquiloculata* (Fig. 12A, b.), *P.*  
438 *primalis* and *Neogloboquadrina dutertrei*. DR49 sample was collected along the scarp at 500 m  
439 water depth, near the East Ngoé pass. The lower part of this scarp corresponds to the top of  
440 seismic unit U1 (Table 3, see location Figs.7A and 7B). Recovered samples comprise a micritic  
441 packstone with algae and LBF of Serravallian age, such as *Alveolinella praequoyi* (Fig. 12B, a.)  
442 and planktonic foraminifera such as, *Globorotalia tumida* (Fig.12C, a.), *Sphaeroidinellopsis*  
443 *subdehiscens*, *Globorotalia menardii* and *Globorotalia inflata* of Early Pliocene age (N19b, 4.2 Ma  
444 to 3.8 Ma) after BouDagher-Fadel (2018a). DR53 is located further south, in front of the Yaté  
445 Pass, in ca. 280 m water depth, and is a micritic packstone containing planktonic foraminifera  
446 such as *Pulleniatina primalis* (Fig.12D, a.), *Prosphaeroidinella parkerae*, *Pulleniatina praecursor*,  
447 *Globigerinoides obliquus* and *Truncorotalia crassaformis* of Late Miocene to Early Pliocene age  
448 (Table 3, see location Fig.2).

#### 449 **4.4.2 Pines Ridge**

450 Seven carbonate rocks were sampled along the Pines Ridge (Table 3, see location Fig. 2  
451 and Fig.8A). These samples are mainly micritic wackestones/packstones with planktonic  
452 foraminifera and algae. Samples DW4737-B, DW4745-B, DW4746-B, DW4747-B1 and DW4747-  
453 X have ages ranging from Pliocene to Late Pleistocene (N19 to N22, 5.33 Ma to 0.12 Ma).  
454 Planktonic foraminifera assemblages of these samples include *Neogloboquadrina pachyderma*,  
455 *Sphaeroidinella dehiscens*, *Truncorotalia truncatulinoides*, *Truncorotalia tosaensis*, and

456 *Pulleniatina obliquiloculata* and LBF, such as *Alanlordia* sp. (Fig.12E, a.), are found reworked  
457 together with Pliocene planktonic foraminifera into the younger assemblages. Further south,  
458 samples DW4757-A and DW4782-A were collected along the eastern slope of Pines Ridge (Table  
459 3, see location Fig.8A and Fig.10). DW4757-A includes Oligocene to earliest middle Miocene LBF  
460 such as *Lepidocyclina* sp. and *Planorbulinella solida* (Fig.12F, a.), while DW4782-A comprises late  
461 Miocene to Pleistocene (N17-N20, 8.6 Ma to 3.4 Ma) planktonic foraminifera such as  
462 *Neogloboquadrina humerosa*, *Sphaeroidinellopsis seminulina*, *Sphaeroidinellopsis subdehiscens*.

#### 463 **4.4.3 Munida seamount**

464 Three carbonate rock samples have been collected along the edges of *Munida* (Table 3,  
465 see location on Fig. 8A and Fig. 9C). Samples from DW4770, located on the northeast flank of the  
466 seamount, comprise micritic and sparitic packstones composed of algae and planktonic  
467 foraminifera, such as *Truncorotalia truncatulinoides* (Fig.12F, a) and *Truncorotalia tosaensis*  
468 (Fig.12F, b) of Pleistocene age (N22, 1.8 Ma to 0.12 Ma). DR4772-A and DR4773-A samples,  
469 located on the southern flank, are grainstones cemented by sparite, with planktonic  
470 foraminiferal assemblages including *Sphaeroidinellopsis subdehiscens*, *Sphaeroidinella dehiscens*,  
471 *Truncorotalia tosaensis* and *Pulleniatina obliquiloculata* of Pliocene to Pleistocene age (N21-N22,  
472 3.4 Ma to 0.12 Ma). These samples also reveal many reworked Miocene and Pliocene planktonic  
473 foraminifera.

474 **4.5. *Paleoenvironmental interpretations***

475           The assemblages of DR44 and DR45 are dominated by Early Pliocene planktonic  
476 foraminiferal assemblages (e.g. *Sphaeroidinellopsis paenedehiscens*, *Globoquadrina dediscens*,  
477 *Orbulina universa*, *Globorotalia plesiotumida*, *G. tumida* and *Dentoglogigerina altispira*). These  
478 mixed, globular and heavily keeled planktonic foraminifera are indicative of inner to outer  
479 neritic environments (BouDagher-Fadel, 2015). Miocene larger benthic foraminifera (e.g.  
480 *Lepidocyclina* sp., *Katacycloclypeus martini*, *Cycloclypeus* sp.) and fragments of corals and  
481 rodophyte species are also frequently reworked within the deeper Early Pliocene platform.  
482 These larger benthic foraminifera are flat in shape and are associated with symbiont-bearing  
483 diatoms (Leutenegger 1984; Romero et al. 2002). They are common in forereef environment  
484 where they adapted to light attenuation with increasing habitat depth (Hottinger, 1983; Hallock  
485 and Schlager, 1986; Hohenegger, 1995; 2005; Yordanova & Hohenegger, 2002; 2007;  
486 BouDagher-Fadel, 2018b).

487           The Late Pliocene to Pleistocene deposits of DR46, DR47 and DR48 contain mainly  
488 planktonic foraminifera of mixed assemblages of globular forms (e.g. *Globigerinoides*  
489 *quadrilobatus*, *Orbulina universa*) and keeled globorotalids (e.g. *Truncorotalia truncatulinoides*,  
490 *Globorotalia tumida*). These assemblages are indicative of an inner to outer neritic environment  
491 (see BouDagher-Fadel, 2015). Micritic patches of older Miocene deposits with mainly globular  
492 small globigerinids (e.g. *Catapsydrax cf. dissimilis*, *Globigerina praebulloides*) are also present  
493 indicating the reworking of an inner neritic Miocene platform within the deeper deposits of the  
494 Pliocene.

495 DR 49 is interpreted as being deposited in an Early Pliocene inner to outer neritic  
496 platform. It contains planktonic foraminifera assemblages dominated by globular forms (e.g.  
497 *Globorotalia menardii*, *G. inflata*, *Globigerinoides trilobus*, *Gldes quadrilobatus*) with occasional  
498 occurrences of keeled forms (e.g., *Globorotalia tumida*, *G. menardii*) and thickly coated forms in a  
499 thick, smooth cortex of calcite, *Sphaeroidinerlla dehiscens*. The latter is an extant thermocline  
500 dweller found rarely in subsurface, tropical, and subtropical waters (Chaisson and Ravelo, 1997;  
501 BouDagher-Fadel, 2018b). Reworked reefal Miocene larger benthic foraminifera (e.g.,  
502 *Alveolinella praequoyi*, *Lepidocyclina sp.*, *Planorbulina larvata*, *Amphistegina lessonii*,  
503 *Operculinoides spp.*, *Gypsina sp.*) are also present. The presence of the large fusiform miliolid, *A.*  
504 *praequoyi* indicates the reworking of shallow reefal facies into the deeper Early Pliocene neritic  
505 environments.

506 The assemblages of DR53 are dominated by Late Miocene to Early Pliocene globular  
507 planktonic foraminifera species (e.g., *Neogloboquadrina pachyderma*, *N. acostaensis*, *Orbulina*  
508 *universa*, *Prosphaeroidinella parkerae*, *Pulleniatina praecursor*, *P. primalis*, *Globigerinoides*  
509 *obliquus*). Occasional keeled forms (e.g., *Truncorotalia crassaformis*, *Globorotalia menardii*,  
510 *Globorotalia tumida*) are also present. Larger benthic foraminifera such as *Amphistegina spp.* and  
511 *Sphaerogypsina spp.* are also found. The extant *Amphistegina* has adapted to high energy  
512 conditions, however, it is also found in mud free sands in areas of sea grass or coralline algae  
513 and in reefal areas down to depths of 35m (McKee et al, 1959), while *Sphaerogypsina* is  
514 generally common in shallow-water reefal environments (Nebelsick et al. 2001). These  
515 assemblages are interpreted as being deposited in an inner to outer neritic platform.

516 All samples from Pines Ridge point to inner to outer neritic settings, except DW4757-A  
517 which is typified by a forereef environment because of the occurrence of larger benthic  
518 foraminifera, such as *Amphistegina lessonii*, *Lepidocyclina sp.*, and *Planorbulinella solida*. All  
519 samples from Munida seamount contain mixed assemblages of globular and keeled planktonic  
520 foraminifera (e.g., *Sphaeroidinellopsis subdehiscens*, *Sphaeroidinella dehiscens*, *Truncorotalia*  
521 *tosaensis*, *Pulleniatina obliquiloculata*, *Globorotalia inflata*) and are thought to reflect inner to  
522 outer neritic settings.

523523

## 524 **5. CARBONATE SYSTEM EVOLUTION ON THE EASTERN MARGIN OF** 525 **NEW CALEDONIA**

### 526 ***5.1 Mio-Pliocene carbonate banks***

527 Carbonate rocks sampled on the upper slope scarp along the eastern margin contain  
528 algae, benthic foraminifera and coral fragments evidencing shallow-water carbonate production  
529 as early as the middle Miocene (Serravalian) and up to the Pliocene (Table 3, Fig. 13). This scarp  
530 corresponds to the top of seismic unit U1, which is bounded by the gently downslope dipping  
531 surface S1 (Figs. 5, 6 and 7). Because of its planar character, Chardon et al., (2008) interpreted  
532 this surface, topping a clastic continental wedge, as a lateritic land surface formed by weathering  
533 during emersion. Because none of the dredges that sampled this scarp (and thus U1) contained  
534 any traces of lateritic deposits, we propose an alternative interpretation where seismic unit U1  
535 corresponds to a Mio-Pliocene carbonate bank, presently located at 300-600 m water depth.  
536 This important subsidence cannot be explained only by eustatism and we suggest that the post-  
537 obduction normal faulting that affected the Peridotite Nappe is likely the main driver of the  
538 subsidence. Surface S1 is interpreted as the top of the carbonate bank characterized by low-  
539 inclination features (Fig. 13A and B). The numerous ultrabasic pebbles/gravels and quartz  
540 grains within the carbonate matrix of samples DR45 and DR47 suggest coeval siliciclastic input

541 with the carbonate buildup development. A similar mixed carbonate-siliciclastic system also  
542 occurs along the coastal domain of the western margin of Grande Terre in the well-constrained  
543 Burdigalian Népoui system (Tournadour et al., 2020) (Fig.13B). The onset of these mixed  
544 systems indicates that both margins of Grande Terre experienced shallow marine conditions  
545 during the Miocene. However, their current positions, up to 20 m above present day sea level for  
546 the Lower Miocene Népoui outcrops of the western margin and up to 500 m water depth for the  
547 middle Miocene samples of the eastern margin, suggest a contrasted tectonic evolution of the  
548 margins.

549 Our results suggest that the Mio-Pliocene carbonate platform (Table 3, Fig.13) extended  
550 southward along the Pines Ridge, over peridotite horsts, which were at that time located in  
551 shallow-water (Fig.13A and B). Within this sedimentary succession, unit UP1 is interpreted as an  
552 attached carbonate platform developing on the western edge of the ridge. The eastward  
553 thickening of unit UP2, which unconformably overlies unit UP1 (Fig.10D), suggests deposition  
554 simultaneous or subsequent to the eastward tectonic tilting of Pines Ridge. The aggrading  
555 mounded reflections of the lower part of UP2 on the eastern edge of the ridge, may be  
556 interpreted as shallow-water, reefal bioconstructions (e.g. Miocene from the Browse basin,  
557 Australia: Belde et al., 2017), or as an oligo-mesophotic bank with dominant algal and  
558 foraminiferal production (e.g. Lower Miocene from Myanmar: Teillet et al., 2020a and 2020b).  
559 However, in the upper part of UP2, the upward change from mounded to flat-topped  
560 morphologies on the eastern margin strongly suggests the development of reef-flat  
561 environments aggrading up to sea-level. Finally, subunit UP3 is also characterized by a slight  
562 overgrowth along the eastern edge as evidenced by low-relief mounded reflectors (Fig.10). Such  
563 an asymmetric feature could be explained by the continuation of an eastward tectonic tilt or  
564 could be related to eastward winds driving carbonate growth (Fig.10).

565 Based on seismic interpretation, two stages of carbonate growth are identified on the  
566 Munida seamount (seismic units UM1 and UM2). A carbonate sample, collected 15 km away  
567 from the seamount (GEO-I-13D; location on Fig.2), contains benthic foraminifera indicative of

568 shallow-water environment, that can be dated Early Miocene (Daniel et al., 1976; Bitoun and  
569 Recy, 1982). This sample suggests a first stage of carbonate growth (UM1) of Miocene age coeval  
570 with carbonate platforms from Pines Ridge (UP1 and/or UP2) (Fig.13A and B). A Miocene  
571 carbonate platform also likely developed on the Crypthelia seamount as suggested by a Middle  
572 to Late Miocene carbonate sample exhibiting forereef facies (GEO-I-9D, see location Fig.2 and  
573 Fig.9A) (Daniel et al., 1976; Bitoun and Recy, 1982).

574           Based on aforementioned observations, we propose the following palaeogeographical  
575 reconstruction of the distribution of Mio-Pliocene shallow-water carbonate systems along the  
576 margin of New Caledonia (Fig. 13B). The Mio-Pliocene carbonate systems extend for about 350  
577 km, along the southeastern margin to Antigonina Seamount. On the western margin, the  
578 Quaternary carbonate reef-lagoon system directly overlies Eocene allochthonous units (see  
579 Fig.1). At that location, the absence of Miocene shallow-water deposits could be explained by a  
580 non-deposition or by erosion in relation to the uplift of the western margin. The thickness of the  
581 Miocene ramp is at least 200 m on the Nepoui area (Maurizot et al., 2016; Tournadour et al.,  
582 2020), but remains unknown along the eastern margin. However, it can be estimated to be  
583 around 750 m on the Pines Ridge (Fig.10B). Similar Miocene carbonate growth rates have been  
584 reported for the southwestern Pacific suggesting that, in addition to local tectonic control  
585 (subsidence) allowing significant volumes of sediments to accumulate, larger-scale  
586 oceanographic or global factors favoured a sufficiently high carbonate production to fill the  
587 created accommodation. For example, the 600 m-thick Marion Plateau platforms, northeast of  
588 Australia, result from robust carbonate growth through early and middle Miocene up to its  
589 terminal demise in the late Miocene (Ehrenberg et al., 2008). Along the northwestern shelf of  
590 Australia, seismic profiles reveal a giant middle Miocene prograding barrier reef that  
591 backstepped in the late Miocene (McCaffrey et al., 2020). Finally, the Gulf of Papua is also  
592 structured by large-scale isolated long-lived carbonate platforms during the late Oligocene-early  
593 Miocene and which demised during late Miocene-early Pliocene (Tcherepanov et al., 2008b). In  
594 our study, the prolific Mio-Pliocene carbonate accumulation is favoured by the subsidence of the

595 shelves of New Caledonia and Pines Ridge, most likely in relation to post-obduction extensional  
596 tectonics (Lagabrielle and Chauvet, 2008; Patriat et al., 2018).

## 597 ***5.2 Transition from Mio-Pliocene to Quaternary platforms***

598 Along the eastern margin of Grande Terre, the Quaternary rimmed platform is thought to  
599 have backstepped onto a Mio-Pliocene carbonate bank (Fig. 13A and 13C). Southward, along the  
600 Pines Ridge and associated seamounts, the Mio-Pliocene carbonate banks are drowned but  
601 several Quaternary flat-topped isolated platforms survived and aggraded.

602 In the vicinity of the study area, the carbonate platform of Maré, on the Loyalty Ridge,  
603 records a significant change in the nature of carbonate production which is rhodalgal-dominated  
604 during the late Miocene, and coralgal-dominated during the Pliocene (McNeill and Pisera, 2010;  
605 Maurizot et al., 2020). These authors explain the switch of carbonate production by the trend of  
606 decreased coralline red algae species richness (Aguirre et al., 2000) combined with the global-  
607 scale Zanclean Flood Event (McKenzie et al., 1999). The exposure of these carbonate records  
608 would result from the local tectonic uplift of the Loyalty Ridge related to Pliocene-Pleistocene  
609 lithospheric flexure associated with the New Hebrides subduction (Dubois et al., 1974 and  
610 1975).

611 Along the western margin of Grande Terre, the coral reef flourished from 400 ky (MIS-  
612 11) considered as a period of luxuriant reef expansion in the southwest Pacific (Cabioch et al.,  
613 2008b). Nevertheless, during the Quaternary, non-reefal carbonates were identified prior to  
614 MIS-11 as early as 1.4 Ma, overlapping the Eocene allochthonous units and could form the  
615 foundation of the Quaternary rimmed platform (Cabioch et al., 2008b; Montaggioni et al., 2011).

616 Along the eastern margin, the occurrence of a Mio-Pliocene platform below the eastern  
617 barrier reef-lagoon suggests that an older carbonate platform developed similarly to what is  
618 observed in Maré Island. The common occurrence of normal faults suggests that the eastern  
619 margin and Pines Ridge were dominated by tectonic subsidence that would have promoted

620 accommodation for Neogene carbonate deposition and preservation, by opposition to the  
621 western margin where the Quaternary carbonates are found on top of Eocene peridotites.  
622 However, high subsidence rates could also explain the demise of the Mio-Pliocene carbonate  
623 systems along the Pines Ridge and the backstepping of Quaternary platforms. After 125 ky, the  
624 southeastern margin is slightly uplifted in the Yaté area and the Isle of Pines (Launay, 1985;  
625 Cabioch et al., 1996). This uplift could be due to the isostatic rebound of the central part of  
626 Grande Terre (Cabioch et al., 1996; Lagabrielle and Chauvet, 2008) or alternatively, could be  
627 associated with the lithospheric bulge of the New Hebrides subduction which is known to have a  
628 regional impact from the Loyalty Islands to the Isle of Pines (Dubois et al., 1974 and 1975;  
629 Cabioch et al., 1996). Hence, both margins of New Caledonia seem to have been affected by long-  
630 term subsidence during the Quaternary which, together with high-amplitude eustatic sea-level  
631 variations, allowed the aggradation and preservation of the reef-lagoon successions.

### 632 ***5.3 Quaternary carbonate platform***

#### 633 ***5.3.1 Late Quaternary mixed carbonate siliciclastic systems along the eastern*** 634 ***margin***

635 At the mouth of the Cap Bayes Pass, seismic unit U2 forms a 200 m-thick prism  
636 comprising five stratigraphic sequences (Fig. 5). In detail, the internal geometries of these  
637 parasequences are characterized by successive sets of aggrading to retrograding mounded  
638 reflections and progradational inclined reflections. We interpret these parasequences as mixed  
639 carbonate-siliciclastic prisms that developed at the mouth of the pass, with aggrading and  
640 retrograding shallow-water carbonate sequences that developed during a transgression (pink  
641 colour on Fig. 5C), deposited during the last glacial-interglacial Quaternary cycles. This  
642 interpretation is consistent with core data collected on the western barrier reef (see location of  
643 Fig. 1), which revealed that the barrier reef itself consist of four to five lithological sequences  
644 deposited during successive transgressions and highstands in sea level since the Mid-Brunhes,  
645 each transgressive reefal units being separated by subaerial unconformities (subaerial

646 exposures) (Cabioch et al., 2008b; Montaggioni et al., 2011). The prograding seismic patterns  
647 (yellow colour on Fig.5C) thus can be interpreted as lowstand siliciclastic wedges that formed  
648 during Late Quaternary glacial lowstands.

649 Siliciclastics might have developed contemporaneously with the Quaternary barrier reef  
650 bordering the eastern lagoon (Figs. 5, 6B and 7). This observation is consistent with the  
651 reciprocal sedimentation concept traditionally developed for carbonate-siliciclastic mixed  
652 systems (see review by Chiarella et al., 2017). According to this concept, siliciclastic deposits  
653 prevailed on the upper slope during sea-level lowstands and at the beginning of the shelf  
654 reflooding, whereas carbonate facies dominate during transgressions and highstand periods.  
655 This configuration is currently observed on the platform edge of Quaternary mixed carbonate-  
656 siliciclastic systems such as the Australia and Papua New Guinea Reef (Tcherepanov et al.,  
657 2008a; 2008b; 2010; Harper et al., 2015; Mallarino et al., 2021) or the Belize Barrier Reef (Esker  
658 et al., 1998; Ferro et al., 1999; Gischler et al., 2010; Droxler and Jorry, 2013). However, the  
659 reciprocal pattern is not expressed everywhere along the upper slope of the eastern margin.  
660 Near the Côte Oubliée, seismic unit U2 is not characterized by sedimentary prograding  
661 clinoforms but rather by a downlapping aggrading wedge with a maximum thickness of 200 m in  
662 front of the Kouakoué Pass (Fig.7). The lack of prograding features associated with the lowstand  
663 clastic wedge could be explained by low terrigenous sedimentation rates as suggested by small  
664 deltas restricted to the coastal domain (Fig. 3A). Moreover, the southeastern part of the lagoon is  
665 characterized by a meandering channel network parallel to the coast and to the barrier reef,  
666 suggesting an alongshore transport which can partly intercept outgoing sedimentary flux from  
667 lagoon (Fig. 3A). In addition, the numerous gullies cutting the upper slope suggest high off-bank  
668 sediment transport toward the deep basin and thus the accumulation of sediments along the  
669 upper slope (Fig. 7A). This off-bank sediment transport could result from density cascading  
670 processes driven by seasonal meteorological conditions (Wilson and Roberts, 1992, 1995). The  
671 alongslope heterogeneity of the eastern margin upper slope deposits clearly shows that the  
672 behaviour of a mixed carbonate-siliciclastic margin is difficult to predict and is not only

673 dependent of relative sea-level changes, as mentioned previously (Chiarella et al., 2017;  
674 O'Connell et al., 2020).

### 675 ***5.3.2 Quaternary isolated flat-topped banks of Pines Ridge and seamounts***

676 Along the Pines Ridge, dredged carbonate rock samples show that shallow-water  
677 carbonate deposition occurred on the Banc de la Torche and Antigonina seamounts during the  
678 Quaternary (Fig.13A and C). The two marine terraces at 80-90 m and 120 m water depth might  
679 evidence reef backstepping during the last deglacial sea-level rise, as reported around the Great  
680 Barrier Reef (Webster et al., 2018), the Gulf of Mexico (Khanna et al. 2017), the Maldives  
681 (Fürstenau et al., 2010; Rovere et al., 2018), the SW Indian Ocean (Jorry et al., 2016), the  
682 Marquesas Island (Cabiocch et al., 2008a) and in Tahiti (Camoin et al., 2012). Carbonate rock  
683 samples dated at the youngest from the Pleistocene and collected on the flat-top of the Munida  
684 seamount that is currently submerged in 93 m water depth, are thought to be representative of  
685 seismic unit UM-2 which would correspond to the last stage of the carbonate platform's growth.  
686 Similarly to the Banc de la Torche and Antigonina, the flat-top of the eastern part of the Munida  
687 seamount is currently located in the photic zone which suggests continuous carbonate  
688 aggradation from the Miocene to the Quaternary. Such a continuous deposition was possibly  
689 favoured by a slower subsidence at that location compared to other seamounts (Fig.13). The  
690 Cryptelia seamount that is submerged at 194 m water depth is affected by three N160°E  
691 normal faults scarps, leading to an overall eastward deepening of the seamount topography  
692 along several stepped terraces at ca 200 m, 300 m and 350 m water depths (Fig.9A). The lack of  
693 samples on these stepped terraces does not allow us to determine if the carbonate factory was  
694 active during the Quaternary and when the isolated carbonate platform was drowned (Fig.13A).

695

## 696 6. CONCLUSIONS

697 The eastern margin of Grande Terre records the evolution of a shallow-water mixed  
698 carbonate-siliciclastic system, with the successive development an aggrading Mio-Pliocene  
699 carbonate bank and a backstepping Quaternary barrier reef.

700 - A Mio-Pliocene shallow-water carbonate platform, presently drowned at 300 to 600 m water  
701 depth, extends about 350 km from Ponerihouen to Antionia seamount and can be up to 750 m  
702 thick along the Pines Ridge.

703 - In front of Grande Terre, the Mio-Pliocene carbonate sediments are mixed with quartz grains  
704 and ultrabasic pebbles, which document terrigenous inputs resulting from high relief of the  
705 island topography dismantling coeval with carbonate production as early as the Serravalian.

706 - The transition between the aggrading Mio-Pliocene carbonate bank and the backstepping  
707 Quaternary carbonate platforms along the eastern margin could be explained by the regional  
708 subsidence context driven by an extensional tectonic regime or by global climate change  
709 associated with Late Quaternary high-amplitude sea-level variations and/or changes of  
710 carbonate producers through time.

711 - The stratigraphic architectures of mixed carbonate-siliciclastic systems, represented by the  
712 Quaternary reef-lagoon complex along the upper slope, vary widely from north to south. In front  
713 of the Cap Bayes Pass, this contribution evidences for the first time in New Caledonia the  
714 presence of a lowstand terrigenous prism alternating with transgressive shallow-water  
715 carbonate sequence, typical to reciprocal sedimentation models. Nevertheless, this configuration  
716 is not observed southward, probably because other control parameters prevailed such as low  
717 terrigenous inputs, the particular morphology of the paleo-drainage network, which appears  
718 parallel to the coastline, or the high by-pass sediment transport toward the deep basin.

719

## 720 7. ACKNOWLEDGEMENTS

721 We thank Editor M. Rebesco, reviewer John J.G. Reijmer and an anonymous reviewer for their  
722 constructive comments on an early version of this paper. We are also grateful to John Butcher  
723 (IRD Nouméa) who provided access to samples.

## 724 REFERENCES

- 725 Adams, C.G., 1984. Neogene larger foraminifera, evolutionary and geological events in the context of datum planes, in:  
726 Ikebe, N., Tsuchi, R. (Eds.), *Pacific Neogene Datum Planes*. Tokyo, pp. 47–67.
- 727 Adams, E., Kenter, J.A.M., 2013. So different, yet so similar: comparing and contrasting siliciclastic and carbonate  
728 slopes, in: Verwer, K., Playton, T.E., Harris, P.M. (Eds.), *Deposits, Architecture and Controls of Carbonate Margin,  
729 Slope and Basinal Settings*, SEPM Special Publication. Tulsa, Oklahoma, pp. 14–25.
- 730 Aguirre, J., Riding, R., Braga, J.C., 2000. Diversity of coralline red algae: origination and extinction patterns from the  
731 Early Cretaceous to the Pleistocene. *Paleobiology* 26, 651–667. [https://doi.org/10.1666/0094-  
732 8373\(2000\)026<0651:DOCRAO>2.0.CO;2](https://doi.org/10.1666/0094-8373(2000)026<0651:DOCRAO>2.0.CO;2)
- 733 Andréfouët, S., Cabioch, G., Flamand, B., Pelletier, B., 2009. A reappraisal of the diversity of geomorphological and  
734 genetic processes of New Caledonian coral reefs: a synthesis from optical remote sensing, coring and acoustic  
735 multibeam observations. *Coral Reefs* 28, 691–707. <https://doi.org/10.1007/s00338-009-0503-y>
- 736 Anselmetti, F.S., Eberli, G.P., 2001. Sonic Velocity in Carbonates— A Combined Product of Depositional Lithology and  
737 Diagenetic Alterations, in: Ginsburg, R.N. (Ed.), *Subsurface Geology of a Prograding Carbonate Platform Margin,  
738 Great Bahama Bank: Results of the Bahamas Drilling Project*. SEPM Society for Sedimentary Geology, p. 0.  
739 <https://doi.org/10.2110/pec.01.70.0193>
- 740 Belde, J., Back, S., Bourget, J., Reuning, L., 2017. Oligocene and Miocene carbonate platform development in the Browse  
741 basin, Australian northwest shelf. *Journal of Sedimentary Research* 87, 795–816.  
742 <https://doi.org/10.2110/jsr.2017.44>
- 743 Bitoun, G., Recy, J., 1982. Origine et évolution du bassin des Loyauté et de ses bordures après la mise en place de la  
744 série ophiolitique de Nouvelle Calédonie, in: *Contribution à l'étude Géodynamique Du Sud-Ouest Pacifique,*  
745 *Travaux et Documents ORSTOM*. pp. 505–540.
- 746 Boudagher-Fadel, M.K., 2018a. *Evolution and Geological Significance of Larger Benthic Foraminifera*, Second edition.  
747 ed. UCL Press.
- 748 Boudagher-Fadel, M.K., 2018b. Revised diagnostic first and last occurrences of Mesozoic and Cenozoic planktonic  
749 foraminifera. UCL Office of the Vice-Provost Research, Professional Papers Series, UCL Press 1–5.
- 750 Boudagher-Fadel, M.K., 2015. *Biostratigraphic and geological of planktonic foraminifera*, Updated second edition. ed.  
751 UCP Press.
- 752 Boudagher-Fadel, M.K., Banner, F.T., 1999. Revision of the stratigraphic significance of the oligocene-miocene “Letter-  
753 Stages.” *Revue de Micropaléontologie* 42, 93–97. [https://doi.org/10.1016/S0035-1598\(99\)90095-8](https://doi.org/10.1016/S0035-1598(99)90095-8)
- 754 Brachert, T.C., Forst, M.H., Pais, J.J., Legoinha, P., Reijmer, J.J.G., 2003. Lowstand carbonates, highstand sandstones?  
755 *Sedimentary Geology* 155, 1–12. [https://doi.org/10.1016/S0037-0738\(02\)00329-9](https://doi.org/10.1016/S0037-0738(02)00329-9)
- 756 Cabioch, G., Montaggioni, L., Frank, N., Seard, C., Sallé, E., Payri, C., Pelletier, B., Paterne, M., 2008a. Successive reef  
757 depositional events along the Marquesas foreslopes (French Polynesia) since 26 ka. *Marine Geology* 254, 18–34.  
758 <https://doi.org/10.1016/j.margeo.2008.04.014>

- 759 Cabioch, G., Montaggioni, L., Thouveny, N., Frank, N., Sato, T., Chazottes, V., Dalamasso, H., Payri, C., Pichon, M., Sémah,  
760 A.-M., 2008b. The chronology and structure of the western New Caledonian barrier reef tracts. *Palaeogeography,*  
761 *Palaeoclimatology, Palaeoecology* 268, 91–105. <https://doi.org/10.1016/j.palaeo.2008.07.014>
- 762 Cabioch, G., Pelletier, B., Boré, J.-M., Panché, J.-Y., Perrier, J., 2002a. Campagne Boisalis 1, Cartographie multifaisceaux et  
763 dragages des pentes du récif barrière Est (Poindimié) et Sud-Est (Goro) de Nouvelle-Calédonie. Transport et  
764 débarquement du matériel de forage sur l'îlot Bayes. (No. 44). Rapports de missions. Sciences de la Terre,  
765 Géologie Géophysique, Centre IRD de Nouméa.
- 766 Cabioch, G., Pelletier, B., Perrier, J., Régnier, M., Varillon, D., 2002b. Campagne Boisalis 2, cartographie multifaisceaux et  
767 dragages des pentes du récif barrière Sud-Est (Goro) et cartographie des passes de Mato et Boulari, Nouvelle-  
768 Calédonie. (No. 45). Rapports de missions. Sciences de la Terre, Géologie Géophysique, Centre IRD de Nouméa.
- 769 Cabioch, G., Recy, J., Jouannic, C., Turpin, L., 1996. Contrôle climatique et tectonique de l'édification récifale en  
770 Nouvelle-Calédonie au cours du Quaternaire terminal. *Bulletin de la Société Géologique de France* 167, 729–742.
- 771 Camoin, G.F., Seard, C., Deschamps, P., Webster, J.M., Abbey, E., Braga, J.C., Iryu, Y., Durand, N., Bard, E., Hamelin, B.,  
772 Yokoyama, Y., Thomas, A.L., Henderson, G.M., Dussouillez, P., 2012. Reef response to sea-level and environmental  
773 changes during the last deglaciation: Integrated Ocean Drilling Program Expedition 310, Tahiti Sea Level.  
774 *Geology* 40, 643–646. <https://doi.org/10.1130/G32057.1>
- 775 Chaisson, W.P., Ravelo, A.C., 1997. Changes in upper water-column structure at Site 925, late Miocene-  
776 Pleistocene: planktonic foraminifer assemblage and isotopic evidence, in: Shackleton, N.J., Curry, W.B., Richter, C.,  
777 Bralower, T.J. (Eds.), *Proceedings of the Ocean Drilling Program, Scientific Results, Ocean Drilling Program.*  
778 College Station, TX, pp. 255–268.
- 779 Chardon, D., Austin, J.A., Cabioch, G., Pelletier, B., Saustrup, S., 2007. NEOMARGES, Imagerie sismique du lagon et des  
780 pentes des marges de la ride de Nouvelle-Calédonie à travers le récif barrière de la Grande Terre, 12-21  
781 décembre 2006 (Rapport de missions, Sciences de la Terre, Géologie-Géophysique No. 72). IRD.  
782 <https://doi.org/10.17600/6100140>
- 783 Chardon, D., Austin, J.A., Cabioch, G., Pelletier, B., Saustrup, S., Sage, F., 2008. Neogene history of the northeastern New  
784 Caledonia continental margin from multichannel reflection seismic profiles. *Comptes Rendus Geoscience* 340,  
785 68–73. <https://doi.org/10.1016/j.crte.2007.09.017>
- 786 Chardon, D., Chevillotte, V., 2006. Morphotectonic evolution of the New Caledonia ridge (Pacific Southwest) from post-  
787 obduction tectonosedimentary record. *Tectonophysics* 420, 473–491.  
788 <https://doi.org/10.1016/j.tecto.2006.04.004>
- 789 Chevillon, C., 1997. Sédimentologie descriptive et cartographie des fonds meubles du lagon de la côte Est de Nouvelle-  
790 Calédonie, in: *Les Fonds Meubles Des Lagons de Nouvelle-Calédonie (Sédimentologie, Benthos)*, Etudes et  
791 Thèses, ORSTOM. pp. 7–30.
- 792 Chiarella, D., Longhitano, S.G., Tropeano, M., 2017. Types of mixing and heterogeneities in siliciclastic-carbonate  
793 sediments. *Marine and Petroleum Geology* 88, 617–627. <https://doi.org/10.1016/j.marpetgeo.2017.09.010>
- 794 Cluzel, D., Aitchison, J.C., Picard, C., 2001. Tectonic accretion and underplating of mafic terranes in the Late Eocene  
795 intraoceanic fore-arc of New Caledonia (Southwest Pacific): geodynamic implications. *Tectonophysics* 340, 23–  
796 59. [https://doi.org/10.1016/S0040-1951\(01\)00148-2](https://doi.org/10.1016/S0040-1951(01)00148-2)
- 797 Cluzel, D., Bosch, D., Paquette, J.-L., Lemennicier, Y., Montjoie, P., Ménot, R.-P., 2005. Late Oligocene post-obduction  
798 granitoids of New Caledonia: A case for reactivated subduction and slab break-off. *Island Arc* 14, 254–271.  
799 <https://doi.org/10.1111/j.1440-1738.2005.00470.x>
- 800 Cohen, K.M., Harper, D.A.T., Gibbard, P.L., 2017. ICS International Chronostratigraphic Chart 2017/02.
- 801 Collot, J., Patriat, M., Etienne, S., Rouillard, P., Soetaert, F., Juan, C., Marcaillou, B., Palazzin, G., Clerc, C., Maurizot, P.,  
802 Pattier, F., Tournadour, E., Sevin, B., Privat, A., 2017. Deepwater Fold-and-Thrust Belt Along New Caledonia's  
803 Western Margin: Relation to Post-obduction Vertical Motions. *Tectonics* 36, 2108–2122.  
804 <https://doi.org/10.1002/2017TC004542>

- 805 Collot, J.Y., Malahoff, A., Recy, J., Latham, G., Missegue, F., 1987. Overthrust emplacement of New Caledonia Ophiolite:  
806 Geophysical evidence. *Tectonics* 6, 215–232. <https://doi.org/10.1029/TC006i003p00215>
- 807 Cotillon, P., Coustillas, F., Gaillard, C., Laurin, B., Liu, D.-J., Pannetier, W., Rigolot, P., Pascal, A., Pascal, F., 1990. Grands  
808 traits de la sédimentation actuelle et récente sur les pentes et dans les bassins au large de la Nouvelle Calédonie  
809 (SW Pacifique): Résultats géologiques de la campagne Biocal Cotillon P, Coustillas F, Gaillard C, Laurin B, Liu D-J,  
810 Pannetier W, Rigolot P, Pascal A, Pascal F. *Oceanologica Acta*, Special issue (0399-1784) Actes du Colloque Tour  
811 du monde Jean Charcot, Paris (France), 2-3 Mar 1989.
- 812 Cotillon, P., Liu, J.D., Gaillard, C., Evin, J., 1989. Evolution du taux de sédimentation au cours des derniers 30 000 ans  
813 aux abords de la Nouvelle-Calédonie (SW Pacifique); résultats de datations au radiocarbone et par la courbe de  
814 l'oxygène 18. *Bulletin de la Société Géologique de France* V, 881–884. <https://doi.org/10.2113/gssgfbull.V.4.881>
- 815 Coudray, J., 1976. Recherches sur le Néogène et le Quaternaire marins de la Nouvelle-Calédonie; contribution de  
816 l'étude sédimentologique à la connaissance de l'histoire géologique post-Eocène, in: Expédition Française Sur  
817 Les Récifs Nouvelle-Calédonie, Fond. Singer-Polignac. Paris, pp. 1–276.
- 818 Coudray, J., 1975. Recherches sur le Néogène et le Quaternaire marin de la Nouvelle-Calédonie. Contribution de l'étude  
819 sédimentologique à la connaissance de l'histoire géologique post-éocène (Thèse de Doctorat). Université des  
820 Sciences et Techniques du Languedoc.
- 821 Daniel, J., Dugas, F., Dupont, J., Jouannic, C., Launay, J., Monzier, M., Recy, J., 1976. La zone charnière Nouvelle-Calédonie  
822 - ride de Norfolk (S.W. Pacifique) : résultats de dragages et interprétation. *Cahiers ORSTOM série Géologie* 8, 95–  
823 105.
- 824 Droxler, A.W., Jorry, S.J., 2013. Deglacial Origin of Barrier Reefs Along Low-Latitude Mixed Siliciclastic and Carbonate  
825 Continental Shelf Edges. *Annu. Rev. Mar. Sci.* 5, 165–190. <https://doi.org/10.1146/annurev-marine-121211-172234>
- 827 Dubois, J., Launay, J., Recy, J., 1975. Some new evidence on lithospheric bulges close to island arcs. *Tectonophysics* 26,  
828 189–196. [https://doi.org/10.1016/0040-1951\(75\)90089-X](https://doi.org/10.1016/0040-1951(75)90089-X)
- 829 Dubois, J., Launay, J., Recy, J., 1974. Uplift movements in New Caledonia-Loyalty Islands area and their plate tectonics  
830 interpretation. *Tectonophysics* 24, 133–150. [https://doi.org/10.1016/0040-1951\(74\)90134-6](https://doi.org/10.1016/0040-1951(74)90134-6)
- 831 Dunbar, G.B., Dickens, G.R., 2003. Massive siliciclastic discharge to slopes of the Great Barrier Reef Platform during sea-  
832 level transgression: constraints from sediment cores between 15°S and 16°S latitude and possible explanations.  
833 *Sediment. Geol.* 162, 141–158. [https://doi.org/10.1016/S0037-0738\(03\)00216-1](https://doi.org/10.1016/S0037-0738(03)00216-1)
- 834 Ehrenberg, S.N., McArthur, J.M., Thirlwall, M.F., 2006. Growth, Demise, and Dolomitization of Miocene Carbonate  
835 Platforms on the Marion Plateau, Offshore NE Australia. *Journal of Sedimentary Research* 76, 91–116.  
836 <https://doi.org/10.2110/jsr.2006.06>
- 837 Esker, D.E., Eberli, G.P., McNeill, D.F., 1998. The Structural and Sedimentological Controls on the Reoccupation of  
838 Quaternary Incised Valleys, Belize Southern Lagoon. *AAPG Bull.* 82, 2075–2109.  
839 <https://doi.org/10.1306/00AA7BE4-1730-11D7-8645000102C1865D>
- 840 Ferro, C.E., Droxler, A.W., Anderson, J.B., Mucciarone, D., 1999. Late Quaternary shift of mixed siliciclastic-carbonate  
841 environments induced by glacial eustatic sea-level fluctuations in Belize. In: *Advances in carbonate sequence*  
842 *stratigraphy: Application to reservoirs, outcrops and models* (Eds P.M. Harris, A.H. Saller and T. Simo), SEPM  
843 Special Publication v. 63, pp. 385–411. SEPM (Society for Sedimentary Geology), Tulsa.
- 844 Flamand, B., 2006. Les pentes externes du récif barrière de la Grande Terre de Nouvelle-Calédonie : morphologie,  
845 lithologie, contrôle de la tectonique et de l'eustatisme. Université de Bretagne occidentale, Brest, France.
- 846 Frank, N., Turpin, L., Cabioch, G., Blamart, D., Tressens-Fedou, M., Colin, C., Jean-Baptiste, P., 2006. Open system U-  
847 series ages of corals from a subsiding reef in New Caledonia: Implications for sea level changes, and subsidence  
848 rate. *Earth and Planetary Science Letters* 249, 274–289. <https://doi.org/10.1016/j.epsl.2006.07.029>
- 849 Fürstenau, J., Lindhorst, S., Betzler, C., Hübscher, C., 2010. Submerged reef terraces of the Maldives (Indian Ocean).  
850 *Geo-Mar Lett* 30, 511–515. <https://doi.org/10.1007/s00367-009-0174-2>

- 851 Gaina, C., Müller, D.R., Royer, J.-Y., Stock, J., Hardebeck, J., Symonds, P., 1998. The tectonic history of the Tasman Sea: A  
852 puzzle with 13 pieces. *Journal of Geophysical Research: Solid Earth* 103, 12413–12433.  
853 <https://doi.org/10.1029/98JB00386>
- 854 Geldart, L.P., Sheriff, R.E., 2004. *Problems in Exploration Seismology and their Solutions*. Society of Exploration  
855 Geophysicists. <https://doi.org/10.1190/1.9781560801733>
- 856 Gischler, E., Ginsburg, R.N., Herrle, J.O., Prasad, S., 2010. Mixed carbonates and siliciclastics in the Quaternary of  
857 southern Belize: Pleistocene turning points in reef development controlled by sea-level change. *Sedimentology*  
858 57, 1049–1068. <https://doi.org/10.1111/j.1365-3091.2009.01133.x>
- 859 Gradstein, F.M., Ogg, J.G., Schmitz, M.D., Ogg, G.M. (Eds.), *The Geologic Time Scale*. Elsevier, Boston, pp. ix–xi.  
860 <https://doi.org/10.1016/B978-0-444-59425-9.10003-4>
- 861 Hallock, P., Schlager, W., 1986. Nutrient Excess and the Demise of Coral Reefs and Carbonate Platforms. *PALAIOS* 1,  
862 389. <https://doi.org/10.2307/3514476>
- 863 Harper, B.B., Puga-Bernabéu, Á., Droxler, A.W., Webster, J.M., Gischler, E., Tiwari, M., Lado-Insua, T., Thomas, A.L.,  
864 Morgan, S., Jovane, L., Röhl, U., 2015. Mixed Carbonate–Siliciclastic Sedimentation Along the Great Barrier Reef  
865 Upper Slope: A Challenge To the Reciprocal Sedimentation Model. *Journal of Sedimentary Research* 85, 1019–  
866 1036. <https://doi.org/10.2110/jsr.2015.58.1>
- 867 Hayes, D.E., Ringis, J., 1973. Seafloor Spreading in the Tasman Sea. *Nature* 243, 454–458.  
868 <https://doi.org/10.1038/243454a0>
- 869 Hohenegger, J., 2005. Estimation of environmental paleogradient values based on presence/absence data: a case study  
870 using benthic foraminifera for paleodepth estimation. *Palaeogeogr. Palaeoclimatol. Palaeoecol.* 217, 115–130.  
871 <https://doi.org/10.1016/j.palaeo.2004.11.020>
- 872 Hohenegger, J., 1995. Depth estimation by proportions of living larger foraminifera. *Mar. Micropal.* 26, 31–47.  
873 [https://doi.org/10.1016/0377-8398\(95\)00044-5](https://doi.org/10.1016/0377-8398(95)00044-5)
- 874 Hottinger, L., 1983. Processes determining the distribution of larger foraminifera in space and time. *Utrecht Micropal.*  
875 *Bull.* 30, 239–253.
- 876 Jorry, S.J., Camoin, G.F., Jouet, G., Roy, P.L., Vella, C., Courgeon, S., Prat, S., Fontanier, C., Paumard, V., Boule, J., Caline, B.,  
877 Borgomano, J., 2016. Modern sediments and Pleistocene reefs from isolated carbonate platforms (Iles Eparses,  
878 SW Indian Ocean): A preliminary study. *Acta Oecologica* 72, 129–143.  
879 <https://doi.org/10.1016/j.actao.2015.10.014>
- 880 Juffroy, F., 2009. *Atlas bathymétrique de la Nouvelle-Calédonie*. Rapport du Service de la Géomatique et de la  
881 Télédétection du Gouvernement de la Nouvelle-Calédonie.
- 882 Kerans, C., Tinker, S.W., 1999. Extrinsic Stratigraphic Controls on Development of the Capitan Reef Complex, in: Saller,  
883 A.H., Harris, P.M. (Mitch), Kirkland, B.L., Mazzullo, S.J. (Eds.), *Geologic Framework of the Capitan Reef*. SEPM  
884 Society for Sedimentary Geology, p. 0.
- 885 Khanna, P., Droxler, A.W., Nittrouer, J.A., Tunnell Jr, J.W., Shirley, T.C., 2017. Coralgall reef morphology records  
886 punctuated sea-level rise during the last deglaciation. *Nature Communications* 8, 1046.  
887 <https://doi.org/10.1038/s41467-017-00966-x>
- 888 Lafoy, Y., Missègue, F., Cluzel, D., Voisset, M., Saget, P., Lenoble, J.-P., Rigaut, F., Lanckneus, J., Lehodey, P., Bouniot, E.,  
889 Cornec, J., De Souza, K., Gallois, F., Garioud, N., Grenard, P., N'Diaye, M., Perchoc, Y., Perrier, J., 1994. Campagne  
890 ZoNéCo 2 (2 au 22 août 1994), RV L'Atalante.
- 891 Lafoy, Y., Van de Beuque, S., Missègue, F., Necessian, A., Bernardel, G., 1998. Campagne de sismique multitraces entre  
892 la marge Est Australienne et le Sud de l'Arc des Nouvelles-Hébrides Rapport de la campagne RIG SEISMIC 206  
893 (21 avril - 24 mai 1998), Programme FAUST (French Australian Seismic Transect). Programme ZoNéCo.
- 894 Lagabrielle, Y., Chauvet, A., 2008. The role of extensional tectonics in shaping Cenozoic New-Caledonia. *Bulletin de la*  
895 *Société Géologique de France* 179, 315–329. <https://doi.org/10.2113/gssgfbull.179.3.315>

- 896 Lagabrielle, Y., Maurizot, P., Lafoy, Y., Cabioch, G., Pelletier, B., Régnier, M., Wabete, I., Calmant, S., 2005. Post-Eocene  
897 extensional tectonics in Southern New Caledonia (SW Pacific): Insights from onshore fault analysis and offshore  
898 seismic data. *Tectonophysics* 403, 1–28. <https://doi.org/10.1016/j.tecto.2005.02.014>
- 899 Launay, J., 1985. Paléoniveaux marins et néotectonique à l'île des Pins (Nouvelle -Calédonie). *Géologie de la France* 1,  
900 77–81.
- 901 Le Roy, P., Cabioch, G., Monod, B., Lagabrielle, Y., Pelletier, B., Flamand, B., 2008. Late Quaternary history of the Nouméa  
902 lagoon (New Caledonia, South West Pacific) as depicted by seismic stratigraphy and multibeam bathymetry: A  
903 modern model of tropical rimmed shelf. *Palaeogeography, Palaeoclimatology, Palaeoecology* 270, 29–45.  
904 <https://doi.org/10.1016/j.palaeo.2008.08.012>
- 905 Le Roy, P., Jorry, S., Jouet, G., Ehrhold, A., Michel, G., Gautier, V., Guérin, C., 2019. Late Pleistocene evolution of the mixed  
906 siliciclastic and carbonate southwestern New Caledonia continental shelf/lagoon. *Palaeogeography, Palaeoclimatology, Palaeoecology* 514, 502–521. <https://doi.org/10.1016/j.palaeo.2018.10.014>
- 908 Mallarino, G., Francis, J.M., Jorry, S.J., Daniell, J.J., Droxler, A.W., Dickens, G.R., Beaufort, L., Bentley, S.J., Opdyke, B.N.,  
909 Peterson, L.C., 2021. Timescale dependent sedimentary record during the past 130 kyr from a tropical mixed  
910 siliciclastic–carbonate shelf edge and slope: Ashmore Trough (southern Gulf of Papua). *Sedimentology*  
911 *sed.12867*. <https://doi.org/10.1111/sed.12867>
- 912 Maurizot, P., Cabioch, G., Fournier, F., Leonide, P., Sebih, S., Rouillard, P., Montaggioni, L., Collot, J., Martin-Garin, B.,  
913 Chaproniere, G., Braga, J.C., Sevin, B., 2016. Post-obduction carbonate system development in New Caledonia  
914 (Népoui, Lower Miocene). *Sedimentary Geology* 331, 42–62. <https://doi.org/10.1016/j.sedgeo.2015.11.003>
- 915 Maurizot, P., Collot, J., Cluzel, D., Patriat, M., 2020. Chapter 6 The Loyalty Islands and Ridge, New Caledonia.  
916 Geological Society, London, *Memoirs* 51, 131. <https://doi.org/10.1144/M51-2017-24>
- 917 Maurizot, P., Vendé-Leclerc, M., 2009. New Caledonia geological map, scale 1/500000. Direction de l'Industrie, des  
918 Mines et de l'Energie-Service de la Géologie de Nouvelle-Calédonie, Bureau de Recherches Géologiques et  
919 Minières.
- 920 McCaffrey, J.C., Wallace, M.W., Gallagher, S.J., 2020. A Cenozoic Great Barrier Reef on Australia's North West shelf.  
921 *Global and Planetary Change* 184, 103048. <https://doi.org/10.1016/j.gloplacha.2019.103048>
- 922 McKee, E.D., Oriol, S.S., Ketner, K.B., MacLachlan, M.E., Goldsmith, J.W., MacLachlan, J.C., Mudge, M.R., 1959.  
923 Paleotectonic maps of the Triassic System. *Miscellaneous Geologic Investigations Map*.
- 924 McKenzie, J.A., Spezzaferri, S., Isern, A., 1999. The Miocene-Pliocene boundary in the Mediterranean Sea and Bahamas;  
925 implications for a global flooding event in the earliest Pliocene. *Memorie della Società Geologica Italiana* 54, 93– 926  
108.
- 927 McNeill, D.F., Pisera, A., 2010. Neogene Lithofacies Evolution on a Small Carbonate Platform in the Loyalty Basin, Mare,  
928 New Caledonia, in: Morgan, W.A., George, A.D., Harris, P.M. (Mitch), Kupecz, J.A., Sarg, J.F. (Rick) (Eds.), *Cenozoic*  
929 *Carbonate Systems of Australasia*. SEPM Society for Sedimentary Geology, p. 0.
- 930 Missègue, F., Saget, P., Desrus, M., Le Suavé, R., Lafoy, Y., 1996. Mission ZoNéCo 3 (30 Aout au 20 Septembre 1996), RV  
931 L'Atalante. <https://doi.org/10.17600/96010070>
- 932 Mitchell, J.K., Holdgate, G.R., Wallace, M.W., Gallagher, S.J., 2007. Marine geology of the Quaternary Bass Canyon system,  
933 southeast Australia: A cool-water carbonate system. *Mar. Geol.* 237, 71–96.  
934 <https://doi.org/10.1016/j.margeo.2006.10.037>
- 935 Mitchum, R.M., Vail, P.R., Sangree, J.B., 1977. Seismic stratigraphy and global changes of sea-level, part 6: stratigraphic  
936 interpretation of seismic reflection patterns in depositional sequences, part 6, in: Payton, C.E. (Ed.), *Seismic*  
937 *Stratigraphy: Applications to Hydrocarbon Exploration*, AAPG Memoir. pp. 117–133.
- 938 Montaggioni, L.F., Cabioch, G., Thouveny, N., Frank, N., Sato, T., Sémah, A.-M., 2011. Revisiting the Quaternary  
939 development history of the western New Caledonian shelf system: From ramp to barrier reef. *Marine Geology*  
940 280, 57–75. <https://doi.org/10.1016/j.margeo.2010.12.001>
- 941 Moretti, I., Turcotte, D.L., 1985. A model for erosion, sedimentation, and flexure with application to New Caledonia.  
942 *Journal of Geodynamics* 3, 155–168. [https://doi.org/10.1016/0264-3707\(85\)90026-2](https://doi.org/10.1016/0264-3707(85)90026-2)

- 943 Mortimer, N., Campbell, H., Tulloch, A.J., King, P.R., Stagpoole, V.M., Wood, R.A., Rattenbury, M.S., Sutherland, R., Adams,  
944 C.J., Collot, J., Seton, M., 2017. Zealandia: Earth's Hidden Continent. *The Geological Society of America* 27, 27–35.
- 945 Nebelsick, J.H., Stingl, V., Rasser, M., 2001. Autochthonous facies and allochthonous debris flows compared: Early  
946 oligocene carbonate facies patterns of the Lower Inn Valley (Tyrol, Austria). *Facies* 44, 31.  
947 <https://doi.org/10.1007/BF02668165>
- 948 O'Connell, B., Dorsey, R.J., Hasiotis, S.T., Hood, A.V.S., 2021. Mixed carbonate–siliciclastic tidal sedimentation in the  
949 Miocene to Pliocene Bouse Formation, palaeo-Gulf of California. *Sedimentology* 68, 1028–1068.  
950 <https://doi.org/10.1111/sed.12817>
- 951 Paquette, J.-L., Cluzel, D., 2007. U–Pb zircon dating of post-obduction volcanic-arc granitoids and a granulite-facies  
952 xenolith from New Caledonia. Inference on Southwest Pacific geodynamic models. *International Journal of Earth  
953 Sciences* 96, 613–622. <https://doi.org/10.1007/s00531-006-0127-1>
- 954 Paris, J.P., 1981. Géologie de la Nouvelle-Calédonie, Un essai de synthèse, Mémoire du BRGM. Orléans, France.
- 955 Patriat, M., Collot, J., Etienne, S., Poli, S., Clerc, C., Mortimer, N., Pattier, F., Juan, C., Roest, W.R., VESPA scientific voyage  
956 team, 2018. New Caledonia Obducted Peridotite Nappe: Offshore Extent and Implications for Obduction and  
957 Postobduction Processes. *Tectonics* 37, 1077–1096. <https://doi.org/10.1002/2017TC004722>
- 958 Pautot, G., Lafoy, Y., Dupont, J., Le Suavé, R., 1993. Campagne ZoNéCo 1 (25 juin au 16 juillet 1993), RV L'Atalante.  
959 <https://doi.org/10.17600/93000130>
- 960 Pelletier, B., Butscher, J., Panché, J.-Y., Perrier, J., Maloune, A., 2002. Cartographie au sondeur multifaisceaux des pentes  
961 externes du récif barrière de la Province Nord de la Nouvelle-Calédonie. Campagne Province Nord 1, côte Est de  
962 la passe de Thio à la passe de Balade (24 juillet au 1er août 2002). (No. 48). Rapports de missions, Sciences de la  
963 Terre, Géologie-Géophysique, Centre IRD Nouméa.
- 964 Pelletier, B., Cabioch, G., Chardon, D., Yamano, H., 2006. Lithologie des pentes externes du récif barrière de Nouvelle-  
965 Calédonie. Campagne de dragages « 2005-NC-DR » du N.O. Alis (30 mai – 7 juin 2005). (No. 68). Rapports de  
966 missions, Sciences de la Terre, Géologie Géophysique, Centre IRD de Nouméa.
- 967 Pelletier, B., Juffroy, F., Flamand, B., Perrier, J., 2012. La bathymétrie des marges de la Grande Terre et des îles Loyauté.  
968 Planche 5, in: Bonvallet, J., Gay, J.C., Habert, E. (Eds.), Atlas de La Nouvelle Calédonie. Nouméa : IRD ; Congrès de  
969 la Nouvelle-Calédonie, Marseille (FRA), pp. 33–36.
- 970 Pelletier, B., Perrier, J., Juffroy, F., Flamand, B., Panché, J.-Y., Gallois, F., 2004. Cartographie systématique par sondeur  
971 multifaisceaux des pentes externes du récif barrière de la Grande Terre et des îles Loyauté, Nouvelle-Calédonie.  
972 Assises de la Recherche Française dans le Pacifique, 24-27 août 2004, Nouméa, Nouvelle-Calédonie. Résumés  
973 des communications scientifiques, p.271-272. Poster. Presented at the Assises de la Recherche Française dans le  
974 Pacifique, 24-27 août 2004, Nouméa, Nouvelle-Calédonie.
- 975 Perrier, J., Flamand, B., Juffroy, F., Panché, J.-Y., Le Houarno, H., 2004a. Cartographie au sondeur multifaisceaux de la  
976 zone côtière de la Province Sud. Campagne Province Sud 1, N.O. Alis (2-5 février et 11-20 février 2004). (No. 62).  
977 Rapports de missions, Sciences de la Terre, Géologie-Géophysique, Centre IRD Nouméa.
- 978 Perrier, J., Flamand, B., Robineau, B., Panché, J.-Y., Le Houarno, H., 2004b. Cartographie au sondeur multifaisceaux de la  
979 zone côtière de la Province Sud, Campagne Province Sud 2. N.O. Alis du 23 septembre au 2 octobre 2004. Côte  
980 Ouest: de la passe de Boulari à la passe Koko; Sud: Corne Sud. (No. 63), Rapports de missions, Sciences de la  
981 Terre, Géologie-Géophysique, Centre IRD de Nouméa.
- 982 Perrier, J., Panché, J.-Y., Juffroy, F., Barazer, J.-F., 2005. Cartographie au sondeur multifaisceaux de la zone côtière de la  
983 Province Sud. Campagne Province Sud 4, NO Alis. 21 au 24 septembre 2005. Hauts fonds à l'extrémité sud de la  
984 Grande Terre : Banc 93, Banc Antigonina, Mont 1 (No. 65). Rapports de missions Sciences de la Terre. Géologie  
985 Géophysique, Centre IRD de Nouméa.
- 986 Perrier, J., Pelletier, B., Panché, J.-Y., Barazer, J.-F., Juffroy, F., 2004c. Cartographie au sondeur multifaisceaux de la zone  
987 côtière de la Province Sud. Campagne Province Sud 3, N.O. Alis du 26 novembre au 30 novembre 2004. Côte Sud  
988 Est : de la passe de la Sarcelle à la terminaison sud de l'île des Pins (banc de la Torche). (No. 64). Rapports de  
989 missions, Sciences de la Terre, Géologie-Géophysique, Centre IRD de Nouméa.

- 990 Puillandre, N., Samadi, S., 2016. Kanacono cruise, RV Alis,. <https://doi.org/10.17600/16003900>
- 991 Purdy, E.G., Gischler, E., 2005. The transient nature of the empty bucket model of reef sedimentation. *Sedimentary*  
992 *Geology* 175, 35–47. <https://doi.org/10.1016/j.sedgeo.2005.01.007>
- 993 Rigolot, P., 1989. Origine et évolution du “système” ride de Nouvelle-Calédonie/Norfolk (Sud -Ouest Pacifique) :  
994 synthèse des données de géologie et de géophysique marine. Etude des marges et bassins associés. UBO, Brest.
- 995 Rovere, A., Khanna, P., Bianchi, C.N., Droxler, A.W., Morri, C., Naar, D.F., 2018. Submerged reef terraces in the Maldivian  
996 Archipelago (Indian Ocean). *Geomorphology* 317, 218–232. <https://doi.org/10.1016/j.geomorph.2018.05.026>
- 997 Schlager, W., 1989. Drowning Unconformities on Carbonate Platforms, in: *Controls on Carbonate Platforms and Basin*  
998 *Development*, SEPM SPECIAL PUBLICATION.
- 999 Sevin, B., Maurizot, P., Cluzel, D., Tournadour, E., Etienne, S., Folcher, N., Jeanpert, J., Collot, J., Iseppi, M., Meffre, S.,  
1000 Patriat, M., 2020. Chapter 7 Post-obduction evolution of New Caledonia. Geological Society, London, *Memoirs*  
1001 51, 147. <https://doi.org/10.1144/M51-2018-74>
- 1002 Smith, W.H.F., Sandwell, D.T., 1997. Global Sea Floor Topography from Satellite Altimetry and Ship Depth Soundings.  
1003 *Science* 277, 1956. <https://doi.org/10.1126/science.277.5334.1956>
- 1004 Sutherland, R., Viskovic, G.P.D., Bache, F., Stagpoole, V.M., Collot, J., Rouillard, P., Hashimoto, T., Hackney, R., Rollet, N.,  
1005 Patriat, M., Roest, W.R., 2012. Compilation of seismic reflection data from the Tasman Frontier region, southwest  
1006 Pacific (GNS Science Report No. 2012/01).
- 1007 Tcherepanov, E.N., Droxler, A.W., Lapointe, P., Dickens, G.R., Bentley, S.J., Beaufort, L., Peterson, L.C., Daniell, J., Opdyke,  
1008 B.N., 2008a. Neogene evolution of the mixed carbonate-siliciclastic system in the Gulf of Papua, Papua New  
1009 Guinea. *J. Geophys. Res.* 113, F01S21. <https://doi.org/10.1029/2006JF000684>
- 1010 Tcherepanov, E.N., Droxler, A.W., Lapointe, P., Mohn, K., 2008b. Carbonate seismic stratigraphy of the Gulf of Papua  
1011 mixed depositional system: Neogene stratigraphic signature and eustatic control. *Basin Res.* 20, 185–209.  
1012 <https://doi.org/10.1111/j.1365-2117.2008.00364.x>
- 1013 Tcherepanov, E.N., Droxler, A.W., Lapointe, P., Mohn, K., Larsen, O.A., 2010. Siliciclastic influx and burial of the Cenozoic  
1014 carbonate system in the Gulf of Papua. *Marine and Petroleum Geology* 27, 533–554.  
1015 <https://doi.org/10.1016/j.marpetgeo.2009.09.002>
- 1016 Teillet, T., Fournier, F., Borgomano, J., Hong, F., 2020a. Origin of seismic reflections in a carbonate gas field, Lower  
1017 Miocene, offshore Myanmar. *Marine and Petroleum Geology* 113, 104110.  
1018 <https://doi.org/10.1016/j.marpetgeo.2019.104110>
- 1019 Teillet, T., Fournier, F., Montaggioni, L.F., BouDagher-Fadel, M., Borgomano, J., Braga, J.C., Villeneuve, Q., Hong, F.,  
1020 2020b. Development patterns of an isolated oligo-mesophotic carbonate buildup, early Miocene, Yadana field,  
1021 offshore Myanmar. *Marine and Petroleum Geology* 111, 440–460.  
1022 <https://doi.org/10.1016/j.marpetgeo.2019.08.039>
- 1023 Terry, J.P., Wotling, G., 2011. Rain-shadow hydrology: Influences on river flows and flood magnitudes across the  
1024 central massif divide of La Grande Terre Island, New Caledonia. *Journal of Hydrology* 404, 77–86.  
1025 <https://doi.org/10.1016/j.jhydrol.2011.04.022>
- 1026 Toomey, M.R., Woodruff, J.D., Donnelly, J.P., Ashton, A.D., Perron, J.T., 2016. Seismic evidence of glacial-age river  
1027 incision into the Tahaa barrier reef, French Polynesia. *Marine Geology* 380, 284–289.  
1028 <https://doi.org/10.1016/j.margeo.2016.04.008>
- 1029 Tournadour, E., Fournier, F., Etienne, S., Collot, J., Maurizot, P., Patriat, M., Sevin, B., Morgans, H.E.G., Martin-Garin, B.,  
1030 Braga, J.C., 2020. Seagrass-related carbonate ramp development at the front of a fan delta (Burdigalian, New  
1031 Caledonia): Insights into mixed carbonate-siliciclastic environments. *Marine and Petroleum Geology* 121,  
1032 104581. <https://doi.org/10.1016/j.marpetgeo.2020.104581>
- 1033 Wallace, M.W., Holdgat, G.R., Daniels, J., Gallagher, S.J., Smith, A., 2002. Sonic velocity, submarine canyons, and burial  
1034 diagenesis in Oligocene-Holocene cool-water carbonates, Gippsland Basin, southeast Australia. *AAPG Bull.* 86,  
1035 1593–1607. <https://doi.org/10.1306/61EEDD14-173E-11D7-8645000102C1865D>

- 1036 Webster, J.M., Braga, J.C., Humblet, M., Potts, D.C., Iryu, Y., Yokoyama, Y., Fujita, K., Bourillot, R., Esat, T.M., Fallon, S.,  
1037 Thompson, W.G., Thomas, A.L., Kan, H., McGregor, H.V., Hinestrosa, G., Obrochta, S.P., Lougheed, B.C., 2018.  
1038 Response of the Great Barrier Reef to sea-level and environmental changes over the past 30,000 years. *Nature*  
1039 *Geoscience* 11, 426–432. <https://doi.org/10.1038/s41561-018-0127-3>
- 1040 Weij, R., Reijmer, J.J.G., Eberli, G.P., Swart, P.K., 2019. The limited link between accommodation space, sediment  
1041 thickness, and inner platform facies distribution (Holocene–Pleistocene, Bahamas). *The Depositional Record* 5,  
1042 400–420. <https://doi.org/10.1002/dep2.50>
- 1043 Wilson, J.L., 1967. Cyclic and Reciprocal Sedimentation in Virgilian Strata of Southern New Mexico. *GSA Bulletin* 78,  
1044 805–818. [https://doi.org/10.1130/0016-7606\(1967\)78\[805:CARSIV\]2.0.CO;2](https://doi.org/10.1130/0016-7606(1967)78[805:CARSIV]2.0.CO;2)
- 1045 Wilson, P.A., Roberts, H.H., 1995. Density cascading; off-shelf sediment transport, evidence and implications, Bahama  
1046 Banks. *Journal of Sedimentary Research* 65, 45–56. [https://doi.org/10.1306/D426801D-2B26-11D7-  
1047 8648000102C1865D](https://doi.org/10.1306/D426801D-2B26-11D7-8648000102C1865D)
- 1048 Wilson, P.A., Roberts, H.H., 1992. Carbonate-periplatform sedimentation by density flows: A mechanism for rapid off-  
1049 bank and vertical transport of shallow-water fines. *Geology* 20, 713–716. [https://doi.org/10.1130/0091-  
1050 7613\(1992\)020<0713:CPSBDF>2.3.CO;2](https://doi.org/10.1130/0091-7613(1992)020<0713:CPSBDF>2.3.CO;2)
- 1051 Yamano, H., Cabioch, G., Pelletier, B., Chevillon, C., Tachikawa, H., Lefèvre, J., Marchesiello, P., 2015. Modern carbonate  
1052 sedimentary facies on the outer shelf and slope around New Caledonia. *Island Arc* 24, 4–15.  
1053 <https://doi.org/10.1111/iar.12085>
- 1054 Yordanova, E.K., Hohenegger, J., 2007. Studies on settling, traction and entrainment of larger benthic foraminiferal  
1055 tests: implications for accumulation in shallow marine sediments. *Sedimentology* 54, 1273–1306.  
1056 <https://doi.org/10.1111/j.1365-3091.2007.00881.x>
- 1057 Yordanova, E.K., Hohenegger, J., 2002. Taphonomy of larger foraminifera: Relationships between living individuals and  
1058 empty tests on flat reef slopes (Sesoko Island, Japan). *Facies* 46, 169–203. <https://doi.org/10.1007/BF02668080>
- 1059 Zeller, M., Verwer, K., Eberli, G.P., Massaferrro, J.L., Schwarz, E., Spalletti, L., 2015. Depositional controls on mixed  
1060 carbonate–siliciclastic cycles and sequences on gently inclined shelf profiles. *Sedimentology* 62, 2009–2037.  
1061 <https://doi.org/10.1111/sed.12215>
- 1062 Zinke, J., Reijmer, J.J.G., Thomassin, B.A., 2001. Seismic architecture and sediment distribution within the Holocene  
1063 barrier reef–lagoon complex of Mayotte (Comoro archipelago, SW Indian Ocean). *Palaeogeography,*  
1064 *Palaeoclimatology, Palaeoecology* 175, 343–368. [https://doi.org/10.1016/S0031-0182\(01\)00379-0](https://doi.org/10.1016/S0031-0182(01)00379-0)
- 1065
- 1066

1067 **FIGURE AND TABLE CAPTIONS**

1068

1069 **Figure 1:** **A.** Regional location map of the study area. **B.** Simplified geological map of Grande  
1070 Terre, New Caledonia (modified after Maurizot and Vendé-Leclerc, 2009) and shaded  
1071 bathymetric map of surrounding offshore areas with the southern extensions of the Peridotite  
1072 Nappe and metamorphic belt (Pines and Félicité ridges, respectively; after Patriat et al., 2018).  
1073 Drill sites of the Quaternary barrier reef (Coudray, 1975; Cabioch et al., 2008; Montaggioni et al.,  
1074 2011) and outcrops of the Lower Miocene mixed carbonate siliciclastic systems of Népoui are  
1075 also indicated (Maurizot et al., 2016 ; Tournadour et al., 2020). **C.** Simplified SW to NE oriented  
1076 geological cross-section of Grande Terre (modified after Lagabrielle et al., 2005 and Collot et al.,  
1077 1987). N: Nouméa ; Pn: Ponérihouen ; Th: Thio ; Yt: Yaté ; IP: Isle of Pines ; T : Banc de la Torche ;  
1078 S : Stylaster seamount ; B : Brachiopod seamount ; A : Antigonie seamount ; C : Crypthelia  
1079 seamount ; M : Munida seamount.

1080 **Figure 2:** Bathymetric map of the eastern margin of Grande Terre, from Poindimié to the Pines  
1081 Ridge with location of the dataset used in this study including seismic profiles AUS-104 (Bitoun  
1082 & Recy, 1982), 206-04 (dashed black lines), NEOMARGES (Chardon, 2006; Chardon et al. 2008,  
1083 black lines), and dredged carbonate samples (yellow circles). T : Banc de la Torche ; S : Stylaster  
1084 seamount ; B : Brachiopod seamount ; A : Antigonie seamount ; C : Crypthelia seamount ; M :  
1085 Munida seamount.

1086 **Figure 3:** **A.** Bathymetric map of the eastern lagoon of Grande Terre from Ponérihouen to Yaté.  
1087 On the outer slope, note the terrace mapped in orange between 300 to 600 m water depths. **B.**  
1088 Bathymetrical profile across the lagoon from the coast of Houailou to the outer barrier reef (see  
1089 location on Figure A) showing three main morphobathymetric zones: 1) a shallow-water coastal  
1090 zone dominated by fine-grained terrigenous sediments; 2) a deeper median lagoon with aligned  
1091 islands and a coast-parallel channel network in front of Cote Oubliée; 3) a barrier reef domain  
1092 cross-cut by passes, dominated by coarse-grained carbonate sedimentation. D: Deltas; D\*:

1093 Restricted deltas; SI: Sandy Islets; PR: Patch Reefs. Red lines are positions of seismic profiles.  
1094 Yellow circles are positions of dredged carbonate samples.

1095 **Figure 4:** Typical bathymetric profiles of the outer slopes of Grande Terre (location on [Fig.2](#))  
1096 highlighting the very steep character of the western margin (dashed green lines; W-01 and W-  
1097 02) contrasting with the more gently inclined eastern margin (solid blue lines; E-01 and E-02).  
1098 The latter illustrate the main morpho-bathymetric domains of the eastern margin slope, which  
1099 can be divided into a low gradient (2-3°) upper slope mostly preserved from erosion, a middle  
1100 slope affected by numerous submarine canyons and a lower slope to to-of-slope region. The  
1101 hatched area shows the elevation difference between the southern and central parts of the  
1102 eastern margin (E-01 and E-02, respectively), highlighting that the slope is better preserved  
1103 from retrogressive erosion by slope canyons processes towards the south.

1104 **Figure 5: A.** 3D bathymetrical map of the outer slope in front of Cap Bayes Pass with location of  
1105 dip-oriented seismic profile NM-1. **B.** Seismic profile NM-1 profile with location of quaternary  
1106 terraces (blue arrow, see details in Flamand, 2006), clinoform slope break of U2 prism (green  
1107 arrow) and the bathymetrical scarp associated with the top of U1 seismic unit (red arrow). **C.**  
1108 Interpretation of seismic profile NM-1 highlighting five sub-units inside U2, interpreted as  
1109 parasequences (numbered from 1 to 5). Each parasequence is typified by an alternation of  
1110 lowstand forced regressive wedges (in beige) and aggrading to retrograding shallow-water  
1111 carbonate transgressive sequences (in pink), consistent with the pattern of reciprocal  
1112 sedimentation model.

1113 **Figure 6: A.** 3D bathymetrical map of the outer slope in front of Canala with location of seismic  
1114 profiles NM-4 and NM-9 and dredged carbonate rocks (see [Table 3](#)). **B.** Uninterpreted seismic  
1115 profile NM-4. **C.** Interpreted seismic profile NM-4. **D.** Uninterpreted seismic profile NM-9. **E.**  
1116 Interpretation of seismic profile NM-9. Both profiles show U1 seismic unit overlain by  
1117 downlapping U2 seismic unit interpreted as external slope deposits derived from the quaternary  
1118 barrier reef.

1119 **Figure 7: A.** 3D bathymetrical map of the outer slope in front of Côte Oubliée with location of  
1120 seismic profiles NM-12B and NM-13 and dredged carbonate rock DR-49 (see [Table 3](#)). **B.**  
1121 Uninterpreted seismic profile NM-12B. **C.** Interpretation of seismic profile NM-12B. **D.**  
1122 Uninterpreted seismic profile NM-13. **E.** Interpretation of seismic profile NM-13. The upper  
1123 slope is characterized by a thick downlapping U1 sedimentary unit incised by numerous gullies  
1124 suggesting significant off-bank transport from the lagoon towards the basin.

1125 **Figure 8: A.** 3D bathymetrical map of the southeastern slope of Grande Terre and Pines Ridge  
1126 with location of AUS-104 and 206-04 seismic profiles. T : Banc de la Torche ; S : Stylaster  
1127 seamount ; B : Brachiopod seamount ; A : Antigonina seamount ; C : Crypthelia seamount ; M :  
1128 Munida seamount. **B.** Seismic profile AUS-14 across the Loyalty Basin bordered by the Loyalty  
1129 and Pines ridges. **C.** Line drawing interpretation of profile AUS-14 showing spectacular normal  
1130 faults affecting the peridotite nappe overlain by post-obduction sedimentary units. This study  
1131 focuses on shallow-water carbonates that cover peridotite horsts of the Pines Ridge and which  
1132 are currently at 300-400 m water depths.

1133 **Figure 9:** Bathymetric map (**A**) and profile (**B**) of Crypthelia seamount located from 200 to 800  
1134 m water depth and marked by N160° oriented faults (f) associated with a channel (Ch) and large  
1135 collapses on its southern edge. Bathymetric map of Munida seamount (**C**) marked by a southern  
1136 terrace noted M1, located between 400 to 600 m water depth, and by a relatively flat top above  
1137 200 m water depth, noted M2.

1138 **Figure 10: A.** Seismic profile 206-04 through the Pines Ridge and Munida seamount (see  
1139 location on [Fig.8A](#) and [10C](#)). **B.** Interpretation of profile 206-04 showing the normally faulted  
1140 geometry the Peridotite Nappe and HP-LT Metamorphic complex resulting from post-obduction  
1141 extensional tectonics (Patriat et al., 2018). Associated flat-topped horsts are capped by a shallow  
1142 water carbonate ramp interpreted as being of Mio-Pliocene age based on biostratigraphic  
1143 analysis of DW-4757 and DW-4782-A dredged samples (see [Table 3](#)). **C.** Close-up view on  
1144 seismic profile 206-04 on the Pines Ridge. **D.** Detailed line drawing interpretation of C. showing

1145 3 subunits UP1 to UP3 and an overall asymmetric configuration suggesting a tilt of Pines Ridge  
1146 before and during deposition of the Mio-Pliocene carbonate ramp. The eastern part of UP2  
1147 subunit is characterized by build-up geometries that could be interpreted as aggrading platform.

1148 **Figure 11:** A. DR44 sample, (a.) *Katacycloclypeus martini*, (b.) *Globigerinoides quadrilobatus*. B.  
1149 DR44 sample, (a.) *small rovaliid* in reworked micrite, (b.) *Dentoglobigerina altispira*, (c.)  
1150 *Globorotalia menardii*, (d.) *Globigerinoides conglobatus*, (e.) *Globigerinoides ruber*. C. DR44  
1151 sample, (a.) *Globorotalia plesiotumida*. D. DR45 sample, (a.) *Lepidocyclina* sp.. E. DR46 sample,  
1152 (a.) *Truncorotalia crassaformis*. F. DR47 sample, (a.) *Globoquadrina dehiscens*. G. DR47 sample,  
1153 (a.) *Globorotalia tumida*.

1154 **Figure 12:** A. DR48 sample, (a.) *Alveolinella praequoyi* (b.) *Pulleniatina obliquiloculata*. B. DR49  
1155 sample, (a.) *Alveolinella praequoyi*. C. DR49 sample, (a.) *Globorotalia tumida* D. DR53 sample,  
1156 (a.) *Pulleniatina primalis* E. DW4737-B sample, (a.) *Alanlordia* sp. F. DW4757-A sample, (a.)  
1157 *Planorbulinella solida*. G. DW4770 sample, (a.) *Truncorotalia truncatulinoides* (d'Orbigny) (b.)  
1158 *Truncorotalia tosaensis* (Takayanagi and Saito).

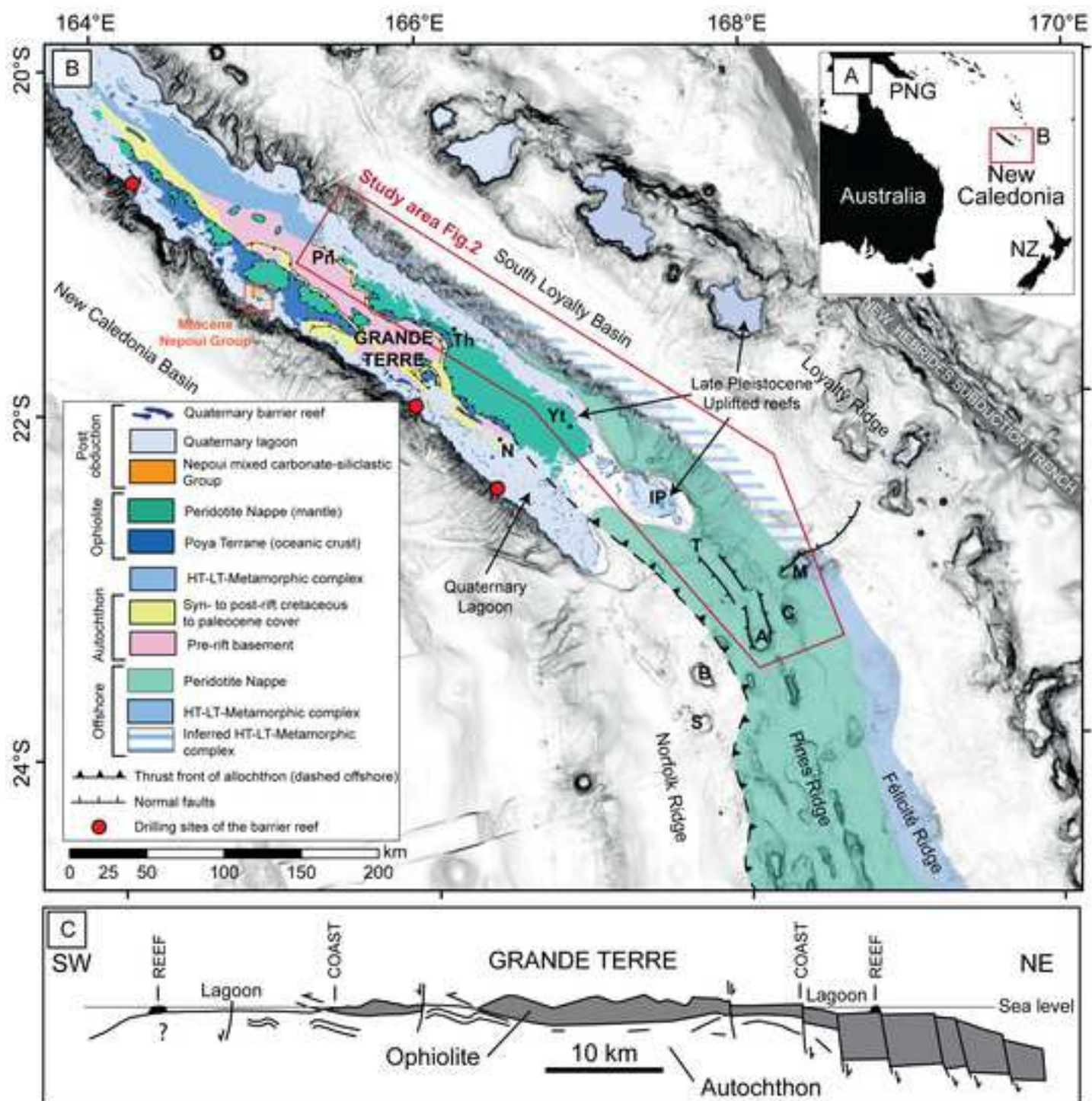
1159 **Figure 13:** A. Schematic cross-sections showing the geometry and evolution of shallow water  
1160 post-obduction systems on the eastern margin of Grande Terre in the vicinity of Poindimié (1),  
1161 north of Pines Ridges along Banc de la Torche (2), south of Pines Ridge (3), and over Cryptelia  
1162 (4) and (5) Munida seamounts. (location in Fig. 13C). B. Paleogeographical reconstruction and  
1163 spatial distribution of Mio-Pliocene carbonate banks. C. Paleogeographical reconstruction and  
1164 spatial distribution of Quaternary barrier reef of Grande Terre and submerged isolated  
1165 platforms along Pines Ridges and seamounts.

1166 **Table 1:** Characteristics of the seismic acquisition devices.

1167 **Table 2:** List of carbonate rock samples analysed in this study

1168 **Table 3:** Table summarizing microfacies description and interpretation of depositional  
1169 environment, age of *in-situ* components and age of reworked components (identified in red in  
1170 Table 4)

1171 **Table 4:** List of the component occurrence with identification of reworked elements (red cross).



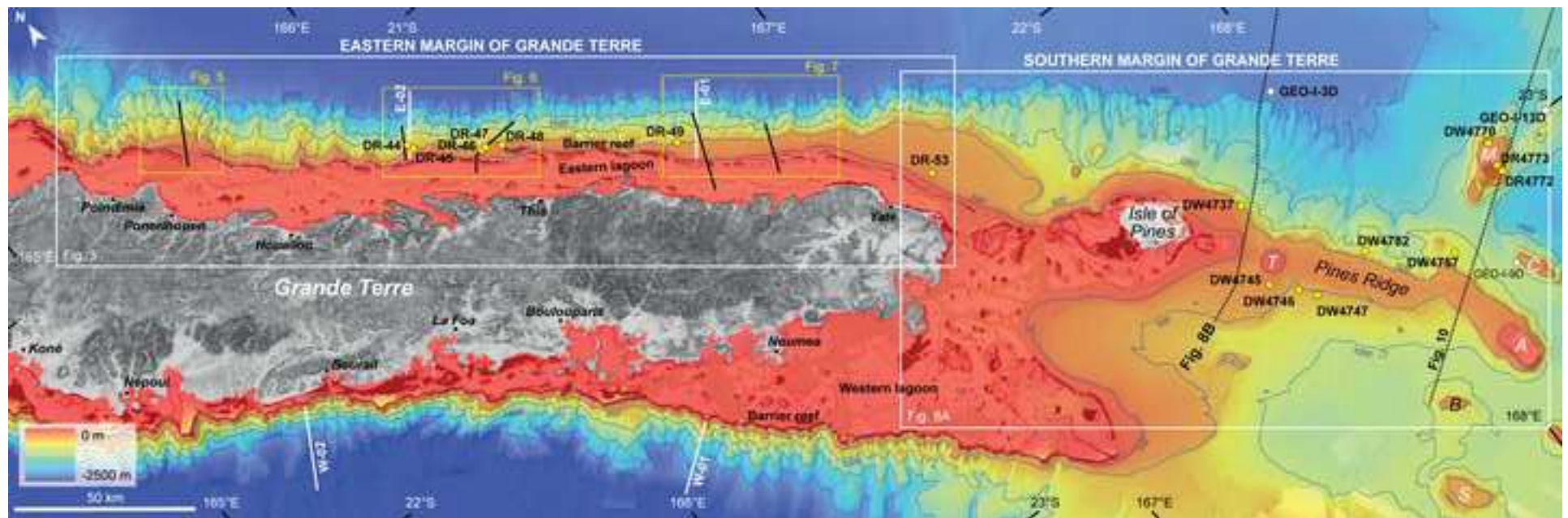


Figure 3

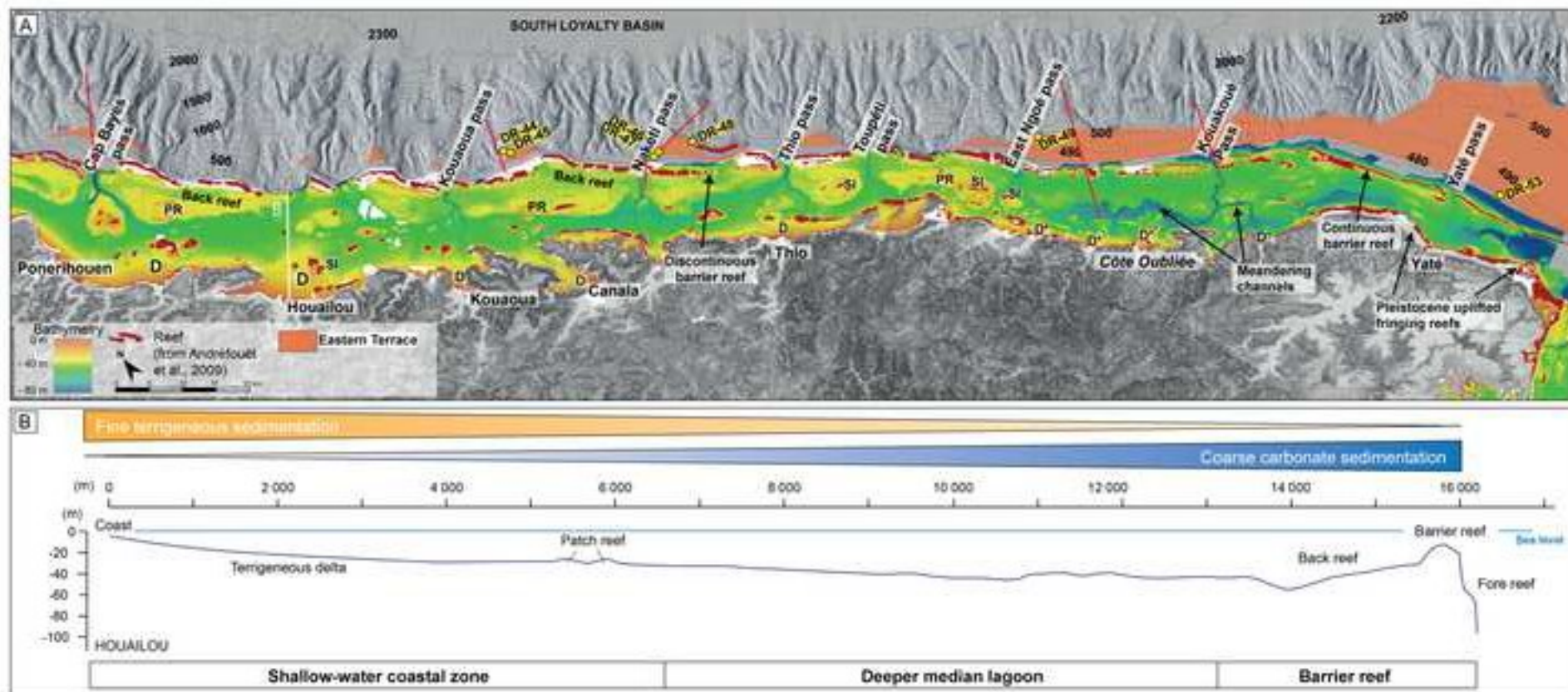
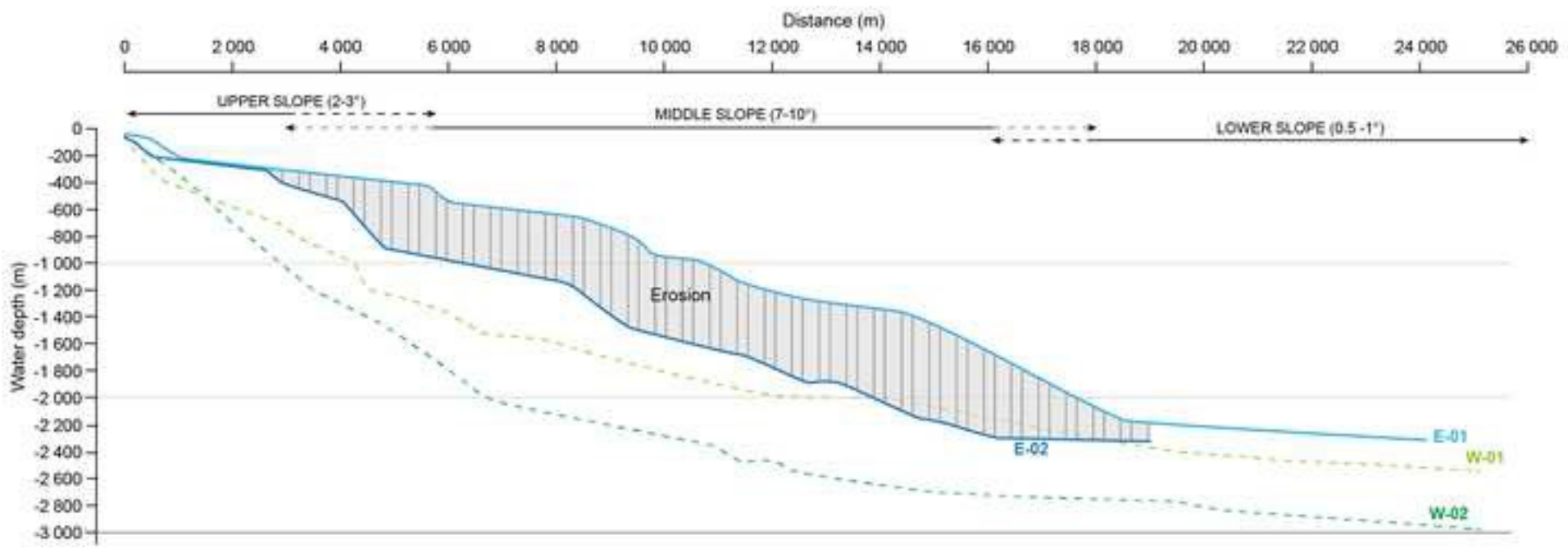
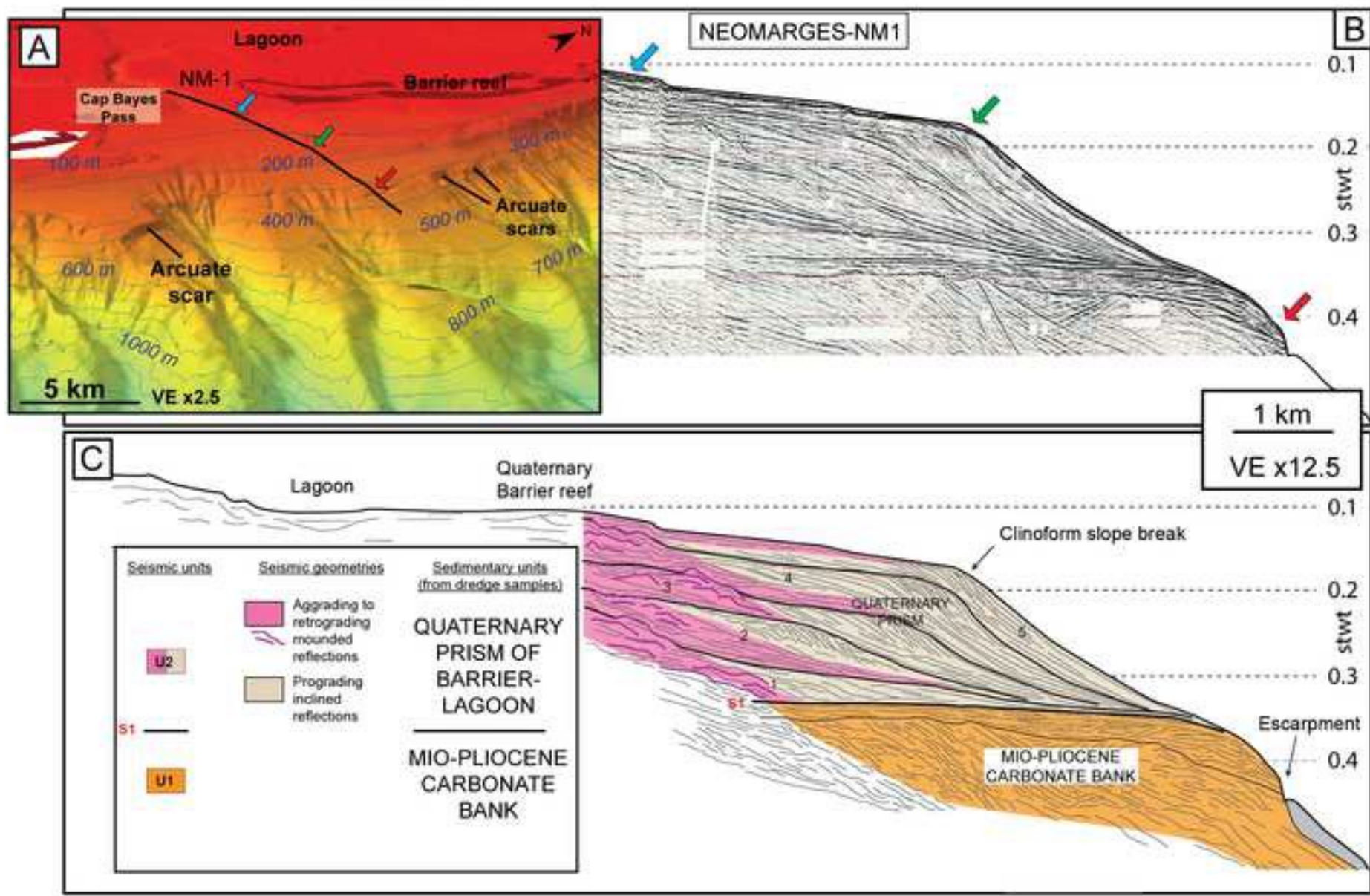
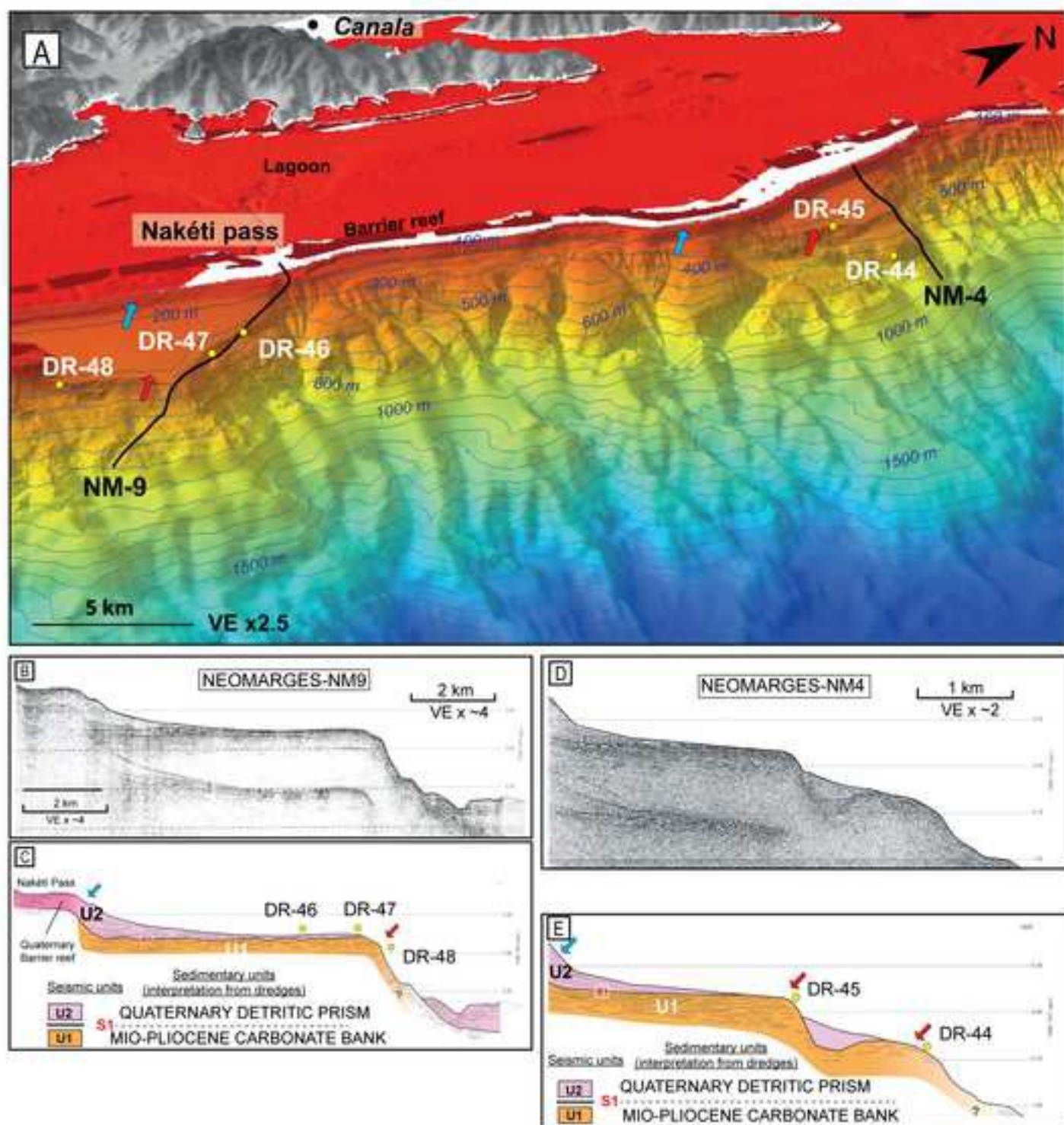
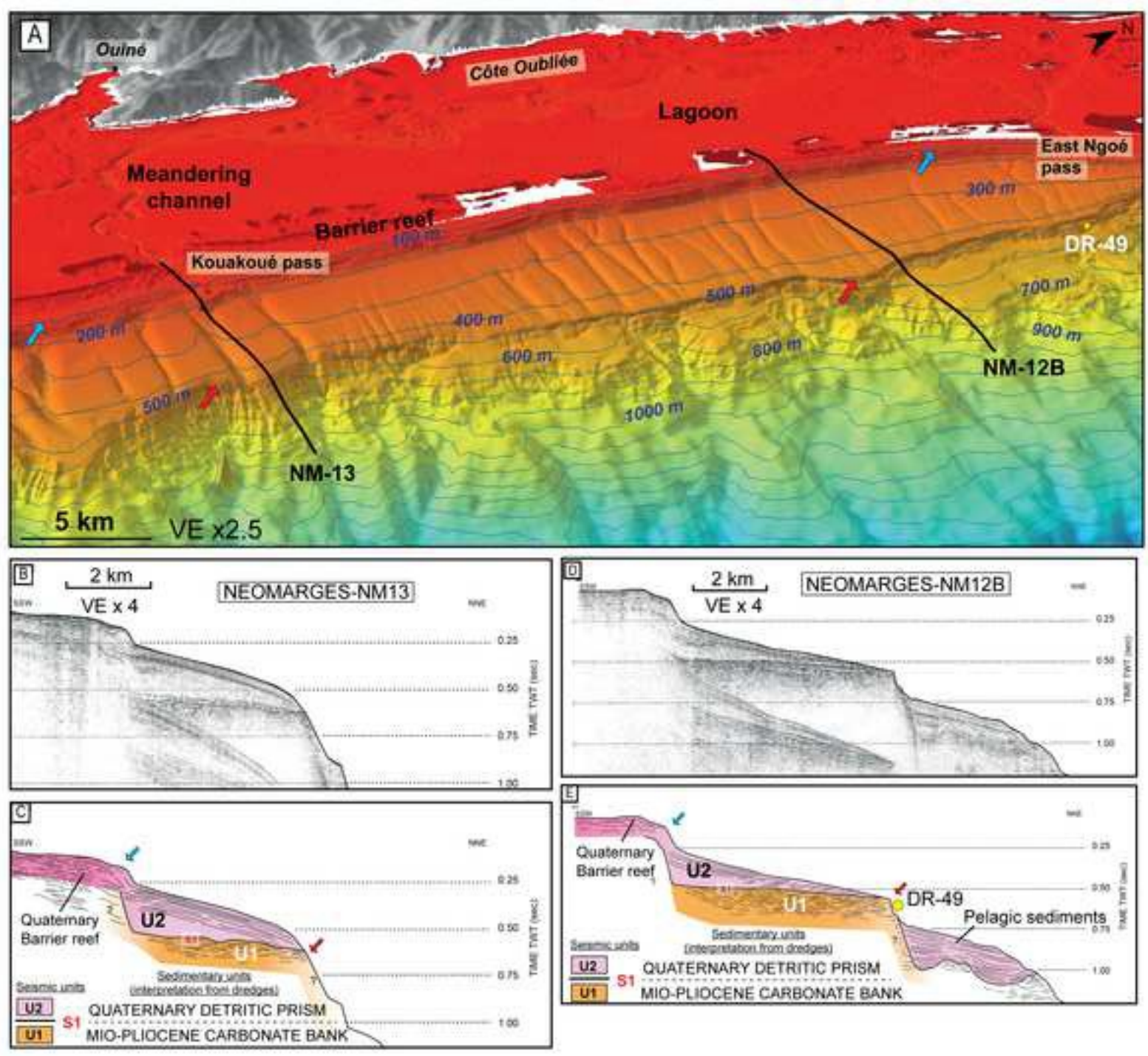


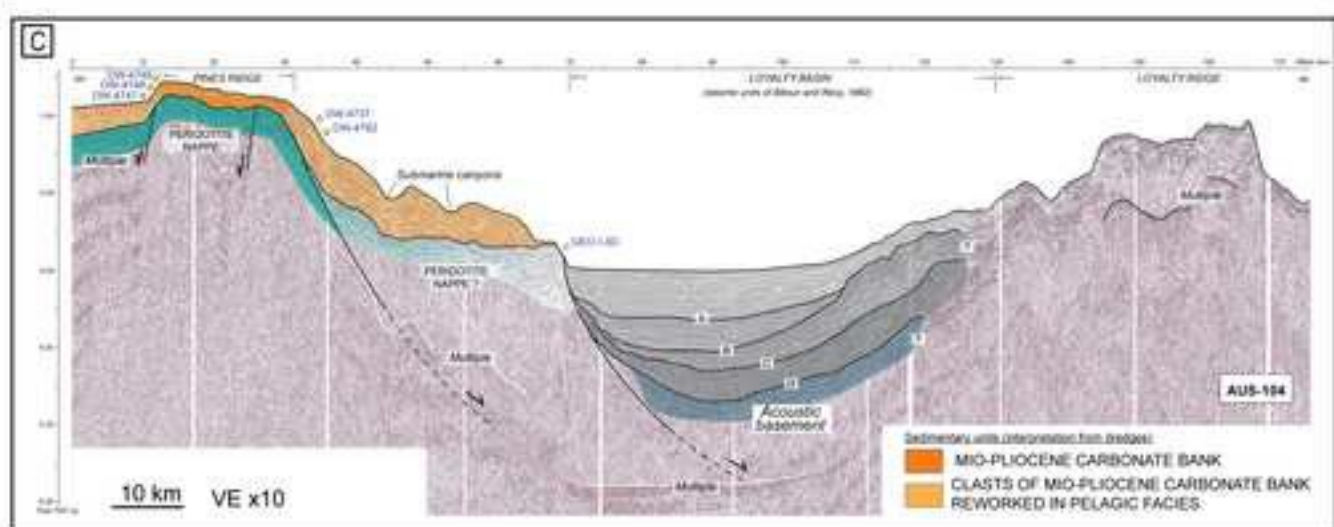
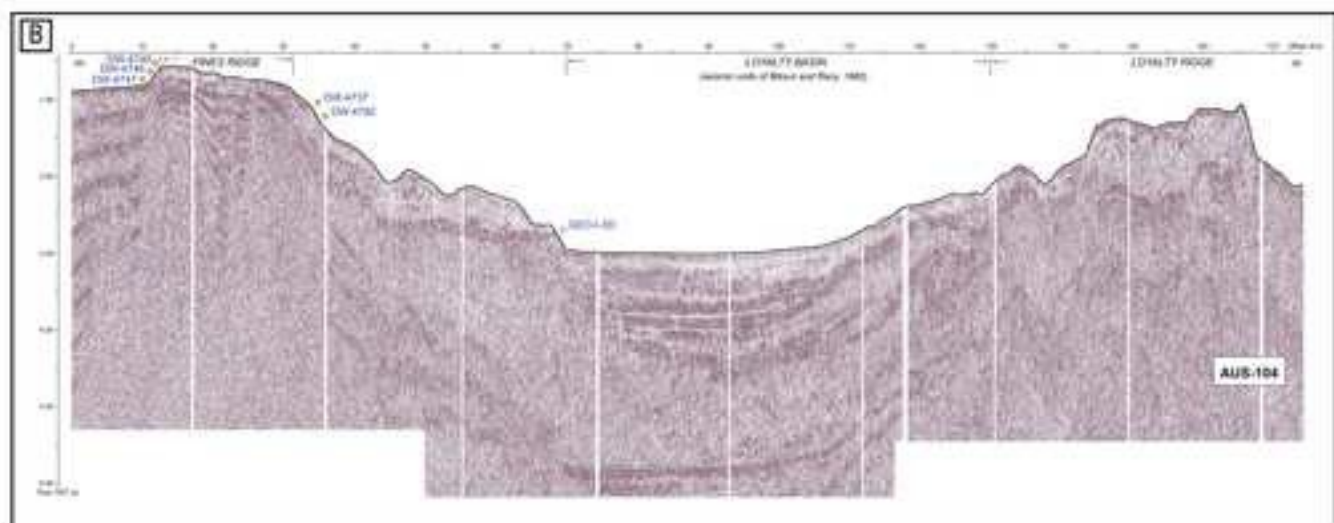
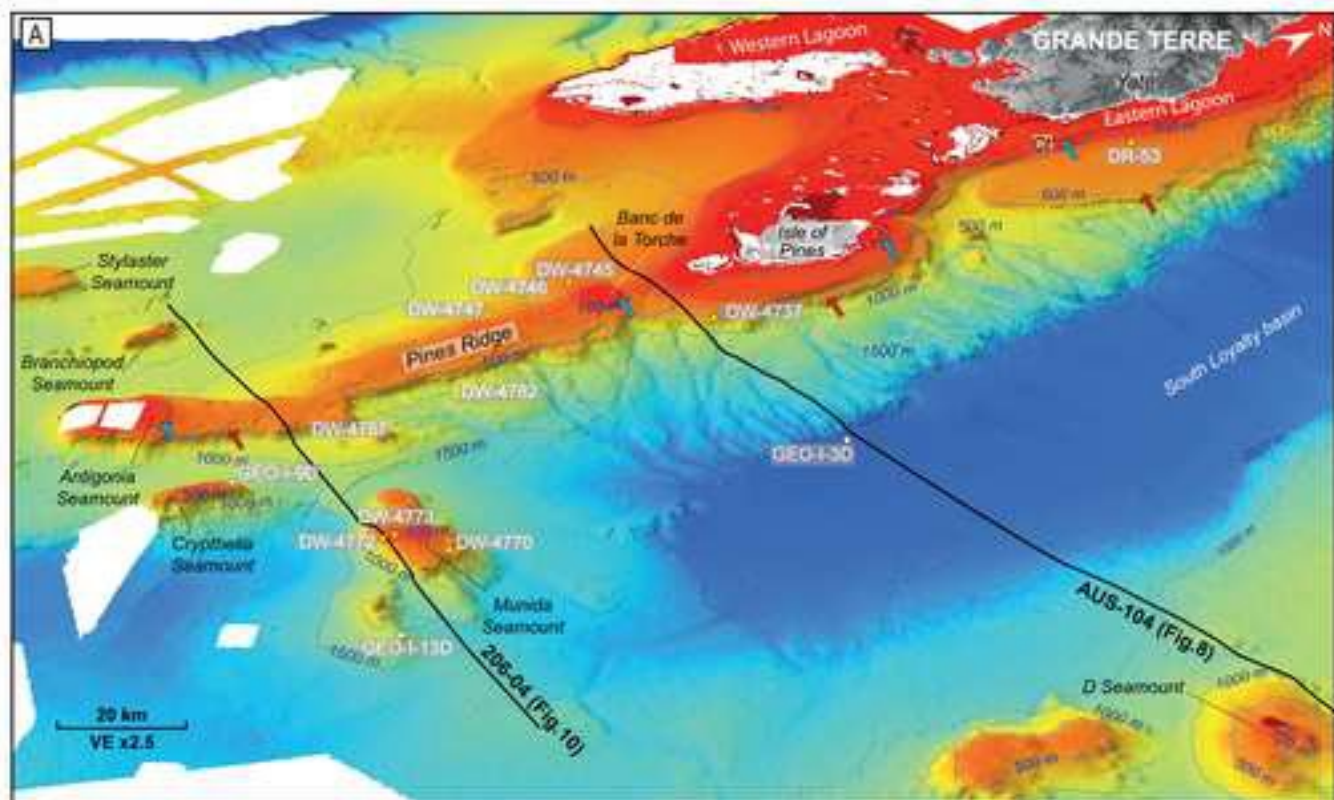
Figure 4



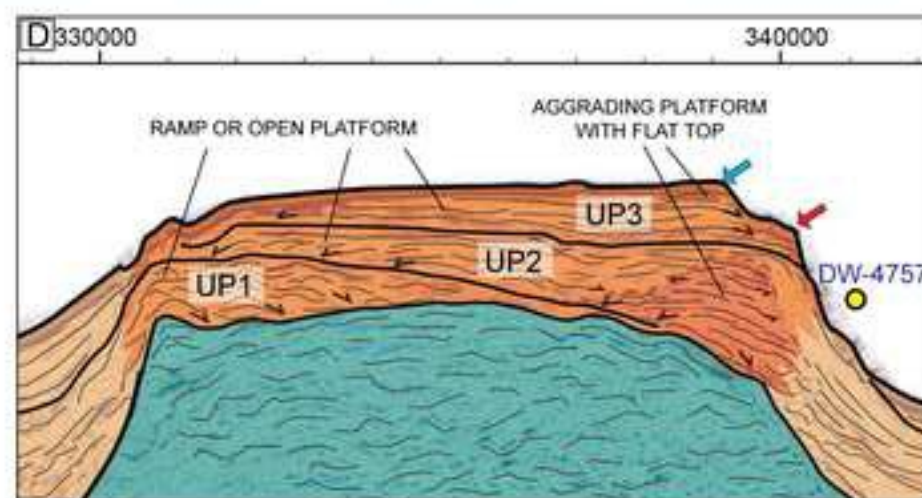
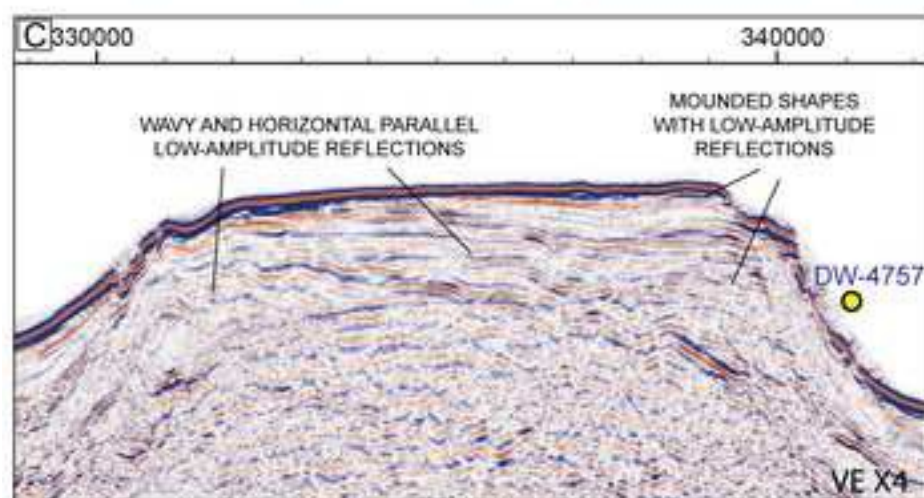
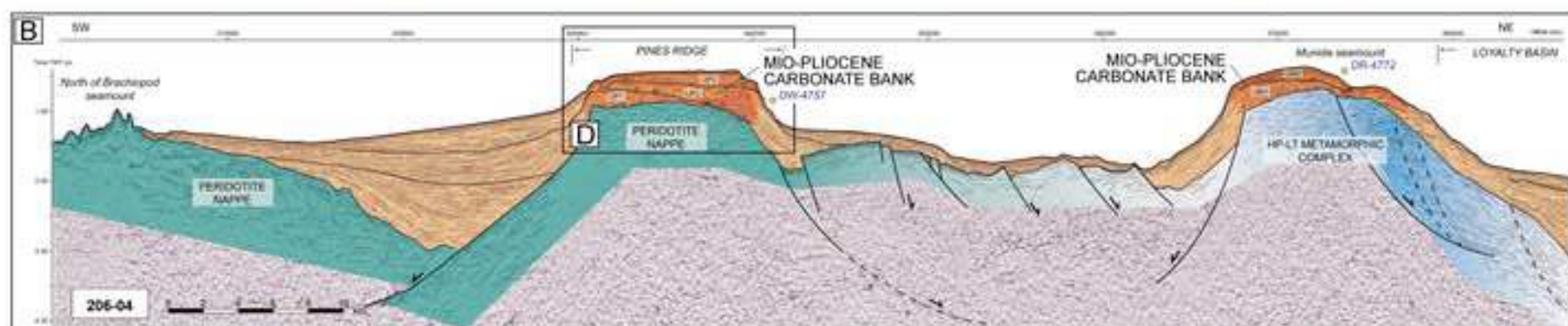
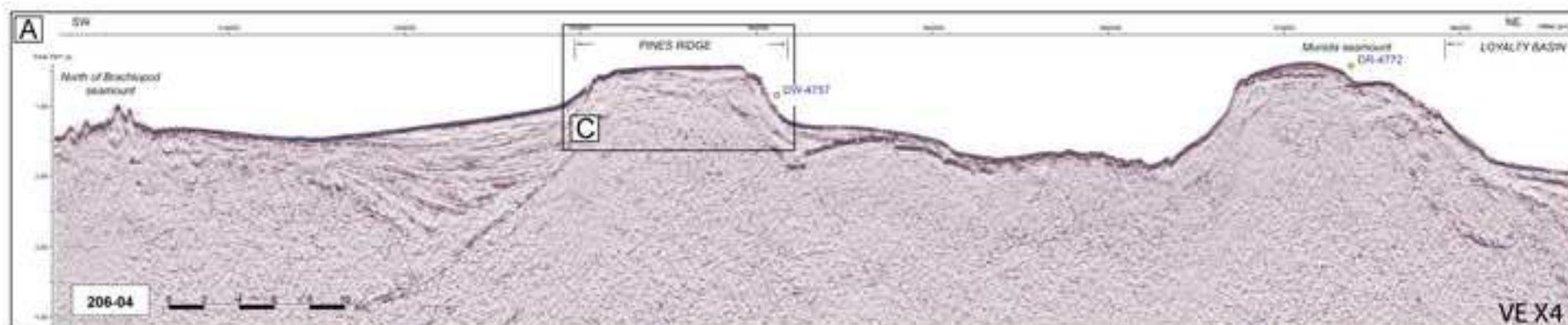


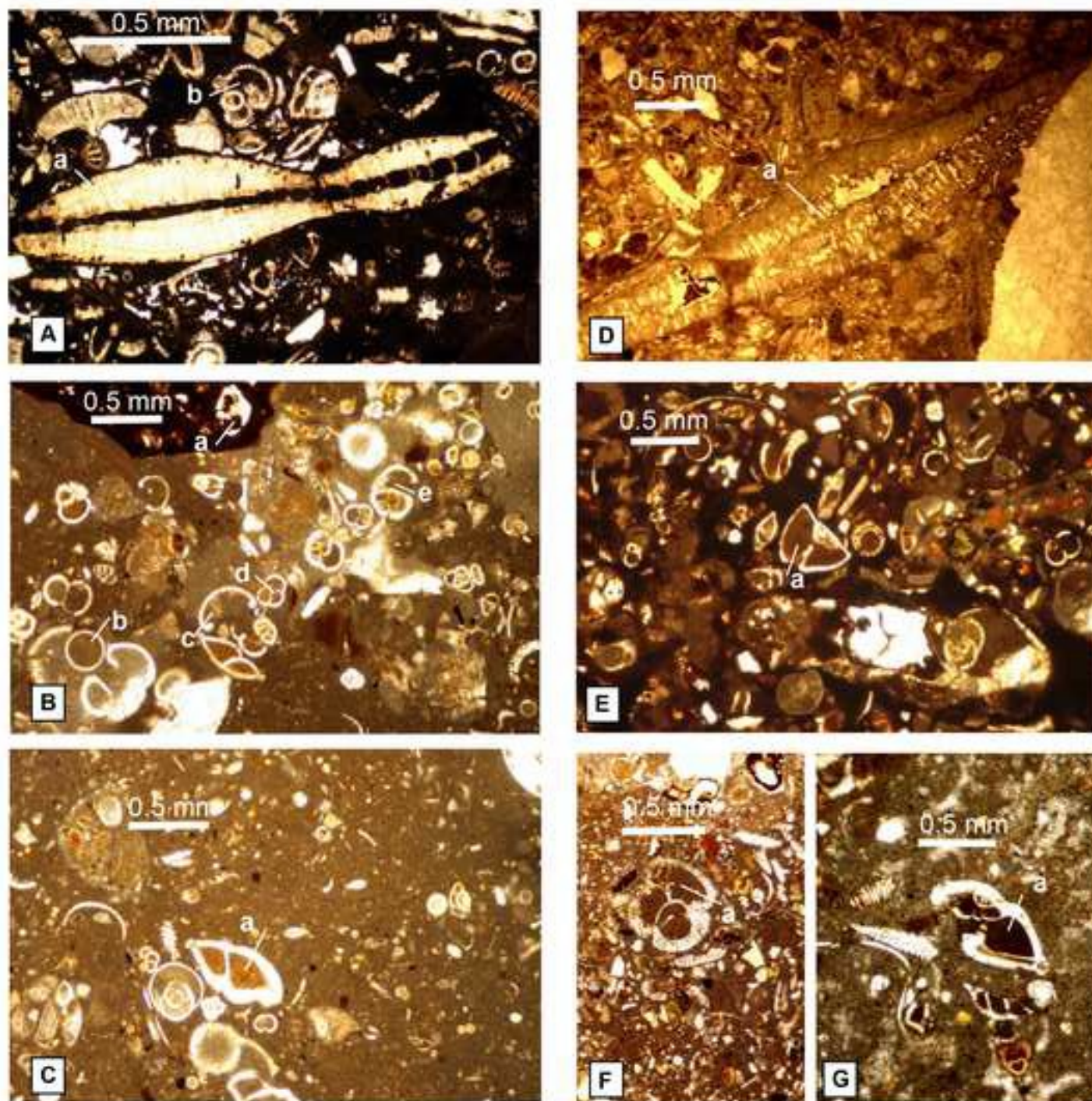


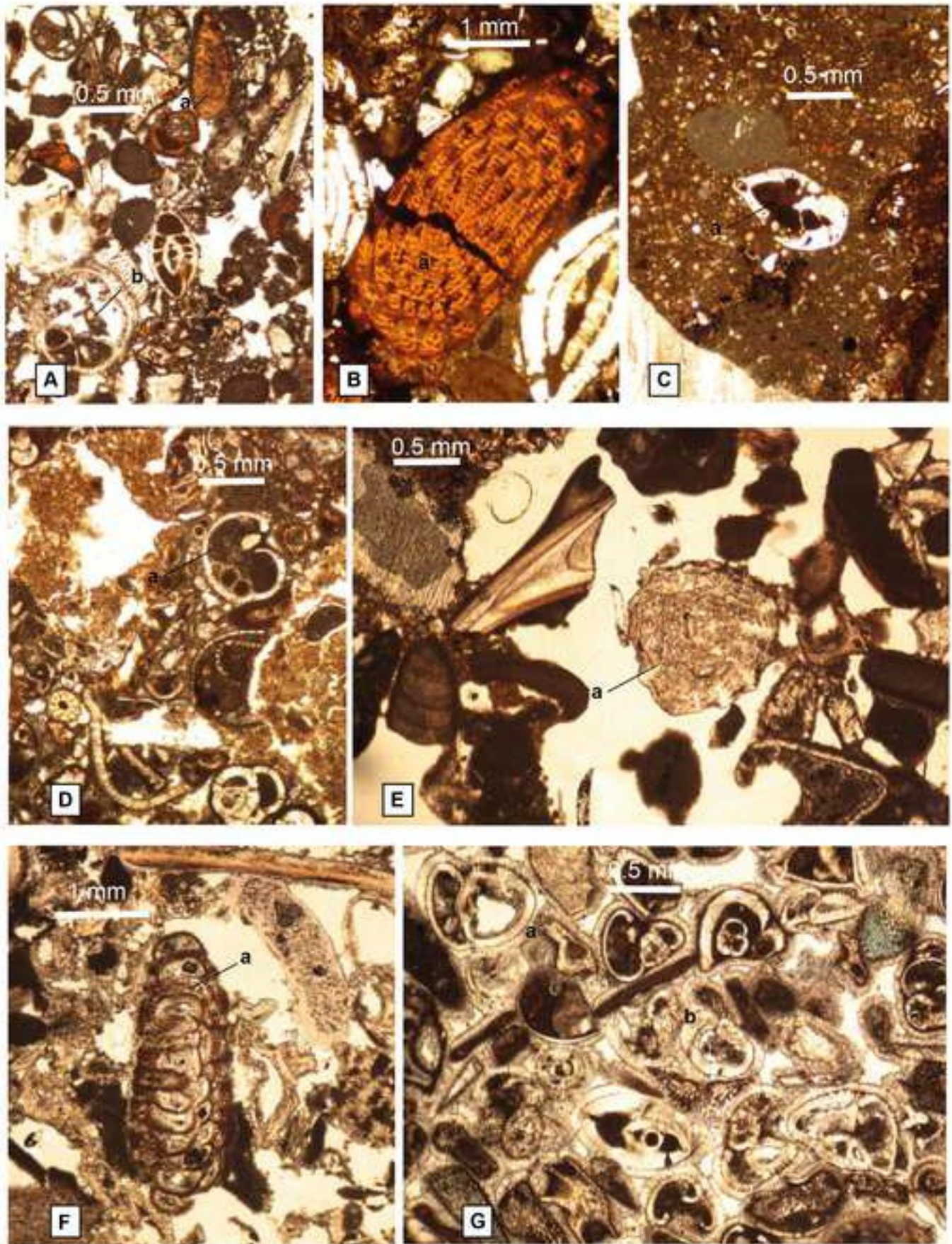


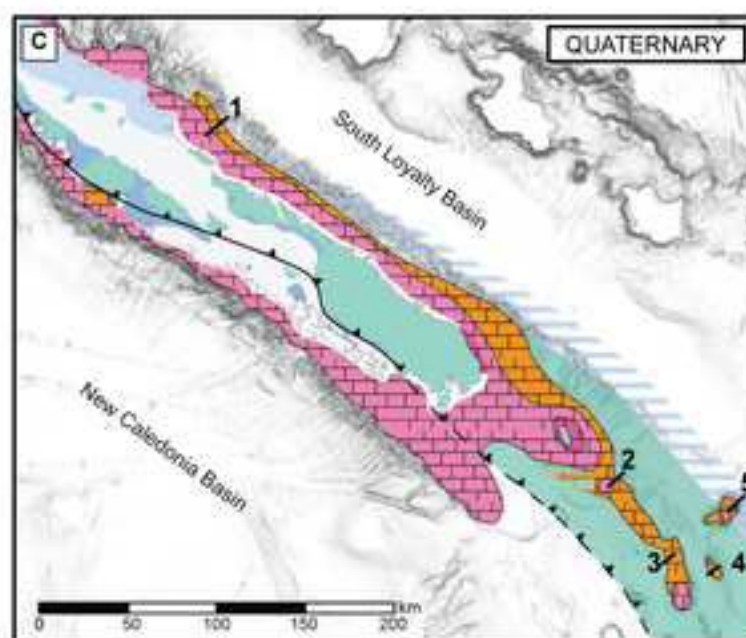
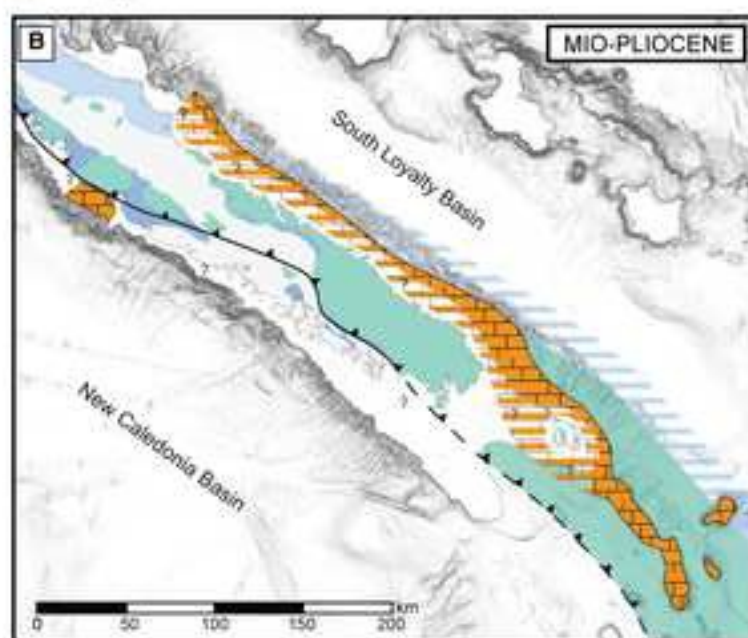
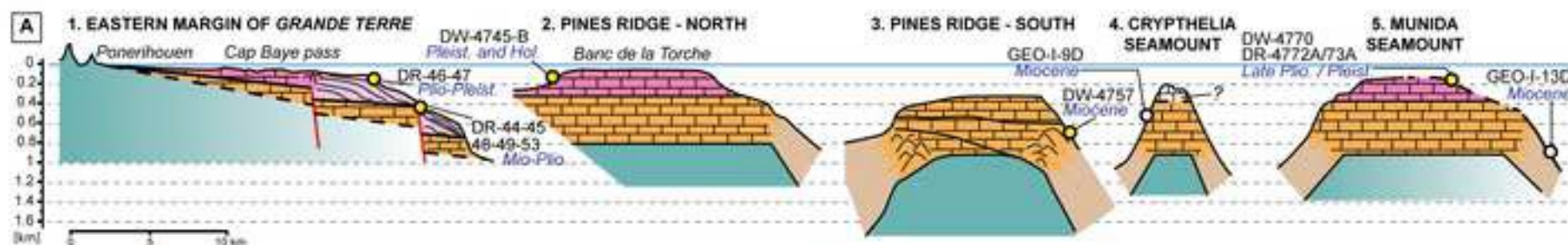




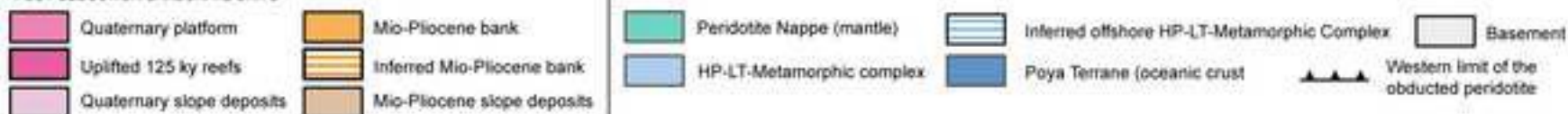








## POST-OBDUCTION CARBONATE UNITS



SEISMIC PROFILE	Figure in this study	CRUISE	STREAMER LENGTH (KM)	NUMBER OF CHANNELS	SOURCE TYPE	SOURCE VOLUME (CU)	SOURCE BAND WIDTH (Hz)	SHOT INTERVAL (m)
NM-1	Fig. 5	NEOMARGES, 2006	0.072	24	Airgun Bolt 600BT	20	50 to 500	5,5 to 8
NM-4	Fig. 6B							
NM-9	Fig. 6C							
NM-12B	Fig. 7B							
NM-13	Fig. 7C							
AUS-104	Fig. 8B	AUSTRADDEC-1, 1972	—	12 or 24	Flexichoc source	—	—	—
206-04	Fig. 10	FAUST-1, 1998	3.3	264	Systems HG Sleeve guns	3000	50-60	50

SAMPLE NAME	CRUISE	SITE	WATER DEPTH (m)	LATITUDE	LONGITUDE
DR44	2005-NC-DR	Eastern margin of <i>Grande Terre</i>	550 to 680	-21.276	166.020
DR45	2005-NC-DR	Eastern margin of <i>Grande Terre</i>	300 to 410	-21.295	166.023
DR46	2005-NC-DR	Eastern margin of <i>Grande Terre</i>	295 to 380	-21.404	166.170
DR47	2005-NC-DR	Eastern margin of <i>Grande Terre</i>	295 to 380	-21.405	166.183
DR48	2005-NC-DR	Eastern margin of <i>Grande Terre</i>	290 to 400	-21.426	166.220
DR49	2005-NC-DR	Eastern margin of <i>Grande Terre</i>	400 to 500	-21.701	166.598
DR53	2005-NC-DR	Eastern margin of <i>Grande Terre</i>	280	-22.168	167.092
DW4737-B	KANACONO	Southern margin of Isle of Pines	387 to 456	-22.716	167.709
DW4746-B	KANACONO	Southern margin of Isle of Pines	494 to 508	-22.975	167.693
DW4745-B	KANACONO	Southern margin of Isle of Pines	310 to 403	-22.918	167.636
DW4747-B1	KANACONO	Southern margin of Isle of Pines	550 to 590	-23.015	167.722
DW4747-X	KANACONO	Southern margin of Isle of Pines	550 to 590	-23.015	167.722
DW4757-A	KANACONO	Southern margin of Isle of Pines	800 to 850	-23.142	168.096
DW4782-A	KANACONO	Southern margin of Isle of Pines	845 to 856	-23.000	167.903
DW4770	KANACONO	Munida seamount	455 to 470	-22.975	168.350
DR4772-A	KANACONO	Munida seamount	230 to 795	-23.051	168.336
DR4773-A	KANACONO	Munida seamount	230 to 400	-23.035	168.334

SAMPLES	SITE	DEPTH	CRUISE	MICROFACIES	DEPOSITIONAL ENVIRONNEMENT	ZONE and AGE	ZONE and AGE of reworked components (in red Table.4)
DR44	Eastern Margin, in front of Canala (Fig.6)	550 to 680 m	2005-NC-DR	Micritic pelagic packstone with reworked micritic patches of planktonic foraminifera, recrystallised algae and larger benthic foraminifera	Forereef environment LBF reworked into inner to outer neritic environment	N19-N20a (5.3 Ma to 3.6 Ma) Early Pliocene	N12 (13.82 Ma to 12.00 Ma) Serravallian
DR45		300 to 410 m	2005-NC-DR	Micritic pelagic packstone with reworked micritic patches of planktonic foraminifera, recrystallised algae and larger benthic foraminifera	Forereef environment LBF reworked into inner to outer neritic environment	N19-N20a (5.33 Ma to 3.6 Ma) Early Pliocene	N12-N13 (13.82 Ma to 11.63 Ma) Serravallian
DR46	Eastern Margin, in front of Nakéti Pass (Fig.6)	295 to 380 m	2005-NC-DR	Micritic packstone of planktonic foraminifera with reworked patches of reworked pelagic micrite	Inner to outer neritic	N22a (1.8 Ma to 1.00 Ma) Pleistocene	N4-N17a (23.03-7.2Ma) Miocene
DR47		295 to 380 m	2005-NC-DR	Micritic wackestone of recrystallised algae with reworked patches of reworked pelagic micrite	Inner to outer neritic	N20a (3.8 Ma-3.6 Ma) Late Pliocene	N4-N17a (23.03-7.2Ma) Miocene
DR48		290 to 400 m	2005-NC-DR	Micritic packstone of algae with reworked patches of reworked pelagic micrite	Forereef environment LBF reworked into inner to outer neritic environment	N22 (1.8 Ma to 0.12 Ma) Pleistocene	N12-N13 (13.82 Ma to 11.63 Ma) Serravallian
DR49	Eastern Margin, in front of Ngoé Pass (Fig.7)	400 to 500 m	2005-NC-DR	Micritic packstone of algae and larger benthic foraminifera reworked into pelagic micrite	Forereef environment LBF reworked into inner to outer neritic environment	N19 (5.3 Ma to 3.8 Ma) Early Pliocene	N12-N13 (13.82 Ma to 11.63 Ma) Serravallian
DR53	Eastern Margin, in front of Yaté (Fig.8)	280 m	2005-NC-DR	Micritic packstone of planktonic foraminifera	Inner to outer neritic	N18-N21a (5.8 Ma to 2.5 Ma) Late Miocene (Messinian) to Early Pliocene (Zanclean)	Serravallian to Pliocene, N12-N21
DW4737-B	SE Isle of Pines (Fig.8)	387 to 456 m	KANACONO	Micritic wackestone of foraminifera and fragments of algae	Inner to outer neritic	N20b-N21 (3.6 Ma to 2.5 Ma) Pliocene	
DW4745-B	West of Pines Ridge (Fig.8)	310 to 403 m	KANACONO	Micritic packstone of foraminifera and algae	Inner to outer neritic	N22-Recent (1.8 Ma to Recent) Pleistocene - Holocene	
DW4746-B		494 to 508 m	KANACONO	Grainstone cemented by sparite of planktonic foraminifera with reworked micritic patches	Inner to outer neritic	N22 (1.8 Ma to 0.12 Ma) Pleistocene	N19-N21 (5.33 Ma to 1.8 Ma) Pliocene
DW4747-B1		550 to 590 m	KANACONO	Micritic packstone of foraminifera and algae	Inner to outer neritic	N19-N22 (5.33 Ma to 0.12 Ma) Pliocene - Pleistocene	
DW4747-X		550 to 590 m	KANACONO	Micritic wackestone of foraminifera	Inner to outer neritic	N21-N22 (2.5 Ma to 0.12 Ma) Late Pliocene - Pleistocene	
DW4757-A	East of Pines Ridges (Fig.8)	800 to 850 m	KANACONO	Micritic wackestone of foraminifera	Forereef environment	N4-N12 (23.03 Ma to 12 Ma) Early Miocene	
DW4782-A		845 to 856 m	KANACONO	Micritic wackestone of foraminifera	Inner to outer neritic	N17-N20 (8.6 Ma to 3.4 Ma) Late Miocene - Early Pliocene	
DW4770	Munida seamount (Fig.8 and Fig.9)	455 to 470 m	KANACONO	Micritic/sparite packstone of foraminifera and algae	Inner to outer neritic	N22 (1.8 Ma to 0.12 Ma) Pleistocene	
DR4772-A		320 to 795 m	KANACONO	Grainstone cemented by sparite of planktonic foraminifera with reworked micritic patches	Inner to outer neritic	N21-N22 (3.4 Ma to 0.12 Ma) Late Pliocene - Pleistocene	N4-N17a Miocene
DR4773-A		230 to 400 m	KANACONO	Grainstone cemented by sparite of planktonic foraminifera with reworked micritic patches	Inner to outer neritic	N21-N22 (3.4 Ma to 0.2 Ma) Late Pliocene - Pleistocene	N4-N17a (23.03-7.2Ma) Miocene

	<i>Planktonic foram</i>																					
	Beella sp.	Catapsydrax cf. dissimilis	Catapsydrax sp.	Dentoglogigerina altispira	Globoquadrina dedicens	Globoquadrina sp.	Globorotalia plesiotumida	Globorotalia tumida	Globorotalia menardii	Globorotalia inflata	Globorotalia scitula	Globorotalia miocenica	Globorotalia unguolata	Globorotalia sp.	Globigerina bulloides	Globigerina praebulloides	Globigerina spp	Globigerinoides quadrilobatus	Globigerinoides conglobatus	Globigerinoides ruber	Globigerinoides trilobus	Globigerinoides obliquus
DR44				X	X	X	X	X	X	X								X	X	X		
DR45					X			X									X	X				
DR46		X						X	X	X						X		X				
DR47					X			X		X	X					X	X	X		X	X	
DR48																		X			X	
DR49								X	X	X				X				X			X	
DR53								X	X	X					X			X				X
DW4737-B												X								X		
DW4745-B													X					X				
DW4746-B	X				X		X	X		X								X			X	
DW4747-B1														X				X			X	
DW4747-X																						
DW4757-A																						
DW4782-A			X															X				
DW4770						X												X				
DR4772-A										X						X					X	
DR4773-A										X						X	X					



																		Amphistegina tuberculata
				x														Amphistegina lessonii
x					x			x	x	x			x	x	x	x	x	Amphistegina spp
										x								Baculogypsina sp.
			x							x		x	x	x			x	Bolivina sp.
																x		Brizalina sp.
					x	x							x					Carpenteria sp.
																		Cycloclypeus spp.
						x												Dasyclad spp.
x												x						Elphidium sp
												x	x					Gypsina sp.
x																		Homotrema sp
																		Katacycloclypeus martini
							x		x									Quasirotalia guamensis
				x													x	Lepidocyclus sp.
		x				x							x	x	x			Lenticulina sp.
x							x		x									Marginopora sp.
x										x	x	x	x	x				Small miliolids
													x	x				Nodosaria sp.
x			x			x									x	x		Operculina spp.
																		Operculinoides spp.
	x																	Paragloborotalia kugleri
																	x	Planorbulinella larvata
				x														Planorbulinella solida
						x												Planorbulina sp.

Benthic Foraminifera

X						X					X						X	Sphaerogypsina sp.
X													X	X				Textularia sp.
													X				X	Radiolaria sp.,
X						X			X		X	X	X	X	X	X	X	Gastropod spp.
	X	X		X		X	X	X	X		X	X	X			X	X	Rodophyte spp.
													X					Halimeda sp.
X	X	X		X	X	X	X	X	X		X	X	X	X	X	X		Echinoid spp.
						X											X	Bryozoa spp.
															X			Ostracod sp.
				X	X	X			X				X	X			X	Coral spp.

Other component

**Declaration of competing interest**

*The authors declare that they have no known competing financial interests or personal relationships that could have appeared to influence the work reported in this paper.*

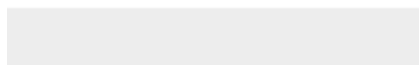
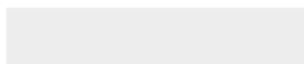


Click here to download Research Data <https://www.gns.cri.nz/Home/Our-Science/Land-and-Marine-Geoscience/Ocean-Floor-Exploration/Oceans-Research/Tasman-Frontier>





Click here to download Research Data <https://georep.nc/plate-forme-de-telechargement>



1 **Neogene to Quaternary evolution of carbonate and mixed**  
2 **carbonate-siliciclastic systems along New Caledonia's eastern**  
3 **margin (SW Pacific)**

4 E. Tournadour<sup>1,2</sup>, S.J. Jorry<sup>1</sup>, S. Etienne<sup>2</sup>, J. Collot<sup>2</sup>, M. Patriat<sup>1</sup>, M.K. BouDagher-Fadel<sup>3</sup>, F.  
5 Fournier<sup>4</sup>, B. Pelletier<sup>5</sup>, P. Le Roy<sup>6</sup>, G. Jouet<sup>1</sup>, P. Maurizot<sup>2</sup>

6 1. IFREMER, Unité Géosciences Marines, 29280 Plouzané, France

7 2. Service Géologique de la Nouvelle-Calédonie, DIMENC, B.P. 465, 98845 Nouméa, New Caledonia

8 3. University College London, Earth Science, 2 Taviton St, London WC1H 0BT, UK

9 4. Aix Marseille Univ, CNRS, IRD, INRAE, Coll France, CEREGE, case 67, 3, Place Victor Hugo 13331 Marseille  
10 cedex 03, France

11 5. Géosciences Azur (UMR 6526), IRD, 101 Promenade R. Laroque, BP A5, 98800 Nouméa, New Caledonia

12 6. Université Européenne de Bretagne Occidentale, UMR-6538 Domaines Océaniques, IUEM/CNRS, Place  
13 Copernic, 29280 Plouzané, France.

14

15 **ABSTRACT**

16 Neogene and Quaternary shallow-water carbonate records surrounding New Caledonia  
17 main island, Grande Terre, provide a good example for understanding the stratigraphic  
18 architecture of tropical mixed carbonate-siliciclastic systems. Due to a southeastern tilt of the  
19 [eastern](#) margin, the eastern shelf of Grande Terre has been better preserved from erosion than  
20 the western part, favouring the development and preservation of shallow-water carbonates.  
21 Based on the integration of bathymetric and seismic data, along with paleoenvironmental and  
22 biostratigraphic constraints derived from dredged carbonate rocks, a comprehensive  
23 geomorphological and architectural characterization of the offshore eastern margin of Grande  
24 Terre has been [performed. We show that duringmade. During](#) the Mio-Pliocene, a wide, up to  
25 750 m-thick carbonate build-up [developed and](#) extended over at least 350 km from north to  
26 south. This Mio-Pliocene build-up, currently lying at 300 to 600 m water depths, is overlain by a  
27 Pleistocene-Holocene barrier reef-lagoon complex and associated slope deposits. The switch  
28 from aggrading Neogene carbonate banks to backstepping Quaternary platforms likely reflects  
29 an increase in accommodation due to a high subsidence rate or to [flooding eventsrelative sea-](#)

30 [level rise](#), and/or results from a switch in carbonate producers associated with global  
31 environmental changes. The internal architecture of the Quaternary barrier reef-lagoon complex  
32 is highlighted, especially the development of lowstand siliciclastic prisms alternating with  
33 transgressive shallow-water carbonate sequences. This pattern agrees with the reciprocal  
34 sedimentation model typically invoked for mixed sedimentary systems. This stratigraphic  
35 pattern is well developed in front of the Cap Bayes inlet [in the north of our study area](#), yet it is  
36 not observed southward along the eastern margin. This difference suggests that other factors  
37 than relative sea-level variations directed the architecture of the margin, such as low  
38 terrigenous inputs, lagoon paleo-drainage networks or sediment by-pass towards deep basins.

39

40 **Keywords:** mixed carbonate-siliciclastic system, reciprocal sedimentation, tropical carbonates,  
41 terrigenous inputs, New Caledonia, SW Pacific.

## 42 1. INTRODUCTION

43 Mixed carbonate-siliciclastic depositional systems are characterized by a high variability in  
44 facies and architectures resulting from ~~a combination of~~ several factors, such as [relative](#) sea-  
45 level change, tectonic motions, carbonate production, terrigenous inputs, sediment transfer and  
46 hydrodynamic conditions, complicating the sequence stratigraphy interpretation (Droxler and  
47 Jorry, 2013; Zeller et al., 2015). According to the classical “reciprocal sedimentation” model  
48 (Wilson, 1967), mixed systems in the tropical realm have been commonly subdivided into  
49 alternating temporal phases where siliciclastic deposits would prevail during low sea-level  
50 periods whereas carbonates would dominate during transgressions and highstands. This  
51 reciprocal concept is yet relevant for several ancient and some modern cases studies (~~e.g.~~ Kerans  
52 & Tinker, 1999; Toomey et al., 2016), but has been shown to be inadequate in describing several  
53 others examples. This model appears not applicable for some mixed cool-water carbonate  
54 platforms, where sandstones can be deposited when wave abrasion depth ~~riserises~~  
55 seafloor during transgressions, whereas ~~shellbeds~~[shell-beds](#) formed during lowstands (Brachert  
56 et al., 2003). Another ~~counter~~ example is the Great Barrier Reef, where siliciclastic deposits are  
57 released to the slope and basin during late transgression, possibly due to the reworking of  
58 significant amounts of fine-grained terrigenous sediment stored on the shelf during lowstand  
59 ([Wallace et al., 2002](#); Dunbar and Dickens, 2003; [Mitchell et al., 2007](#); Harper et al., 2015). In  
60 addition, wave and/or current energy might prevent the infill of the lagoon during highstands,  
61 during which carbonate production is thought to be maximal, inducing, thus, an “empty bucket”  
62 pattern (Schlager, 1989; Purdy and Gischler, 2005; Zinke et al., 2001; Weij et al., 2019). This  
63 variability in the ~~stratigraphiesedimentological~~ response of mixed systems to relative sea-level  
64 changes demonstrates that other ~~control~~[controlling](#) parameters should also be considered in  
65 order to improve the prediction of their complex depositional architectures.

66 Around the main island of New Caledonia, “Grande Terre”, Neogene to Quaternary shallow-  
67 water carbonate systems ~~areoccur~~ coeval with high terrigenous fluxes derived from the erosion

68 of rugged mountain ranges ~~located all across the island and~~ primarily composed of obduction-  
69 related thrust sheets. The oldest known Neogene shallow-water carbonates on Grande Terre are  
70 ~~the~~ lower Miocene mixed carbonate-~~siliclastic~~~~siliciclastic~~ series cropping out in the ~~restricted~~  
71 Népoui area, on the western part of the island, close to the present day coastline (Fig. 1). These  
72 outcrops were interpreted as reflecting ~~sediment~~ deposition ~~of~~ Aquitanian and Burdigalian  
73 ramps where seagrass-related and scleractinian carbonate production occurred simultaneously  
74 to strong fluvio-deltaic terrigenous inputs (Maurizot et al., 2016; Tournadour et al., 2020).  
75 However, the offshore extent of this Miocene mixed system remains unknown.

76 At the present day, Grande Terre is surrounded by one of the largest modern barrier reef in  
77 the world. This barrier reef has been drilled on the western margin and past studies (Coudray,  
78 1975; Cabioch et al., 2008b ; Montaggioni et al., 2011) showed that it initiated ~~from~~at 400 cal  
79 kyr B.P. or Marine Isotope Stage 11 (MIS 11), over non-reefal shallow water carbonates ~~that~~  
80 ~~were~~ deposited ~~from~~as of ca. 1.2 Ma ~~ago~~ on a carbonate ramp or ~~an~~ non-rimmed platform  
81 (Montaggioni et al., 2011). The inner lagoon, in turn, started its infill only since 200 cal kyr, B.P.  
82 or Marine Isotope Stage 7 (MIS7) (Le Roy et al., 2008). This points to the fact that the  
83 southwestern shelf of New Caledonia does not follow a classic reciprocal sedimentation pattern  
84 but constitutes a unique mixed ~~carbonate-siliclastic~~ tropical system with a strong temporal  
85 and spatial partitioning between the outer coral plateau and the inner lagoon depression where  
86 terrigenous clastic sediments prevail (Le Roy et al., 2019).

87 In contrast, the Neogene to Quaternary shallow-water mixed systems of the eastern margin  
88 of Grande Terre are much less documented than ~~in the west~~their western counterparts, largely  
89 because of a lack of boreholes, rare outcrops onshore and few acoustic data offshore. However,  
90 this margin is thought to have a very different tectonic history than the western margin, ~~most~~  
91 ~~likely~~probably a ~~greater~~higher subsidence that ~~most likely~~would have resulted in a better  
92 preservation of shallow-water systems on the shelf, thus allowing to improve our understanding  
93 of the onset of Neogene carbonate systems and the transition to ~~quaternary~~Quaternary barrier  
94 reef lagoon in the regional tectonic context. In addition, those ~~sedimentary~~ records allow to

95 discuss the potential controlling factors ~~on~~[determining the](#) stratigraphic architectures along the  
96 margin, such as terrigenous inputs or paleo-drainage networks. With that aim, we have compiled  
97 both existing and newly acquired geophysical data and dredged carbonate rock samples from  
98 Ponérihouen to Antigonía seamount (Fig. 1) to perform a comprehensive analysis of slope  
99 morphologies ~~as well as a reconstruction of~~[and to reconstruct](#) the depositional environments  
100 and ages of the main terraces and seismic units observed along the eastern margin.

## 101 **2. GENERAL SETTINGS**

### 102 **2.1. Geography**

103 New Caledonia is a remote archipelago located in the South West Pacific (Fig.1). Its main  
104 island, Grande Terre, is a 50 to 80 km wide and approximately 400 km long land stripe  
105 oriented in a N140° direction. Highest summits are *ca.* 1600 m high. Because of dominant  
106 southeastward trade winds (N110-120°) its eastern margin is [positioned on the](#) windward [side](#),  
107 whereas the western margin is [the](#) leeward [side](#). Its eastern part is typified by steep reliefs,  
108 deeply incised valleys and short coastal plains, whereas the western part has more extended  
109 valleys, wider alluvial lowlands and large coastal plains. This landform dissymmetry impacts the  
110 spatial distribution of rainfall, [with](#) the eastern windward coast receiving twice as much  
111 precipitation than the western leeward coast. Such differences induce [a](#) one-and-a-half-time  
112 higher river discharge along the eastern coast compared to the western coast (Terry & Wolting,  
113 2011).

### 114 **2.2. Tectonics**

115 Grande Terre marks the northeastern tip of Zealandia (Mortimer et al., 2017), a mostly  
116 submerged fragment of continental crust isolated from Gondwana during the Late Cretaceous to  
117 Paleocene due to regional rifting followed by seafloor spreading in the Tasman Sea (Hayes &  
118 Ringis, 1973; Gaina et al., 1998). During the Eocene Grande Terre underwent a convergence

119 phase that led to the NE-SW emplacement of several tectonic nappes and finally, in the late  
120 Eocene-early Oligocene, to the obduction of a prominent kilometres-thick ophiolite mostly  
121 constituted of serpentized peridotites (Paris, 1981; Maurizot et al., 2020). Once obduction  
122 terminated, extensional tectonics prevailed all over Grande Terre (Lagabrielle et al., 2005;  
123 Chardon & Chevillotte, 2006; Lagabrielle & Chauvet, 2008). During this post-obduction  
124 extensional phase, that may still be active today, widespread normal faulting affected both [island](#)  
125 [margins of the island](#). The assymmetric morphology of Grande Terre is likely the result of these  
126 obduction and post-obduction tectonics. Drivers of the extension are either attributed to a plate  
127 tectonic divergent phase (i.e. far-field stresses related to initiation of east-verging subduction of  
128 the Australian plate beneath the Pacific Plate, Chardon & Chevillotte, 2006) and/or to post-  
129 orogenic collapse, dismantling and combined isostatic rebound (Lagabrielle et al. 2005,  
130 Lagabrielle & Chauvet, 2008; Moretti & Turcotte 1985; Collot et al., 2017). In this second  
131 hypothesis, unroofing the ridge of dense allochthonous mantle material and loading the adjacent  
132 basins resulted in subsidence of the basins and uplift of the ridge. The latter uplift is thus  
133 interpreted as being at the origin of the steepening of both the western and eastern margins of  
134 Grande Terre. The deep structure of the eastern margin has not been imaged by seismic data but  
135 is interpreted to be structured by a series of normal faults (see simplified geological cross-  
136 section of Fig. 1 and Collot et al. (1987)). Timing and amplitudes of these extensional events and  
137 vertical motions over the post-obduction period are not constrained as no continuous Oligocene  
138 to present day geological records exist. The Neogene to Quaternary carbonates that are the focus  
139 of this paper have developed on these structures. Offshore, towards the south, major listric  
140 normal faults bordering the obducted mantle sheets are imaged by seismic data along Pines  
141 Ridge (Chardon & Chevillotte, 2006; Flamand, 2006; Chardon et al., 2008; Patriat et al., 2018)  
142 (Fig.1). Apart from post-obduction extension, since the late Miocene, the southern part of Grande  
143 Terre and the Loyalty Islands are the foreland area of the Vanuatu Subduction Zone where the  
144 Australian Plate subducts beneath the Pacific Plate. A lithospheric flexure associated to this  
145 process is observed and results in the uplifts of the Loyalty Islands, the southern tip of Grande

146 Terre and the Isles of Pines. As a result, Quaternary 125 ka fringing reefs around Yaté and Isle of  
147 Pines are uplifted [between and now are positioned](#) 10 to 20 m [high above present-day sea level](#)  
148 (Cabioch et al., 1996).

### 149 **2.3. Miocene mixed carbonate siliciclastic systems**

150 ~~On land~~[On land](#), the post-obduction geology is characterized by an Oligocene sedimentary  
151 hiatus and the oldest known marine sediments that overlie allochthonous units are Miocene  
152 mixed carbonate-siliciclastic sedimentary rocks only cropping out in a restricted nearshore area  
153 located west of Grande Terre, in the region of Népoui (Coudray, 1975; Maurizot et al., 2016;  
154 Tournadour et al., 2020). These successions have been interpreted to reflect deposition of an  
155 Aquitanian carbonate ramp dominated by seagrass-related carbonate production, overlain by  
156 Burdigalian fan delta deposits that laterally evolve towards a carbonate ramp dominated by  
157 seagrass meadows and small-sized coral bioconstructions (Tournadour et al., 2020).

158 Offshore, despite a lack of drill core data, a few dredged carbonate samples were  
159 recovered from the outer slope of the eastern margin of Grande Terre (Chardon et al., 2008;  
160 Yamano et al., 2015) and close to *Munida* and *Crypthelia* seamounts (Daniel et al., 1976; Bitoun  
161 and Recy, 1982) (Fig. 2). These samples, collected between 400 m and 800 m water depths, are  
162 the only evidences of Miocene shallow-water carbonate deposits along the eastern margin of  
163 Grande Terre and Pines Ridge. Based on the interpretation of seismic profiles along Grande  
164 Terre's southeastern margin, Chardon et al. (2008) identified several normal faults that they  
165 interpret as being related to Late Miocene extensional tectonics. These authors also interpreted  
166 two planar surfaces as post-obduction erosional lateritic land surfaces resulting from  
167 weathering processes overlain by shallow-water carbonate deposits.

### 168 **2.4. Quaternary carbonate systems**

169 Our knowledge on the nature, structure and chronology of the New Caledonian  
170 ~~quaternary~~[Quaternary](#) carbonate systems primarily comes from coring investigations carried

171 out through the western parts of the New Caledonian barrier system (Coudray, 1976, Cabioch et  
172 al., 2008b; Montaggioni et al., 2011). Four cores, ~~ranging from~~ 120 to ~~226m~~226 m-long, reached  
173 the upper Cretaceous and Eocene bedrock and allowed to characterize the Quaternary  
174 development history of the western carbonate shelf margin. The recovered carbonate sequences  
175 result from stacking of about ten sedimentary carbonate units that ~~havewere~~ deposited during  
176 successive transgressive and high sea-level stands corresponding to interglacial periods  
177 (Cabioch et al., 2008b). These units are separated from each other by unconformities formed  
178 during sea-level drops in glacial periods. The succession of depositional events was  
179 reconstructed using lithostratigraphy, magnetostratigraphy, uranium-series dating and  
180 nannofossil stratigraphy (Cabioch et al., 2008b; Montaggioni et al., 2011). Carbonate  
181 ~~initiationsediment production~~ was initiated prior to 1.2 Ma ~~fromwithin~~ an open shallow-water  
182 shelf margin, ~~believed to havewhich~~ acted as a carbonate ramp system until 0.48 Ma.  
183 Corresponding deposits forming the lower units recovered in ~~borehole~~boreholes (red dots on  
184 Fig. 1) include grainstone, packstone and wackstone rich in corals, coralline algae, encrusting  
185 foraminifera with locally thick rodoliths accumulations (Montaggioni et al., 2011). The ramp  
186 system is assumed to have evolved into a rimmed, reef platform ~~fromas of~~ 0.40 Ma. The  
187 initiation of ~~typical~~ coral reef tracts and the associated reef-rimmed platform are thus  
188 considered to have begun after MIS 11 (Montaggioni et al., 2011), i.e. the Mid-Brunhes Event.  
189 Corresponding sedimentary units are made up of stacked ~~poritid-rich framework beds~~  
190 correlated to reef-flat environments with moderate to lower-water energy, and coralgal  
191 frameworks partly including arborescent acroporids suggesting deposition ~~at in~~ a protected reef-  
192 flat setting (Montaggioni et al., 2011). Complementary studies of the Quaternary evolution of  
193 the ~~SW-NC~~south-west lagoon ~~were performed by~~obtained seismic, bathymetric and coring data  
194 (Le Roy et al., 2008; Le Roy et al., 2019). Results ~~have shown~~showed that infill is composed of  
195 two or three 100 ka sedimentary sequences with a first significant flooding of the lagoon  
196 assumed to have started during MIS7, at 220 cal kyr B.P. The disparate ages of the lagoon and  
197 reefs can be reconciled with the fact that the first reefs were probably initially fringing

Formatted: Font: Italic

198 structures without a significant lagoon that has expanded later in response to subsidence of the  
199 margin and reef growth (Le Roy et al., 2018). Offshore, the outer barrier reef slopes of Grande  
200 Terre are marked by five marine terraces located between ca. 20 and ca. 120 m water depths  
201 that Flamand (2006) tentatively correlated to the five reefal lithological sequences cored on the  
202 western barrier reef and interpreted as the morphological expressions of Quaternary  
203 interglacials. However, a younger, last deglacial origin for these terraces located above 120 m  
204 water depth cannot be ruled out. Note that these ~~quaternary~~Quaternary marine terraces are  
205 located in the area indicated by the blue arrow on bathymetrical and seismic data. (Figs. 5 to 8).

## 206 **2.5. Quaternary subsidence rates**

207 Based on cores of the ~~quaternary~~Quaternary barrier reef of the western margin of Grande Terre,  
208 subsidence rates are estimated to range between 0.03 to 0.20 mm.yr<sup>-1</sup> since the last 400 ka  
209 (Coudray, 1975; Cabioch et al., 1996; Flamand, 2006; Frank et al., 2006) and ~~to have display~~  
210 mean rates of  $\leq 0.08$  mm.yr<sup>-1</sup> over the past 1 Ma (Montaggioni et al., 2011). Such values ~~are~~  
211 ~~believed to possibly~~ reflect a long-term subsidence of the western margin of Grande Terre  
212 suggesting that post-obduction extensional tectonics are still active and allowing sufficient  
213 accommodation space to record most Quaternary sea-level highstands. Unfortunately, the lack of  
214 core data on the eastern margin does not allow reconstructing any Neogene to Quaternary  
215 vertical motions.

## 216 **3. DATA AND METHODS**

217 Our morphological and stratigraphic analyses are based on the integration of existing and  
218 newly acquired bathymetrical and 2D seismic reflection data supplemented by dredged rock  
219 samples (Fig. 2). Existing bathymetrical data are derived from four datasets. The former covers  
220 the lagoon of Grande Terre and was essentially acquired during hydrographic surveys of the  
221 French Navy (SHOM), compiled by ~~the~~ New Caledonia Government within a 25 m resolution  
222 grid. The second dataset corresponds to data acquired between 2002 and 2006 onboard RV *Alis*

223 (EM1002 multibeam echosounder) along all the outer slopes of Grande Terre and Loyalty  
224 islands, as well as on seamounts of the Pines Ridges (down to *ca.* 1000 m of water depth), in the  
225 framework of the ZoNéCo program (*egge.g.* Pelletier et al., 2002, 2004, 2012; Perrier et al., 2004a,  
226 2004b, 2004c, 2005) and IRD research projects (*egge.g.* Cabioch et al., 2002a, 2002b). The third  
227 dataset ~~corresponds to~~ consists of data acquired in the 90's and 2000's in deeper waters (>1000  
228 m of water depth), such as in the South Loyalty Basin, onboard RV *L'Atalante* (EM12D multibeam  
229 echosounder), again through ZoNéCo (*eg.* ZoNéCo-1, Pautot et al., 1993; ZoNéCo-2, Lafoy et al.,  
230 1994; and ZoNéCo-3; Missègue et al., 1996). These two multibeam datasets were compiled in  
231 2009 in 25 m (EM1002) and 100 m (EM12D) resolution grids by New Caledonia Government  
232 (Juffroy, 2009) and included in the 2012 atlas of New Caledonia (Pelletier et al., 2012). The  
233 fourth dataset is the global seafloor topography derived from satellite altimetry and ship depth  
234 soundings (Smith and Sandwell, 1997). Newly acquired bathymetrical data corresponds to those  
235 gathered by the KANACONO cruise onboard R/V *Alis* (Puillandre & Samadi, 2016).

236 The seismic dataset mainly consists of published multichannel seismic reflection profiles  
237 located on the upper slope of the eastern margin of Grande Terre, acquired onboard R/V *Alis*  
238 during the NEOMARGES cruise (Chardon et al., 2007), using a 24 channel streamer and a 20  
239 cubic-inch air gun source. The high-resolution images have a maximum penetration of 0.25 s two  
240 way time (twt) (Table 1) and were reinterpreted in this study through detailed line drawings.  
241 Seismic profiles 206-04 (Lafoy et al. 1998) and AUS-104 (Bitoun & Recy et al. 1982), which are  
242 publicly available in the *Tasman Frontier seismic database* (Sutherland et al., 2012), were also  
243 interpreted. These profiles were acquired using lower frequency seismic devices (see Table 1)  
244 and hence have a lower resolution but a higher penetration, reaching 3 s twt in the offshore  
245 basins. Seismic stratigraphic analysis was performed on these profiles including identification of  
246 seismic facies, unconformities and sequences following Mitchum et al. (1977). To estimate the  
247 thickness of the carbonate units on the Pines Ridge, we assumed that they are composed of  
248 shallow-water carbonates with a low-porosity, affected by early compaction and dissolution, for  
249 which we attributed a mean velocity of 3000 m.s<sup>-1</sup> (Anselmetti & Eberli, 2001).

250 Sedimentary facies determinations were made on 17 carbonate rock samples dredged  
251 during the DR-2005-NC and KANACONO cruises onboard R/V *Alis* (Pelletier et al., 2006;  
252 Puillandre & Samadi, 2016; respectively) in water depths between 250 and 900 m (Table 2).  
253 Samples were described from large thin sections in order to identify textures and main  
254 components and ultimately reconstruct depositional environments. Biostratigraphic datings and  
255 paleoenvironmental reconstructions were based on the interpretation of foraminiferal  
256 assemblages (larger benthic and planktonic foraminifera). In our definitions of stratigraphic  
257 ranges, the planktonic foraminiferal zonal scheme of BouDagher-Fadel (2015, 2018a) is used.  
258 This scheme is tied to the time scale of Gradstein et al. (2012) and the revision by Cohen et al.  
259 (2017).

## 260 4. PHYSIOGRAPHY, STRUCTURE AND STRATIGRAPHY OF THE

### 261 EASTERN MARGIN

#### 262 4.1. Lagoon

263 The eastern lagoon, extending from the shoreline to the external barrier reef, is 10-15  
264 km wide between Poindimié and Yaté with an average water depth of 40 m, whereas the  
265 western lagoon does not exceed a width of 5-10 km wide with an average water depth of 20 m,  
266 except in its southern part where it is deeper and wider (Le Roy et al., 2008, 2019). Another  
267 difference with the western lagoon, which is bounded by continuous barrier reefs, is that the  
268 eastern lagoon is typified by a discontinuous external barrier reef with drowned segments in its  
269 southern part, off Yaté (Cabioch et al., 1996; Andrefouet et al., 2009) (Fig. 2). The eastern lagoon  
270 can be divided into three morphological domains: (1) the shallow-water coastal zone, (2) the  
271 median lagoon and (3) the external barrier reef (Fig. 3B).

272 The shallow-water coastal zone is particularly well-developed between Ponérihouen to  
273 Thio, where coastal bays are shallow and have gentle slopes, due to terrigenous deltas located at  
274 river and estuarine mouths (Fig.3). The latter are deltaic deposits extend for 2.5 to 7 km long and

275 can reach the central part of the lagoon. Between Côte Oubliée and Yaté, deltas are very  
276 restricted and do not exceed 2 km in length (Fig.3A). Previous studies on unconsolidated  
277 seafloor sediments revealed that these deltas are mainly composed of terrigenous sediments  
278 (Chevillon, 1997).

279 The deeper median lagoon, is relatively flat in its central part and contains isolated patch reefs  
280 as well as sandy islets aligned parallel to the coastline (Fig.3A). Southeast of the East Ngoé Pass,  
281 the median lagoon deepens (with an average water depth of 60-70 m) and contains a  
282 meandering channel that runs parallel to the coastline (Fig. 3A). This channel extends over 30  
283 km, incises the lagoon up to 40 m deep and is connected to the Kouakoué Pass, where it runs  
284 perpendicular to the coastline thanks to a *ca.* 90° bend (Fig.3A).

285 The barrier reef domain comprises the reef crest, close to sea-level, as well as a back-  
286 reef and reef flats within a 5 km-wide shallow-water area (20 to 40 m water depths). The latter  
287 is dominated by carbonate sediments of heterogeneous grain size, ranging from fine-grained  
288 sands to gravels (Chevillon, 1997). The barrier reef domain is interrupted by numerous passes  
289 (ie. inlets) connected to lagoonal channels that cross-cut the back-reef domain and that are  
290 oriented roughly perpendicular to the coastline and the reef crest (Fig.3).

## 291 **4.2. Outer slope**

### 292 **4.2.1 Overall slope profile**

293 The outer slope morphologies of Grande Terre were previously described by Bitoun and  
294 Récy (1982), Rigolot (1989), Flamand (2006) and Pelletier et al. (2012). The outer slope of the  
295 western margin is very steep with values up to 20° between 0 to 2000 m water depths. This  
296 margin is very abrupt as the upper part of the slope is also very steep (see W-01 and W-02  
297 profiles Fig.4). In comparison, the outer slope of the eastern margin, from Poindimié to Yaté, is  
298 smoother and extends over 15 to 20 km from the platform edge to the toe of slope at a water  
299 depth of approximately 2200 m (Fig. 4). It is composed of 3 domains: (1) the upper slope,

300 characterized by a slope gradient lower than 3°, between 100 to approximately 500 m water  
301 depths and extending up to 20 km in areas preserved from the erosion (e.g. offshore Côte  
302 Oubliée and Yaté, see E-01 profile Fig.4). On the contrary, some areas are devoid of an upper  
303 slope domain and canyon heads are ~~there~~ in ~~closed~~direct contact with the external barrier reef  
304 (e.g. offshore Houailou, see E-02 profile Fig.4); (2) the middle slope shows a slope gradient ~~of~~ up  
305 to 10° between 400-500 m to approximately 2200 m water ~~depths~~depth; (3) the lower slope and  
306 toe-of-slope domain shows a gentle slope gradient ranging from 0.5 ~~to~~to 1°. This slope section  
307 starts approximately at 2200 m water depth, which corresponds ~~to~~with the transition to ~~the~~  
308 Loyalty Basin floor. The slope section contains numerous erosional by-pass features such as  
309 submarine canyons that incise the slope up to a depth of 200 m. Backscatter imagery reveals  
310 depositional lobes at canyon mouths, offshore Thio and Yaté, as previously reported by Cotillon  
311 et al. (1989, 1990). The cut off angles are intended to characterize the morphology of the slope  
312 and have no universal value. Even in the case of a Gaussian slope angle evolution (*sensu* Adams  
313 and Kenter, 2013) angle values may vary between different carbonate systems.

#### 314 **4.2.2 Physiography of the upper slope**

315 The upper slope is delimited by a major scarp located at 300-400 m water depth close to  
316 the Cap Bayes Pass (Fig. 5A) and the Nakéti Pass (Fig. 6A), at 400-500 m water ~~depths~~depth in  
317 front of Côte Oubliée (Fig. 7A) and at 500-600 m water depths close to the Yaté Pass. The low-  
318 angle upper slope is only 3 to 4 km wide close to Nakéti Pass and widens southward to reach a  
319 width of 20 km in the vicinity of Yaté (Fig. 3A). Arcuate scars occur along the scarp, suggesting  
320 slope failure processes along the upper slope (Fig.5A and 6A). In front of Côte Oubliée, the 5-6  
321 km wide upper slope is incised by low sinuosity, U-shaped, 40 to 80 m deep gullies (Fig.7A).  
322 Gullies are of variable extension along the upper slope, some start at 150 m water depth close to  
323 the outer reef slope, whereas others, shorter, gullies start at 300 m water depth, 3-4 km away  
324 from the shelf edge. The majority of gullies are located in front of Kouakoué Pass through which  
325 they are connected to the meandering lagoonal channel (Fig.3A).

#### 326 **4.2.3 Stratigraphy of the upper slope**

327 Seismic profiles covering the platform edge to the upper slope region reveal two main  
328 seismic units, U1 and U2 separated by unconformity S1 (Fig. 5, 6 and 7). These profiles also  
329 show that U1 is exposed on the seafloor along a major scarp (see red arrows on maps and  
330 profiles of Fig. 5, 6 and 7). U1 comprises wavy reflections and is delimited at its top by erosional  
331 truncations and toplap terminations ~~on~~at bounding surface S1. The latter is overlain by unit 2  
332 (U2) which shows well-layered reflections downlapping onto S1 (Figs. 5, 6 and 7). The maximal  
333 thickness of U2 varies between 0.1 to 0.25 s twt. In front of Côte Oubliée, on profile NM-13, at  
334 the mouth of the Kouakoué Pass, U2 is twice ~~thicker~~as thick than on profile NM-12b located 20  
335 km further north at distance from any pass (Fig. 7).

336 Seismic profile NM1 at the mouth of the Cap Bayes Pass displays a well-developed unit  
337 U2 which forms a 0.2-0.25 s twt thick sedimentary prism (Fig. 5) composed of five stratigraphic  
338 sequences each composed of retrogradational sets (in pink on Fig. 5) overlain by progradational  
339 clinoform foresets (in beige on Fig. 5), noted 1 to 5. The slope break of the youngest (5<sup>th</sup>)  
340 clinoform foreset (annotated "Clinoform slope break" on Fig. 5) is located at 150 m water depth.  
341 Retrogradational sets contain low-amplitude, mound-shaped seismic reflections that are only  
342 observed in topsets. Progradational sets show high-amplitude sigmoidal oblique reflections that  
343 downlap onto the underlying unit and are mainly located in the distal part of the sedimentary  
344 prism.

#### 345 **4.3. Pines Ridge**

346 The Pines Ridge corresponds to the structural extension of the eastern margin of Grande  
347 Terre towards the South (Fig. 2). It is a NNW-SSE trending structure extending from the Isle of  
348 Pines to the Cook Fracture Zone.

349 **4.3.1 Basement structure and first-order seismic stratigraphy of the Pines**

350 **Ridge**

351 The Pines Ridge is a horst of peridotite bounded by normal faults (Bitoun & Recy, 1982;  
352 Patriat et al., 2018) and is the southern offshore extension of the Peridotite Nappe cropping out  
353 onland (Patriat et al., 2018). In this paper, we have studied the area comprised between the Isle  
354 of Pines and Antigonía seamount, where Pines Ridge is the shallowest (Fig. 8A). Seismic profile  
355 AUS-104 (Fig. 8B) reveals that the Pines Ridge comprises at its top high-amplitude subparallel  
356 reflections between 0.7 and 0.9 s twt, which contrast with the transparent seismic character of  
357 the underlying acoustic basement. Along the eastern flank of the Pines Ridge, the acoustic  
358 basement crops out on the seafloor at 2000 m water depth and was sampled by dredge GEO-I-  
359 3D (Daniel et al., 1976; Bitoun & Recy, 1982) (Fig. 8). The samples comprised altered basalt  
360 pebbles within a carbonate mud matrix containing planktonic foraminifera from the late  
361 Oligocene – earliest Miocene (Daniel et al., 1976). At that location, the acoustic basement forms a  
362 slightly tilted plateau located between 2.5 and 2.7 s twt, interpreted as an erosional weathering  
363 surface on top of peridotites by Bitoun and Recy (1982). This peridotite platform constitutes the  
364 western edge of the South Loyalty Basin (Figs. 8B and 8C). The peridotite basement is covered  
365 by a seismic unit composed of discontinuous low-amplitude subparallel reflections that is about  
366 0.2 s twt thick at the crest of the ridge and up to 0.6 s twt-thick on its eastern flank. This unit is  
367 interpreted as a post-obduction sedimentary sequence (Bitoun & Recy, 1982 ; Patriat et al.,  
368 2018). The unit is incised by several submarine canyons along the eastern slope that extend  
369 from the Pines Ridge to the South Loyalty Basin (Fig. 8).

370 **4.3.2 Physiography of the Pines Ridge**

371 Along the northern part of the Pines Ridge, on the upper slope, the terrace identified on  
372 the eastern outer slopes of Grande Terre is continuously present between 300 to 600 m water  
373 depths (red arrows on Fig. 8A). East of the Isle of Pines, this terrace is affected by arcuate scarps  
374 most likely corresponding to submarine gravity collapses. Towards the Antigonía seamount, the

375 top of the Pines Ridge is capped by this terrace (Fig. 2). Indeed, between the Banc de la Torche  
376 and Antigonina seamounts, the ridge's top remains positioned at 400-500 m water depth and its  
377 eastern slope is again characterized by a steep gradient and collapse features (red arrows on Fig.  
378 8A). In turn, the Banc de la Torche and Antigonina display flat tops in 30 m to 60 m water depths  
379 (blue arrows on Fig. 8A). These two submerged isolated banks are surrounded by two terraces  
380 at 80-90 m and 120 m water depth.

381 The isolated Cryphelia and Munida seamounts are delimited by a main scarp at 400-500  
382 m water depths (Figs.2 and 8). Their tops are located at 194 m and 93 m water depths,  
383 respectively. The Cryphelia seamount is 3 km wide and 12 km long elongated in a N160°  
384 direction (Fig. 9A and 9B). Three fault scarps located approximately in 250, 350 and 500 m  
385 water ~~depths~~ affect the seamount across its entire length ~~with~~. Fault scarp heights ~~are~~  
386 comprised between 30 m and 100 m (see map and cross section of Fig. 9B). In the northern part,  
387 the eastern fault scarp is associated with a channel probably formed by ~~the action of~~ bottom  
388 currents circulating along the footwall of the fault (Fig. 9A and 9B). The southern edge of the  
389 seamount is marked by two 2-3 km wide failure scars, evidenced by arcuate headscarps located  
390 between 350 to 600 m water ~~depths~~. The Munida seamount, located further to the  
391 northeast, extends over 8 km wide and 18 km long with a N60° direction (Fig. 9C). Its edges are  
392 bordered by N60° and N160° oriented fractures. On its southern flank, a terrace (M1) bordered  
393 by fault scarps is identified between 400 m and 600 m water depth. Above 200 m water depth,  
394 the top of the seamount (M2) is relatively flat (Fig. 9C) but still shows terraces at 100 m and  
395 120-130 m water depth.

#### 396 **4.3.3 Stratigraphy of the Pines Ridge**

397 The internal architecture of the post-obduction sedimentary sequence overlying  
398 basement of Pines Ridge and Munida seamount are imaged by seismic profile 206-04 (Fig.10).  
399 Over the Pines Ridge, the capping sedimentary unit reaches up to 0.5 s twt thick, i.e.  
400 approximately 750 m thick considering a velocity of 3000 m.s<sup>-1</sup> for a 30% porosity limestones

401 according to Geldart (2004). In details, this interval is composed of 3 units, UP1 to UP3 (Fig.10C  
402 and 10D). Unit UP1 mainly developed on the SW edge of the ridge and is composed of low-  
403 amplitude reflections northeastwardly downlapping on basement. Unit UP2 downlaps basement  
404 on the eastern edge of the ridge with very low-amplitude reflections that form mounded  
405 morphologies. To the west, the seismic character of UP2 laterally evolves into low-amplitude,  
406 wavy to horizontal parallel reflections onlapping onto UP1 towards the southwest. Unit UP3 is  
407 typified by low-amplitude, sub-parallel and nearly horizontal reflections with low relief,  
408 mounded morphologies on the eastern edge of the ridge. Because seismic line 206-04 runs along  
409 the south-eastern slope of Munida Seamount (Fig. 9C), seismic imaging is poor due to 3D lateral  
410 effects. However, the profile intersects a part of the seamount with less slope that reveals that  
411 the sedimentary sequence has a minimum thickness of 0.4 s twt, i.e. approximately 600 m-thick  
412 (Fig.10A and 10B). It is composed of two distinct seismic units, UM1 and UM2 (Fig.10). Unit UM1  
413 overlies the basement and comprises low-amplitude subparallel mounded reflections with  
414 downlapping and onlapping terminations. Unit UM2 overlies UM1 and comprises high-  
415 amplitude subparallel reflections with downlapping terminations.

#### 416 **4.4. Lithologies and biostratigraphic ages**

##### 417 **4.4.1 Eastern margin of Grande Terre**

418 Seven carbonate rock samples have been collected along the upper slope of the eastern  
419 margin (Table 3, see location on Fig. 2). DR44 and DR45 were recovered on scarps located at  
420 400 m and 600 m water depths, at the seafloor exposure of seismic unit U1 (see location on Figs.  
421 6A and 6B). DR44 is a micritic packstone with recrystallised algae, large benthic foraminifera  
422 (LBF) of Serravallian age (PZ N12, Tf2, 13.82 Ma to 12.00 Ma) (see BouDagher-Fadel, 2018b)  
423 and corals. These elements are reworked within a pelagic mud dominated by plancktonic  
424 foraminifera (Table 4) that comprise *Globigerinoides quadrilobatus* (Fig.11A, b.),  
425 *Dentoglobigerina altispira* (Fig.11B, b.), *Globorotalia menardii* (Fig.11B, c.), *Globigerinoides*  
426 *conglobatus* (Fig.11B, d.), *Globigerinoides ruber* (Fig.11B, e.), *Truncorotalia crassaformis*, *Orbulina*

427 *universa*, *Globorotalia plesiotumida* (Fig.11C, a), *Sphaeroidinella dehiscons* of Early Pliocene age  
428 (N19-N20a, 5.3 Ma to 3.6 Ma). DR45 comprises ultramafic pebbles and gravels encrusted by  
429 algae incorporated in a micritic packstone similar to that of DR44 and also includes  
430 *Lepidocyclina* sp. (Fig. 11D) and *Alveolinella praequoyi*, with the same Serravallian age. DR46,  
431 DR47 and DR48 were collected on the edge of the terrace located between 200 to 400 m water  
432 depths near the Nakéti Pass (Figs. 6A and 6C). These three samples consist of micritic  
433 wackestone/packstones with patches of reworked pelagic micritic facies. DR46 assemblages are  
434 dominated by planktonic foraminifera such as *Truncorotalia crassaformis* (Fig. 11E, a.) *T.*  
435 *truncatulinoides*, *Globorotalia inflata*, *Globorotalia menardii* and *Orbulina univesa* of Pleistocene  
436 age (N22, 1.8 Ma to 0.12 Ma). DR47 sample shows numerous terrigenous grains (quartz, altered  
437 serpentine and undifferentiated clasts). Planktonic foraminifera are common and include  
438 *Globoquadrina dehiscons* (Fig. 11F, a.), *Globigerinoides quadrilobatus*, *Globigerinoides trilobus*,  
439 *Globigerinoides ruber*, *Globorotalia tumida*, *Globigerinoides spp.*, and *Pulleniatina obliquiloculata*  
440 of Late Pliocene age (N20a, 3.8 Ma to 3.6 Ma). DR48 contains numerous recrystallized algae and  
441 reworked LBF, such as *Alveolinella praequoyi* (Fig. 12A, a.) of Serravallian age (see Adams, 1984;  
442 BouDagher-Fadel and Banner, 1999; BouDagher-Fadel, 2018b), planktonic foraminifera of  
443 Pleistocene in age (N22, 1.8 Ma to 0.12 Ma) such as *Pulleniatina obliquiloculata* (Fig. 12A, b.), *P.*  
444 *primalis* and *Neogloboquadrina dutertrei*. DR49 sample was collected along the scarp at 500 m  
445 water depth, near the East Ngoé pass. The lower part of this scarp corresponds to the top of  
446 seismic unit U1 (Table 3, see location Figs.7A and 7B). Recovered samples comprise a micritic  
447 packstone composed of with algae and LBF of Serravallian age, such as *Alveolinella praequoyi*  
448 (Fig. 12B, a.) and planktonic foraminifera such as, *Globorotalia tumida* (Fig.12C, a.),  
449 *Sphaeroidinellopsis subdehiscons*, *Globorotalia menardii* and *Globorotalia inflata* of Early Pliocene  
450 age (N19b, 4.2 Ma to 3.8 Ma) after BouDagher-Fadel (2018a). DR53 is located further south, in  
451 front of the Yaté Pass, in ca. 280 m water depth, and is a micritic packstone containing  
452 planktonic foraminifera such as *Pulleniatina primalis* (Fig.12D, a.), *Prosphaeroidinella parkerae*,

453 *Pulleniatina praecursor*, *Globigerinoides obliquus* and *Truncorotalia crassaformis* of Late Miocene  
454 to Early Pliocene age (Table 3, see location Fig.2).

#### 455 **4.4.2 Pines Ridge**

456 Seven carbonate rocks were sampled along the Pines Ridge (Table 3, see location Fig. 2  
457 and Fig.8A). These samples are mainly micritic wackestones/packstones with planktonic  
458 foraminifera and algae. Samples DW4737-B, DW4745-B, DW4746-B, DW4747-B1 and DW4747-  
459 X have ages ranging from Pliocene to Late Pleistocene (N19 to N22, 5.33 Ma to 0.12 Ma).  
460 Planktonic foraminifera assemblages of these samples include *Neogloboquadrina pachyderma*,  
461 *Sphaeroidinella dehiscens*, *Truncorotalia truncatulinoides*, *Truncorotalia tosaensis*, and  
462 *Pulleniatina obliquiloculata* and LBF, such as *Alanlordia* sp. (Fig.12E, a.), are found reworked  
463 together with Pliocene planktonic foraminifera into the younger assemblages. Further south,  
464 samples DW4757-A and DW4782-A were collected along the eastern slope of Pines Ridge (Table  
465 3, see location Fig.8A and Fig.10). DW4757-A includes Oligocene to earliest middle Miocene LBF  
466 such as *Lepidocyclina* sp. and *Planorbulinella solida* (Fig.12F, a.), while DW4782-A comprises late  
467 Miocene to Pleistocene (N17-N20, 8.6 Ma to 3.4 Ma) planktonic foraminifera such as  
468 *Neogloboquadrina humerosa*, *Sphaeroidinellopsis seminulina*, *Sphaeroidinellopsis subdehiscens*.

#### 469 **4.4.3 Munida seamount**

470 Three carbonate rock samples have been collected along the edges of *Munida* (Table 3,  
471 see location on Fig. 8A and Fig. 9C). Samples from DW4770, located on the northeast flank of the  
472 seamount, comprise micritic and sparitic packstones composed of algae and planktonic  
473 foraminifera, such as *Truncorotalia truncatulinoides* (Fig.12F, a) and *Truncorotalia tosaensis*  
474 (Fig.12F, b) of Pleistocene age (N22, 1.8 Ma to 0.12 Ma). DR4772-A and DR4773-A samples,  
475 located on the southern flank, are grainstones cemented by sparite, with planktonic  
476 foraminiferal assemblages including *Sphaeroidinellopsis subdehiscens*, *Sphaeroidinella dehiscens*,  
477 *Truncorotalia tosaensis* and *Pulleniatina obliquiloculata* of Pliocene to Pleistocene age (N21-N22,

478 3.4 Ma to 0.12 Ma). These samples also reveal many reworked Miocene and Pliocene planktonic  
479 foraminifera.

#### 480 4.5. *Paleoenvironmental interpretations*

481 The assemblages of DR44 and DR45 are dominated by Early Pliocene planktonic  
482 foraminiferal assemblages (e.g. *Sphaeroidinellopsis paenedehiscens*, *Globoquadrina dediscens*,  
483 *Orbulina universa*, *Globorotalia plesiotumida*, *G. tumida* and *Dentoglogigerina altispira*). These  
484 mixed, globular and heavily keeled planktonic foraminifera are indicative of inner to outer  
485 neritic environments (BouDagher-Fadel, 2015). Miocene larger benthic foraminifera (e.g.  
486 *Lepidocyclina* sp., *Katacycloclypeus martini*, *Cycloclypeus* sp.) and fragments of corals and  
487 rodophyte species are also frequently reworked within the deeper Early Pliocene platform.  
488 These larger benthic foraminifera are flat in shape and are associated with symbiont-bearing  
489 diatoms (Leutenegger 1984; Romero et al. 2002). They are common in forereef environment  
490 where they adapted to light attenuation with increasing habitat depth ([Hottinger, 1983](#); Hallock  
491 and Schlager, 1986; [Hohenegger, 1995; 2005; Yordanova & Hohenegger, 2002; 2007](#);  
492 BouDagher-Fadel, 2018b).

493 The Late Pliocene to Pleistocene deposits of DR46, DR47 and DR48 contain mainly  
494 planktonic foraminifera of mixed assemblages of globular forms (e.g. *Globigerinoides*  
495 *quadrilobatus*, *Orbulina universa*) and keeled globorotalids (e.g. *Truncorotalia truncatulinoides*,  
496 *Globorotalia tumida*). These assemblages are indicative of an inner to outer neritic environment  
497 (see BouDagher-Fadel, 2015). Micritic patches of older Miocene deposits with mainly globular  
498 small globigerinids (e.g. *Catapsydrax cf. dissimilis*, *Globigerina praebulloides*) are also present  
499 indicating the reworking of an inner neritic Miocene platform within the deeper deposits of the  
500 Pliocene.

501 DR 49 is interpreted as being deposited in an Early Pliocene inner to outer neritic  
502 platform. It contains planktonic foraminifera assemblages dominated by globular forms (e.g.  
503 *Globorotalia menardii*, *G. inflata*, *Globigerinoides trilobus*, *Gldes quadrilobatus*) with occasional  
504 occurrences of keeled forms (e.g., *Globorotalia tumida*, *G. menardii*) and thickly coated forms in a  
505 thick, smooth cortex of calcite, *Sphaeroidinerlla dehiscens*. The latter is an extant thermocline  
506 dweller found rarely in subsurface, tropical, and subtropical waters (Chaisson and Ravelo, 1997;  
507 BouDagher-Fadel, 2018b). Reworked reefal Miocene larger benthic foraminifera (e.g.,  
508 *Alveolinella praequoyi*, *Lepidocyclina* sp., *Planorbulina larvata*, *Amphistegina lessonii*,  
509 *Operculinoides* spp., *Gypsina* sp.) are also present. The presence of the large fusiform miliolid, *A.*  
510 *praequoyi* indicates the reworking of quiet shallow reefal facies into the deeper Early Pliocene  
511 neritic environments.

512 The assemblages of DR53 are dominated by Late Miocene to Early Pliocene globular  
513 planktonic foraminifera species (e.g., *Neogloboquadrina pachyderma*, *N. acostaensis*, *Orbulina*  
514 *universa*, *Prosphaeroidinella parkerae*, *Pulleniatina praecursor*, *P. primalis*, *Globigerinoides*  
515 *obliquus*). Occasional keeled forms (e.g., *Truncorotalia crassaformis*, *Globorotalia menardii*,  
516 *Globorotalia tumida*) are also present. Larger benthic foraminifera such as *Amphistegina* spp. and  
517 *Sphaerogypsina* spp. are also found. The extant *Amphistegina* has adapted to high energy  
518 conditions, however, it is also found in mud free sands in areas of sea grass or coralline algae  
519 and in reefal areas down to depths of 35m (McKee et al, 1959), while *Sphaerogypsina* is  
520 generally common in shallow-water reefal environments (Nebelsick et al. 2001). These  
521 assemblages are interpreted as being deposited in an inner to outer neritic platform.

Formatted: Font: Italic

522 All samples from Pines Ridge point to inner to outer neritic settings, except DW4757-A  
523 which is typified by a forereef environment because of the occurrence of larger benthic  
524 foraminifera, such as *Amphistegina lessonii*, *Lepidocyclina sp.*, and *Planorbulinella solida*. All  
525 samples from Munida seamount contain mixed assemblages of globular and keeled planktonic  
526 foraminifera (e.g., *Sphaeroidinellopsis subdehiscens*, *Sphaeroidinella dehiscens*, *Truncorotalia*  
527 *tosaensis*, *Pulleniatina obliquiloculata*, *Globorotalia inflata*) and are thought to reflect inner to  
528 outer neritic settings.

529

## 530 **5. CARBONATE SYSTEM EVOLUTION ON THE EASTERN MARGIN OF** 531 **NEW CALEDONIA**

### 532 ***5.1 Mio-Pliocene carbonate banks***

533 Carbonate rocks sampled on the upper slope scarp along the eastern margin contain  
534 algae, benthic foraminifera and coral fragments evidencing shallow-water carbonate production  
535 as early as the middle Miocene (Serravalian) and up to the Pliocene (Table 3, Fig. 13). This scarp  
536 corresponds to the top of seismic unit U1, which is bounded by the gently downslope dipping  
537 surface S1 (Figs. 5, 6 and 7). Because of its planar character, Chardon et al., (2008) interpreted  
538 this surface, topping a clastic continental wedge, as a lateritic land surface formed by weathering  
539 during emersion. Because none of the dredges that sampled this scarp (and thus U1) contained  
540 any traces of lateritic deposits, we propose an alternative interpretation where seismic unit U1  
541 corresponds to a Mio-Pliocene carbonate bank, presently located at 300-600 m water depth.  
542 This important [drowningsubsidence](#) cannot be explained only by eustatism and we suggest that  
543 the post-obduction normal faulting that affected the Peridotite Nappe is likely the main driver of  
544 the [drowningsubsidence](#). Surface S1 is interpreted as the top of the carbonate bank  
545 characterized by low-inclination features (Fig. 13A and B). The numerous ultrabasic  
546 pebbles/gravels and quartz grains within the carbonate matrix of samples DR45 and DR47

547 suggest coeval siliciclastic ~~inputs~~input with the carbonate buildup development. A similar mixed  
548 carbonate-siliciclastic system also occurs along the coastal domain of the western margin of  
549 Grande Terre in the well-constrained Burdigalian Népoui system (Tournadour et al., 2020)  
550 (Fig.13B). The onset of these mixed systems indicates that both margins of Grande Terre ~~were~~  
551 ~~inexperienced~~ shallow marine conditions during the Miocene. However, their current positions,  
552 up to 20 m above present day sea-level for the Lower Miocene ~~Népoui~~Népoui outcrops of the  
553 western margin and up to 500 m water depth for the middle Miocene samples of the eastern  
554 margin, suggest a contrasted tectonic evolution of the margins.

555 Our results suggest that the Mio-Pliocene carbonate platform (Table 3, Fig.13) extended  
556 southward along the Pines Ridge, over peridotite horsts, which were at that time located in  
557 shallow-water (Fig.13A and B). Within this sedimentary succession, unit UP1 is interpreted as an  
558 attached carbonate platform developing on the western edge of the ridge. The eastward  
559 thickening of unit UP2, which unconformably overlies unit UP1 (Fig.10D), suggests a deposition  
560 simultaneous or subsequent to the eastward tectonic tilting of Pines Ridge. The aggrading  
561 mounded reflections of the lower part of UP2 on the eastern edge of the ridge, may be  
562 interpreted as shallow-water, reefal bioconstructions (e.g. Miocene from the Browse basin,  
563 Australia: Belde et al., 2017), or as an oligo-mesophotic bank with dominant algal and  
564 foraminiferal production (e.g. Lower Miocene from Myanmar: Teillet et al., 2020a and 2020b).  
565 However, in the upper part of UP2, the upward change from mounded to flat-topped  
566 morphologies on the eastern margin strongly suggests the development of reef-flat  
567 environments aggrading up to sea-level. Finally, subunit UP3 is also characterized by a slight  
568 overgrowth along the eastern edge as evidenced by low-relief mounded reflectors (Fig.10). Such  
569 an asymmetric feature could be explained by the continuation of an eastward tectonic tilt or  
570 could be related to eastward winds driving carbonate growth (Fig.10).

571 Based on seismic interpretation, two stages of carbonate growth are identified on the  
572 Munida seamount (seismic units UM1 and UM2). A carbonate sample, collected 15 km away  
573 from the seamount (GEO-I-13D, ~~located;~~ location on Fig.2), contains benthic foraminifera

574 indicative of shallow-water environment, that can be dated Early Miocene (Daniel et al., 1976;  
575 Bitoun and Recy, 1982). This sample suggests a first stage of carbonate growth (UM1) of  
576 Miocene age coeval ~~to~~with carbonate platforms from Pines Ridge (UP1 and/or UP2) (Fig.13A  
577 and B). A Miocene carbonate platform also likely developed on the Crypthelia seamount as  
578 suggested by a Middle to Late Miocene carbonate sample exhibiting forereef facies (GEO-I-9D,  
579 see location Fig.2 and Fig.9A) (Daniel et al., 1976; Bitoun and Recy,1982).

580 Based on ~~these~~forementioned observations, we propose ~~at~~he following  
581 palaeogeographical reconstruction of the distribution of Mio-Pliocene shallow-water carbonate  
582 systems along the margin of New Caledonia (Fig. 13B). The Mio-Pliocene carbonate systems  
583 extend for about 350 km, along the southeastern margin to Antignonia Seamount. On the western  
584 margin, the Quaternary carbonate reef-lagoon system directly overlies Eocene allochthonous  
585 units (see Fig.1). At that location, the absence of Miocene shallow-water deposits could be  
586 explained by a non-deposition or by erosion in relation to the uplift of the western margin. The  
587 thickness of the Miocene ramp is a least 200 m on the Nepoui area (Maurizot et al., 2016;  
588 Tournadour et al, 2020), but remains unknown along the eastern margin, ~~but~~ However, it can  
589 be estimated to be around 750 m on the Pines Ridge (Fig.10B). Similar Miocene carbonate  
590 ~~growths~~growth rates have been reported ~~in~~for the southwestern Pacific suggesting that, in  
591 addition to local tectonic control (subsidence) allowing significant volumes of sediments to  
592 accumulate, larger-scale oceanographic or global factors favoured a sufficiently high carbonate  
593 production to fill the created accommodation ~~space~~. For example, the 600 m-thick Marion  
594 Plateau platforms, northeast of Australia, result from a robust carbonate growth through early  
595 and middle Miocene up to ~~its~~ terminal demise in ~~the~~ late Miocene (Ehrenberg et al., 2008). Along  
596 the northwestern shelf of Australia, seismic profiles reveal a giant middle Miocene prograding  
597 barrier reef that backstepped in the late Miocene (McCaffrey et al., 2020). Finally, the Gulf of  
598 Papua is also structured by large-scale isolated long-lived carbonate platforms during the late  
599 Oligocene-early Miocene and which demised during late Miocene-early Pliocene (Tcherepanov  
600 et al., 2008,2008b). In our study, the prolific Mio-Pliocene carbonate accumulation is favoured by

601 the subsidence of the shelves of New Caledonia and Pines Ridge, most likely in relation to post-  
602 obduction extensional tectonics (Lagabrielle and Chauvet, 2008; Patriat et al., 2018).

## 603 **5.2 Transition from Mio-Pliocene to Quaternary platforms**

604 Along the eastern margin of Grande Terre, the Quaternary rimmed platform is thought to  
605 have backstepped onto a Mio-Pliocene carbonate bank (Fig. 13A and 13C). Southward, along the  
606 Pines Ridge and associated seamounts, the Mio-Pliocene carbonate banks are drowned but  
607 several Quaternary flat-topped isolated platforms survived and aggraded.

608 In the vicinity of the study area, the carbonate platform of Maré, on the Loyalty Ridge,  
609 records a significant change in the nature of carbonate production which is rhodalgal-dominated  
610 during the late Miocene, and coralgal-dominated during the Pliocene (McNeill and Pisera, 2010;  
611 Maurizot et al., 2020). These authors explain the switch of carbonate production by the trend of  
612 decreased coralline red algae species richness (Aguirre et al., 2000) combined ~~to~~with the global-  
613 scale Zanclean Flood Event (McKenzie et al., 1999). The exposure of these carbonate records  
614 would result from the local tectonic uplift of the Loyalty Ridge related to Pliocene-Pleistocene  
615 lithospheric flexure associated with the New Hebrides subduction (Dubois et al., 1974 and  
616 1975).

617 Along the western margin of Grande Terre, the coral reef flourished from 400 ky (MIS-  
618 11) considered as a period of luxuriant reef expansion in the southwest Pacific (Cabiocch et al.,  
619 2008b). Nevertheless, during the Quaternary, non-reefal carbonates were identified prior to  
620 MIS-11 as early as 1.4 Ma, overlapping the Eocene allochthonous units and could form the  
621 foundation of the Quaternary rimmed platform (Cabiocch et al., 2008b; Montaggioni et al., 2011).

622 Along the eastern margin, the occurrence of a Mio-Pliocene platform below the eastern  
623 barrier reef-lagoon suggests that an older carbonate platform developed similarly to what is  
624 observed in Maré Island. The common occurrence of normal faults suggests that the eastern  
625 margin and Pines Ridge were dominated by tectonic subsidence that would have promoted

626 accommodation for Neogene carbonate deposition and preservation, by opposition to the  
627 western margin where the Quaternary carbonates are found on top of ~~eocene~~Eocene peridotites.  
628 However, high subsidence rates could also explain the demise of the Mio-Pliocene carbonate  
629 systems along the Pines Ridge and the backstepping of Quaternary platforms. After 125 ky, the  
630 southeastern margin is slightly uplifted in the Yaté area and the Isle of Pines (Launay, 1985;  
631 Cabioch et al., 1996). This uplift could be due to the isostatic rebound of the central part of  
632 Grande Terre (Cabioch et al., 1996; Lagabrielle and Chauvet, 2008) or alternatively, could be  
633 associated with the lithospheric bulge of the New Hebrides subduction which is known to have a  
634 regional impact from the Loyalty Islands to the Isle of Pines (Dubois et al., 1974 and 1975;  
635 Cabioch et al., 1996). ~~In any cases~~Hence, both margins of New Caledonia seem to have been  
636 affected by long-term subsidence during the Quaternary which, together with high-amplitude  
637 eustatic sea-level variations, allowed the aggradation and preservation of the reef-lagoon  
638 successions.

### 639 **5.3 Quaternary carbonate platform**

#### 640 **5.3.1 Late Quaternary mixed carbonate siliciclastic systems along the eastern** 641 **margin**

642 At the mouth of the Cap Bayes Pass, seismic unit U2 forms a 200 m-thick prism  
643 comprising five stratigraphic sequences (Fig. 5). In detail, the internal geometries of these  
644 parasequences are characterized by successive sets of aggrading to retrograding mounded  
645 reflections and progradational inclined reflections. We interpret these parasequences as mixed  
646 carbonate-siliciclastic prisms that developed at the mouth of the pass, with aggrading ~~teand~~  
647 retrograding shallow-water carbonate ~~transgressive~~ sequences that developed during a  
648 transgression (pink colour on Fig. 5C), deposited during the last glacial-interglacial Quaternary  
649 cycles. This interpretation is consistent with core data collected on the western barrier reef (see  
650 location of Fig. 1), which revealed that the barrier reef itself ~~is constituted by~~consist of four to  
651 five lithological sequences deposited during successive transgressions and highstands in sea

652 [level](#) since the Mid-Brunhes, each transgressive reefal units being separated by subaerial  
653 unconformities (subaerial exposures) (Cabiocch et al., 2008b; Montaggioni et al., 2011). The  
654 prograding seismic patterns (yellow colour on [Fig.5C](#)) [are thus can be](#) interpreted as lowstand  
655 siliciclastic [wedgewedges that](#) formed during Late Quaternary glacial lowstands.

656 Siliciclastics might have [thus](#) developed contemporaneously with the Quaternary barrier  
657 reef bordering the eastern lagoon ([Figs. 5, 6B and 7](#)). This observation is consistent with the  
658 reciprocal sedimentation concept traditionally developed for carbonate-siliciclastic mixed  
659 systems (see review by Chiarella et al., 2017). According to this concept, siliciclastic deposits  
660 prevailed on the upper slope during [low](#) sea-level [periods/lowstands](#) and at the beginning of the  
661 [platformshelf](#) reflooding, whereas carbonate facies dominate during transgressions and  
662 highstand periods. This configuration is currently observed on the platform edge of Quaternary  
663 mixed carbonate-siliciclastic systems such as the Australia and Papua New Guinea Reef  
664 ([Tcherepanov et al., 2008a; 2008b; 2010](#); Harper et al., 2015; Mallarino et al., 2021) or the Belize  
665 Barrier Reef ([Esker et al., 1998; Ferro et al., 1999](#); Gischler et al., 2010; Droxler and Jorry, 2013).

666 However, the reciprocal pattern is not expressed everywhere along the upper slope of the  
667 eastern margin. Near the Côte Oubliée, seismic unit U2 is not characterized by sedimentary  
668 prograding [clineform/clinoforms](#) but rather by a downlapping aggrading wedge with a maximum  
669 thickness of 200 m in front of the Kouakoué Pass ([Fig.7](#)). The lack of prograding features  
670 associated with [the](#) lowstand clastic wedge could be explained by low terrigenous sedimentation  
671 rates as suggested by small deltas restricted to [the](#) coastal domain ([Fig. 3A](#)). Moreover, the  
672 southeastern part of the lagoon is characterized by a meandering channel network parallel to  
673 the coast and to the barrier reef, suggesting an alongshore transport which can partly intercept  
674 outgoing sedimentary flux from lagoon ([Fig. 3A](#)). In addition, the numerous gullies cutting the  
675 upper slope suggest ~~a~~ high off-bank sediment transport toward the deep basin and thus the  
676 accumulation of sediments along the upper slope ([Fig. 7A](#)). This off-bank sediment transport  
677 could result from density cascading processes driven by seasonal meteorological conditions  
678 (Wilson and Roberts, 1992, 1995). The alongslope heterogeneity of the eastern margin upper

679 slope deposits clearly shows that the behaviour of a mixed carbonate-siliciclastic margin is  
680 difficult to predict and is not only dependent of relative sea-level changes, as mentioned  
681 previously (Chiarella et al., 2017; O'Connell et al., 2020).

### 682 **5.3.2 Quaternary isolated flat-topped banks of Pines Ridge and seamounts**

683 Along the Pines Ridge, dredged carbonate rock samples show that shallow-water  
684 carbonate deposition occurred on the Banc de la Torche and Antigonina seamounts during the  
685 Quaternary (Fig.13A and C). The two marine terraces at 80-90 m and 120 m water depth might  
686 evidence reef backstepping during the last deglacial sea-level rise, as reported around the Great  
687 Barrier Reef (Webster et al., 2018), the Gulf of Mexico (Khanna et al. 2017), the Maldives  
688 (Fürstenau et al., 2010; Rovere et al., 2018), the SW Indian Ocean (Jorry et al., 2016), the  
689 Marquesas Island (Cabiocch et al., 2008a) and in Tahiti (Camoin et al., 2012). Carbonate rock  
690 samples dated at the youngest from the Pleistocene and collected on the flat-top of the Munida  
691 seamount that is currently submerged in 93 m water depth, are thought to be representative of  
692 seismic unit UM-2 which would correspond to the last stage of the carbonate platform's growth.  
693 Similarly to the Banc de la Torche and Antigonina, the flat-top of the eastern part of the Munida  
694 seamount is currently located in the photic zone which suggests a continuous carbonate  
695 aggradation from the Miocene to the Quaternary. Such a continuous deposition was possibly  
696 favoured by a slower subsidence at that location compared to other seamounts (Fig.13). The  
697 Cryptothelia seamount that is submerged at 194 m water depth is affected by three N160°E  
698 normal faults scarps, leading to an overall eastward deepening of the seamount topography  
699 along several stepped terraces at ca 200 m, 300 m and 350 m water depths (Fig.9A). The lack of  
700 samples on these stepped terraces does not allow us to determine if the carbonate factory was  
701 active during the Quaternary and when the isolated carbonate platform was drowned (Fig.13A).

702

703 **6. CONCLUSIONS**

704 The eastern margin of Grande Terre records the evolution of a shallow-water mixed  
705 carbonate-siliciclastic system, with the successive development an aggrading Mio-Pliocene  
706 carbonate bank and a backstepping Quaternary barrier reef.

707 - ~~a~~A Mio-Pliocene shallow-water carbonate platform, presently drowned at 300 to 600 m water  
708 depth, extends about 350 km from Ponerihouen to Antigonja seamount and can be up to 750 m  
709 thick along the Pines Ridge.

710 - ~~in~~In front of Grande Terre, the Mio-Pliocene carbonate sediments are mixed with quartz grains  
711 and ultrabasic pebbles, which ~~attests-of-document~~ terrigenous inputs resulting from high relief of  
712 ~~the island topography~~ dismantling coeval with carbonate production as early as ~~the~~ Serravalian.

713 - ~~The~~ transition between the aggrading Mio-Pliocene carbonate bank and the backstepping  
714 Quaternary carbonate platforms along the eastern margin could be explained by ~~the~~ regional  
715 subsidence context driven by ~~an~~ extensional tectonic regime or by global climate change  
716 associated with Late Quaternary high-amplitude sea-level variations and/or changes of  
717 carbonate producers through time.

718 - ~~The~~ stratigraphic architectures of mixed carbonate-siliciclastic systems, represented by the  
719 Quaternary reef-lagoon complex along the upper slope, vary widely from north to south. In front  
720 of the Cap Bayes Pass, this contribution evidences for the first time in New Caledonia the  
721 presence of ~~a~~ lowstand terrigenous prism alternating with transgressive shallow-~~water~~  
722 carbonate sequence, typical to reciprocal sedimentation models. ~~Nerveless~~Nevertheless, this  
723 configuration is not observed southward, probably because other control parameters prevailed  
724 such as low terrigenous inputs, the particular morphology of the paleo-drainage network, which  
725 appears parallel to the coastline, or the high by-pass ~~sediment~~ transport toward the deep basin.

726

727 **7. ACKNOWLEDGEMENTS**

728 We thank Editor M. Rebesco, reviewer John J.G. Reijmer and an anonymous reviewer for their  
729 constructive comments on an early version of this paper. We are also grateful to John Butcher  
730 (IRD Nouméa) who provided access to samples.

731 **REFERENCES**

- 732 Adams, C.G., 1984. Neogene larger foraminifera, evolutionary and geological events in the context of datum planes, in:  
733 Ikebe, N., Tsuchi, R. (Eds.), Pacific Neogene Datum Planes. Tokyo, pp. 47–67.
- 734 Adams, E., Kenter, J.A.M., 2013. So different, yet so similar: comparing and contrasting siliciclastic and carbonate  
735 slopes, in: Verwer, K., Playton, T.E., Harris, P.M. (Eds.), Deposits, Architecture and Controls of Carbonate Margin,  
736 Slope and Basinal Settings, SEPM Special Publication. Tulsa, Oklahoma, pp. 14–25.
- 737 Aguirre, J., Riding, R., Braga, J.C., 2000. Diversity of coralline red algae: origination and extinction patterns from the  
738 Early Cretaceous to the Pleistocene. *Paleobiology* 26, 651–667. [https://doi.org/10.1666/0094-  
739 8373\(2000\)026<0651:DOCRAO>2.0.CO;2](https://doi.org/10.1666/0094-8373(2000)026<0651:DOCRAO>2.0.CO;2)
- 740 Andréfouët, S., Cabioch, G., Flaman, B., Pelletier, B., 2009. A reappraisal of the diversity of geomorphological and  
741 genetic processes of New Caledonian coral reefs: a synthesis from optical remote sensing, coring and acoustic  
742 multibeam observations. *Coral Reefs* 28, 691–707. <https://doi.org/10.1007/s00338-009-0503-y>
- 743 Anselmetti, F.S., Eberli, G.P., 2001. Sonic Velocity in Carbonates— A Combined Product of Depositional Lithology and  
744 Diagenetic Alterations, in: Ginsburg, R.N. (Ed.), Subsurface Geology of a Prograding Carbonate Platform Margin,  
745 Great Bahama Bank: Results of the Bahamas Drilling Project. SEPM Society for Sedimentary Geology, p. 0.  
746 <https://doi.org/10.2110/pec.01.70.0193>
- 747 Belde, J., Back, S., Bourget, J., Reuning, L., 2017. Oligocene and Miocene carbonate platform development in the Browse  
748 basin, Australian northwest shelf. *Journal of Sedimentary Research* 87, 795–816.  
749 <https://doi.org/10.2110/jsr.2017.44>
- 750 Bitoun, G., Recy, J., 1982. Origine et évolution du bassin des Loyauté et de ses bordures après la mise en place de la  
751 série ophiolitique de Nouvelle Calédonie, in: Contribution à l'étude Géodynamique Du Sud-Ouest Pacifique,  
752 Travaux et Documents ORSTOM. pp. 505–540.
- 753 Boudagher-Fadel, M.K., 2018a. Evolution and Geological Significance of Larger Benthic Foraminifera, ~~Seconde~~Second  
754 edition. ed. UCL Press.
- 755 Boudagher-Fadel, M.K., 2018b. Revised diagnostic first and last occurrences of Mesozoic and Cenozoic planktonic  
756 foraminifera. UCL Office of the Vice-Provost Research, Professional Papers Series, UCL Press 1–5.
- 757 Boudagher-Fadel, M.K., 2015. Biostratigraphic and geological of planktonic foraminifera, Updated second edition. ed.  
758 UCP Press.
- 759 Boudagher-Fadel, M.K., Banner, F.T., 1999. Revision of the stratigraphic significance of the oligocene-miocene "Letter-  
760 Stages." *Revue de Micropaléontologie* 42, 93–97. [https://doi.org/10.1016/S0035-1598\(99\)90095-8](https://doi.org/10.1016/S0035-1598(99)90095-8)
- 761 Brachert, T.C., Forst, M.H., Pais, J.J., Legoinha, P., Reijmer, J.J.G., 2003. Lowstand carbonates, highstand sandstones?  
762 *Sedimentary Geology* 155, 1–12. [https://doi.org/10.1016/S0037-0738\(02\)00329-9](https://doi.org/10.1016/S0037-0738(02)00329-9)
- 763 Cabioch, G., Montaggioni, L., Frank, N., Seard, C., Sallé, E., Payri, C., Pelletier, B., Paterne, M., 2008a. Successive reef  
764 depositional events along the Marquesas foreslopes (French Polynesia) since 26 ka. *Marine Geology* 254, 18–34.  
765 <https://doi.org/10.1016/j.margeo.2008.04.014>

Field Code Changed

Formatted: English (United States)

Field Code Changed

- 766 Cabioch, G., Montaggioni, L., Thouveny, N., Frank, N., Sato, T., Chazottes, V., Dalamasso, H., Payri, C., Pichon, M., Sémah,  
767 A.-M., 2008b. The chronology and structure of the western New Caledonian barrier reef tracts. *Palaeogeography,*  
768 *Palaeoclimatology, Palaeoecology* 268, 91–105. <https://doi.org/10.1016/j.palaeo.2008.07.014>
- 769 Cabioch, G., Pelletier, B., Boré, J.-M., Panché, J.-Y., Perrier, J., 2002a. Campagne Boisalis 1, Cartographie multifaisceaux et  
770 dragages des pentes du récif barrière Est (Poindimié) et Sud-Est (Goro) de Nouvelle-Calédonie. Transport et  
771 débarquement du matériel de forage sur l'îlot Bayes. (No. 44). Rapports de missions. Sciences de la Terre,  
772 Géologie Géophysique, Centre IRD de Nouméa.
- 773 Cabioch, G., Pelletier, B., Perrier, J., Régnier, M., Varillon, D., 2002b. Campagne Boisalis 2, cartographie multifaisceaux et  
774 dragages des pentes du récif barrière Sud-Est (Goro) et cartographie des passes de Mato et Boulari, Nouvelle-  
775 Calédonie. (No. 45). Rapports de missions. Sciences de la Terre, Géologie Géophysique, Centre IRD de Nouméa.
- 776 Cabioch, G., Recy, J., Jouannic, C., Turpin, L., 1996. Contrôle climatique et tectonique de l'édification récifale en  
777 Nouvelle-Calédonie au cours du Quaternaire terminal. *Bulletin de la Société Géologique de France* 167, 729–742.
- 778 Camoin, G.F., Seard, C., Deschamps, P., Webster, J.M., Abbey, E., Braga, J.C., Iryu, Y., Durand, N., Bard, E., Hamelin, B.,  
779 Yokoyama, Y., Thomas, A.L., Henderson, G.M., Dussouillez, P., 2012. Reef response to sea-level and environmental  
780 changes during the last deglaciation: Integrated Ocean Drilling Program Expedition 310, Tahiti Sea Level.  
781 *Geology* 40, 643–646. <https://doi.org/10.1130/G32057.1>
- 782 Chaisson, W.P., Ravelo, A.C., 1997. Changes in upper water-column structure at Site 925, late Miocene-  
783 Pleistocene planktonic foraminifer assemblage and isotopic evidence, in: Shackleton, N.J., Curry, W.B., Richter, C.,  
784 Bralower, T.J. (Eds.), *Proceedings of the Ocean Drilling Program, Scientific Results, Ocean Drilling Program.*  
785 College Station, TX, pp. 255–268.
- 786 Chardon, D., Austin, J.A., Cabioch, G., Pelletier, B., Sastrup, S., 2007. NEOMARGES, Imagerie sismique du lagon et des  
787 pentes des marges de la ride de Nouvelle-Calédonie à travers le récif barrière de la Grande Terre, 12-21  
788 décembre 2006 (Rapport de missions, Sciences de la Terre, Géologie-Géophysique No. 72). IRD.  
789 <https://doi.org/10.17600/6100140>
- 790 Chardon, D., Austin, J.A., Cabioch, G., Pelletier, B., Sastrup, S., Sage, F., 2008. Neogene history of the northeastern New  
791 Caledonia continental margin from multichannel reflection seismic profiles. *Comptes Rendus Geoscience* 340,  
792 68–73. <https://doi.org/10.1016/j.crte.2007.09.017>
- 793 Chardon, D., Chevillotte, V., 2006. Morphotectonic evolution of the New Caledonia ridge (Pacific Southwest) from post-  
794 obduction tectonosedimentary record. *Tectonophysics* 420, 473–491.  
795 <https://doi.org/10.1016/j.tecto.2006.04.004>
- 796 Chevillon, C., 1997. Sédimentologie descriptive et cartographie des fonds meubles du lagon de la côte Est de Nouvelle-  
797 Calédonie, in: *Les Fonds Meubles Des Lagons de Nouvelle-Calédonie (Sédimentologie, Benthos), Etudes et*  
798 *Thèses, ORSTOM.* pp. 7–30.
- 799 Chiarella, D., Longhitano, S.G., Tropeano, M., 2017. Types of mixing and heterogeneities in siliciclastic-carbonate  
800 sediments. *Marine and Petroleum Geology* 88, 617–627. <https://doi.org/10.1016/j.marpetgeo.2017.09.010>
- 801 Cluzel, D., Aitchison, J.C., Picard, C., 2001. Tectonic accretion and underplating of mafic terranes in the Late Eocene  
802 intraoceanic fore-arc of New Caledonia (Southwest Pacific): geodynamic implications. *Tectonophysics* 340, 23–  
803 59. [https://doi.org/10.1016/S0040-1951\(01\)00148-2](https://doi.org/10.1016/S0040-1951(01)00148-2)
- 804 Cluzel, D., Bosch, D., Paquette, J.-L., Lemennicier, Y., Montjoie, P., Ménot, R.-P., 2005. Late Oligocene post-obduction  
805 granitoids of New Caledonia: A case for reactivated subduction and slab break-off. *Island Arc* 14, 254–271.  
806 <https://doi.org/10.1111/j.1440-1738.2005.00470.x>
- 807 Cohen, K.M., Harper, D.A.T., Gibbard, P.L., 2017. ICS International Chronostratigraphic Chart 2017/02.
- 808 Collot, J., Patriat, M., Etienne, S., Rouillard, P., Soetaert, F., Juan, C., Marcaillou, B., Palazzin, G., Clerc, C., Maurizot, P.,  
809 Pattier, F., Tournadour, E., Sevin, B., Privat, A., 2017. Deepwater Fold-and-Thrust Belt Along New Caledonia's  
810 Western Margin: Relation to Post-obduction Vertical Motions. *Tectonics* 36, 2108–2122.  
811 <https://doi.org/10.1002/2017TC004542>

Field Code Changed

Field Code Changed

Formatted: French (France)

812 Collot, J.Y., Malahoff, A., Recy, J., Latham, G., Missegue, F., 1987. Overthrust emplacement of New Caledonia Ophiolite:  
813 Geophysical evidence. *Tectonics* 6, 215–232. <https://doi.org/10.1029/TC006i003p00215>

814 Cotillon, P., Coustillas, F., Gaillard, C., Laurin, B., Liu, D.-J., Pannetier, W., Rigolot, P., Pascal, A., Pascal, F., 1990. Grands  
815 traits de la sédimentation actuelle et récente sur les pentes et dans les bassins au large de la Nouvelle Calédonie  
816 (SW Pacifique): Résultats géologiques de la campagne Biocal Cotillon P, Coustillas F, Gaillard C, Laurin B, Liu D-J,  
817 Pannetier W, Rigolot P, Pascal A, Pascal F. *Oceanologica Acta*, Special issue (0399-1784) Actes du Colloque Tour  
818 du monde Jean Charcot, Paris (France), 2-3 Mar 1989.

819 Cotillon, P., Liu, J.D., Gaillard, C., Evin, J., 1989. Evolution du taux de sédimentation au cours des derniers 30 000 ans  
820 aux abords de la Nouvelle-Calédonie (SW Pacifique); résultats de datations au radiocarbone et par la courbe de  
821 l'oxygène 18. *Bulletin de la Société Géologique de France* V, 881–884. <https://doi.org/10.2113/gssgfbull.V4.881>

822 Coudray, J., 1976. Recherches sur le Néogène et le Quaternaire marins de la Nouvelle-Calédonie; contribution de  
823 l'étude sédimentologique à la connaissance de l'histoire géologique post-Eocène, in: *Expédition Française Sur*  
824 *Les Récifs Nouvelle-Calédonie*, Fond. Singer-Polignac. Paris, pp. 1–276.

825 Coudray, J., 1975. Recherches sur le Néogène et le Quaternaire marin de la Nouvelle-Calédonie. Contribution de l'étude  
826 sédimentologique à la connaissance de l'histoire géologique post-éocène (Thèse de Doctorat). Université des  
827 Sciences et Techniques du Languedoc.

828 Daniel, J., Dugas, F., Dupont, J., Jouannic, C., Launay, J., Monzier, M., Recy, J., 1976. La zone charnière Nouvelle-Calédonie  
829 - ride de Norfolk (S.W. Pacifique) : résultats de dragages et interprétation. *Cahiers ORSTOM série Géologie* 8, 95–  
830 105.

831 Droxler, A.W., Jorry, S.J., 2013. Deglacial Origin of Barrier Reefs Along Low-Latitude Mixed Siliciclastic and Carbonate  
832 Continental Shelf Edges. *Annu. Rev. Mar. Sci.* 5, 165–190. [https://doi.org/10.1146/annurev-marine-121211-  
833 172234](https://doi.org/10.1146/annurev-marine-121211-172234)

834 Dubois, J., Launay, J., Recy, J., 1975. Some new evidence on lithospheric bulges close to island arcs. *Tectonophysics* 26,  
835 189–196. [https://doi.org/10.1016/0040-1951\(75\)90089-X](https://doi.org/10.1016/0040-1951(75)90089-X)

836 Dubois, J., Launay, J., Recy, J., 1974. Uplift movements in New Caledonia-Loyalty Islands area and their plate tectonics  
837 interpretation. *Tectonophysics* 24, 133–150. [https://doi.org/10.1016/0040-1951\(74\)90134-6](https://doi.org/10.1016/0040-1951(74)90134-6)

838 Dunbar, G.B., Dickens, G.R., 2003. Massive siliciclastic discharge to slopes of the Great Barrier Reef Platform during sea-  
839 level transgression: constraints from sediment cores between 15°S and 16°S latitude and possible explanations.  
840 *Sediment. Geol.* 162, 141–158. [https://doi.org/10.1016/S0037-0738\(03\)00216-1](https://doi.org/10.1016/S0037-0738(03)00216-1)

841 Ehrenberg, S.N., McArthur, J.M., Thirlwall, M.F., 2006. Growth, Demise, and Dolomitization of Miocene Carbonate  
842 Platforms on the Marion Plateau, Offshore NE Australia. *Journal of Sedimentary Research* 76, 91–116.  
843 <https://doi.org/10.2110/jsr.2006.06>

844 Esker, D.E., Eberli, G.P., McNeill, D.F., 1998. The Structural and Sedimentological Controls on the Reoccupation of  
845 Quaternary Incised Valleys, Belize Southern Lagoon. *AAPG Bull.* 82, 2075–2109.  
846 <https://doi.org/10.1306/00AA7BE4-1730-11D7-8645000102C1865D>

847 Ferro, C.E., Droxler, A.W., Anderson, J.B., Mucciarone, D., 1999. Late Quaternary shift of mixed siliciclastic-carbonate  
848 environments induced by glacial eustatic sea-level fluctuations in Belize. In: *Advances in carbonate sequence  
849 stratigraphy: Application to reservoirs, outcrops and models* (Eds P.M. Harris, A.H. Saller and T. Simo), SEPM  
850 *Special Publication v. 63*, pp. 385–411. SEPM (Society for Sedimentary Geology), Tulsa.

851 Flamand, B., 2006. Les pentes externes du récif barrière de la Grande Terre de Nouvelle-Calédonie : morphologie,  
852 lithologie, contrôle de la tectonique et de l'eustatisme. Université de Bretagne occidentale, Brest, France.

853 Frank, N., Turpin, L., Cabioch, G., Blamart, D., Tressens-Fedou, M., Colin, C., Jean-Baptiste, P., 2006. Open system U-  
854 series ages of corals from a subsiding reef in New Caledonia: Implications for sea level changes, and subsidence  
855 rate. *Earth and Planetary Science Letters* 249, 274–289. <https://doi.org/10.1016/j.epsl.2006.07.029>

856 Fürstenau, J., Lindhorst, S., Betzler, C., Hübscher, C., 2010. Submerged reef terraces of the Maldives (Indian Ocean).  
857 *Geo-Mar Lett* 30, 511–515. <https://doi.org/10.1007/s00367-009-0174-2>

Formatted: French (France)

Field Code Changed

Field Code Changed

Field Code Changed

Formatted: Hyperlink, Font: 11 pt, French (France)

Formatted: French (France)

858 Gaina, C., Müller, D.R., Royer, J.-Y., Stock, J., Hardebeck, J., Symonds, P., 1998. The tectonic history of the Tasman Sea: A  
859 puzzle with 13 pieces. *Journal of Geophysical Research: Solid Earth* 103, 12413–12433.  
860 <https://doi.org/10.1029/98JB00386>

861 Geldart, L.P., Sheriff, R.E., 2004. *Problems in Exploration Seismology and their Solutions*. Society of Exploration  
862 Geophysicists. <https://doi.org/10.1190/1.9781560801733>

863 Gischler, E., Ginsburg, R.N., Herrle, J.O., Prasad, S., 2010. Mixed carbonates and siliciclastics in the Quaternary of  
864 southern Belize: Pleistocene turning points in reef development controlled by sea-level change. *Sedimentology*  
865 57, 1049–1068. <https://doi.org/10.1111/j.1365-3091.2009.01133.x>

866 Gradstein, F.M., Ogg, J.G., Schmitz, M.D., Ogg, G.M. (Eds.), *The Geologic Time Scale*. Elsevier, Boston, pp. ix–xi.  
867 <https://doi.org/10.1016/B978-0-444-59425-9.10003-4>

868 Hallock, P., Schlager, W., 1986. Nutrient Excess and the Demise of Coral Reefs and Carbonate Platforms. *PALAIOS* 1,  
869 389. <https://doi.org/10.2307/3514476>

870 Harper, B.B., Puga-Bernabéu, Á., Droxler, A.W., Webster, J.M., Gischler, E., Tiwari, M., Lado-Insua, T., Thomas, A.L.,  
871 Morgan, S., Jovane, L., Röhl, U., 2015. Mixed Carbonate–Siliciclastic Sedimentation Along the Great Barrier Reef  
872 Upper Slope: A Challenge To the Reciprocal Sedimentation Model. *Journal of Sedimentary Research* 85, 1019 –  
873 1036. <https://doi.org/10.2110/jsr.2015.581>

874 Hayes, D.E., Ringis, J., 1973. Seafloor Spreading in the Tasman Sea. *Nature* 243, 454–458.  
875 <https://doi.org/10.1038/243454a0>

876 Hohenegger, J., 2005. Estimation of environmental paleogradient values based on presence/absence data: a case study  
877 using benthic foraminifera for paleodepth estimation. *Palaeogeogr. Palaeoclimatol. Palaeoecol.* 217, 115 –130.  
878 <https://doi.org/10.1016/j.palaeo.2004.11.020>

879 Hohenegger, J., 1995. Depth estimation by proportions of living larger foraminifera. *Mar. Micropal.* 26, 31–47.  
880 [https://doi.org/10.1016/0377-8398\(95\)00044-5](https://doi.org/10.1016/0377-8398(95)00044-5)

881 Hottinger, L., 1983. Processes determining the distribution of larger foraminifera in space and time. *Utrecht Micropal.*  
882 *Bull.* 30, 239–253.

883 Jorry, S.J., Camoin, G.F., Jouet, G., Roy, P.L., Vella, C., Courgeon, S., Prat, S., Fontanier, C., Paumard, V., Boule, J., Caline, B.,  
884 Borgomano, J., 2016. Modern sediments and Pleistocene reefs from isolated carbonate platforms (Iles Eparses,  
885 SW Indian Ocean): A preliminary study. *Acta Oecologica* 72, 129–143.  
886 <https://doi.org/10.1016/j.actao.2015.10.014>

887 Juffroy, F., 2009. Atlas bathymétrique de la Nouvelle-Calédonie. Rapport du Service de la Géomatique et de la  
888 Télé-détection du Gouvernement de la Nouvelle-Calédonie.

889 Kerans, C., Tinker, S.W., 1999. Extrinsic Stratigraphic Controls on Development of the Capitan Reef Complex, in: Saller,  
890 A.H., Harris, P.M. (Mitch), Kirkland, B.L., Mazzullo, S.J. (Eds.), *Geologic Framework of the Capitan Reef*. SEPM  
891 Society for Sedimentary Geology, p. 0.

892 Khanna, P., Droxler, A.W., Nittrouer, J.A., Tunnell Jr, J.W., Shirley, T.C., 2017. Coralgall reef morphology records  
893 punctuated sea-level rise during the last deglaciation. *Nature Communications* 8, 1046.  
894 <https://doi.org/10.1038/s41467-017-00966-x>

895 Lafoy, Y., Missègue, F., Cluzel, D., Voisset, M., Saget, P., Lenoble, J.-P., Rigaut, F., Lanckneus, J., Lehodey, P., Bouniot, E.,  
896 Cornec, J., De Souza, K., Gallois, F., Garioud, N., Grenard, P., N'Diaye, M., Perchoc, Y., Perrier, J., 1994. Campagne  
897 ZoNéCo 2 (2 au 22 août 1994), RV L'Atalante.

898 Lafoy, Y., Van de Beuque, S., Missègue, F., Nercessian, A., Bernardel, G., 1998. Campagne de sismique multitraces entre  
899 la marge Est Australienne et le Sud de l'Arc des Nouvelles-Hébrides Rapport de la campagne RIG SEISMIC 206  
900 (21 avril - 24 mai 1998). Programme FAUST (French Australian Seismic Transect). Programme ZoNéCo.

901 Lagabrielle, Y., Chauvet, A., 2008. The role of extensional tectonics in shaping Cenozoic New-Caledonia. *Bulletin de la*  
902 *Société Géologique de France* 179, 315–329. <https://doi.org/10.2113/gssgfbull.179.3.315>

Field Code Changed

Formatted: English (United States)

Field Code Changed

Formatted: English (United States)

Formatted: Hyperlink, Font: 11 pt, English (United States)

903 Lagabriele, Y., Maurizot, P., Lafoy, Y., Cabioch, G., Pelletier, B., Régnier, M., Wabete, I., Calmant, S., 2005. Post-Eocene  
904 extensional tectonics in Southern New Caledonia (SW Pacific): Insights from onshore fault analysis and offshore  
905 seismic data. *Tectonophysics* 403, 1–28. <https://doi.org/10.1016/j.tecto.2005.02.014>

906 Launay, J., 1985. Paléoniveaux marins et néotectonique à l'île des Pins (Nouvelle-Calédonie). *Géologie de la France* 1,  
907 77–81.

908 Le Roy, P., Cabioch, G., Monod, B., Lagabriele, Y., Pelletier, B., Flamand, B., 2008. Late Quaternary history of the Nouméa  
909 lagoon (New Caledonia, South West Pacific) as depicted by seismic stratigraphy and multibeam bathymetry: A  
910 modern model of tropical rimmed shelf. *Palaeogeography, Palaeoclimatology, Palaeoecology* 270, 29–45.  
911 <https://doi.org/10.1016/j.palaeo.2008.08.012>

912 Le Roy, P., Jorry, S., Jouet, G., Ehrhold, A., Michel, G., Gautier, V., Guérin, C., 2019. Late Pleistocene evolution of the mixed  
913 siliciclastic and carbonate southwestern New Caledonia continental shelf/lagoon. *Palaeogeography,  
914 Palaeoclimatology, Palaeoecology* 514, 502–521. <https://doi.org/10.1016/j.palaeo.2018.10.014>

915 Mallarino, G., Francis, J.M., Jorry, S.J., Daniell, J.J., Droxler, A.W., Dickens, G.R., Beaufort, L., Bentley, S.J., Opdyke, B.N.,  
916 Peterson, L.C., 2021. [Time-scale](#) [Timescale](#) dependent sedimentary record during the past 130 [kaky](#) from a  
917 tropical mixed siliciclastic–carbonate shelf edge and slope: Ashmore Trough (southern Gulf of Papua).  
918 *Sedimentology*. [sed.12867](https://doi.org/10.1111/sed.12867). <https://doi.org/10.1111/sed.12867>

919 Maurizot, P., Cabioch, G., Fournier, F., Leonide, P., Sebih, S., Rouillard, P., Montaggioni, L., Collot, J., Martin-Garin, B.,  
920 Chaproniere, G., Braga, J.C., Sevin, B., 2016. Post-obduction carbonate system development in New Caledonia  
921 (Népoui, Lower Miocene). *Sedimentary Geology* 331, 42–62. <https://doi.org/10.1016/j.sedgeo.2015.11.003>

922 Maurizot, P., Collot, J., Cluzel, D., Patriat, M., 2020. Chapter 6 The Loyalty Islands and Ridge, New Caledonia.  
923 Geological Society, London, *Memoirs* 51, 131. <https://doi.org/10.1144/M51-2017-24>

924 Maurizot, P., Vendé-Leclerc, M., 2009. New Caledonia geological map, scale 1/500000. Direction de l'Industrie, des  
925 Mines et de l'Energie-Service de la Géologie de Nouvelle-Calédonie, Bureau de Recherches Géologiques et  
926 Minières.

927 McCaffrey, J.C., Wallace, M.W., Gallagher, S.J., 2020. A Cenozoic Great Barrier Reef on Australia's North West shelf.  
928 *Global and Planetary Change* 184, 103048. <https://doi.org/10.1016/j.gloplacha.2019.103048>

929 McKee, E.D., Oriol, S.S., Ketner, K.B., MacLachlan, M.E., Goldsmith, J.W., MacLachlan, J.C., Mudge, M.R., 1959.  
930 Paleotectonic maps of the Triassic System. *Miscellaneous Geologic Investigations Map*.

931 McKenzie, J.A., Spezzaferri, S., Isern, A., 1999. The Miocene-Pliocene boundary in the Mediterranean Sea and Bahamas;  
932 implications for a global flooding event in the earliest Pliocene. *Memorie della Società Geologica Italiana* 54, 93–  
933 108.

934 McNeill, D.F., Pisera, A., 2010. Neogene Lithofacies Evolution on a Small Carbonate Platform in the Loyalty Basin, Mare,  
935 New Caledonia, in: Morgan, W.A., George, A.D., Harris, P.M. (Mitch), Kupez, J.A., Sarg, J.F. (Rick) (Eds.), *Cenozoic  
936 Carbonate Systems of Australasia*. SEPM Society for Sedimentary Geology, p. 0.

937 Missègue, F., Saget, P., Desrus, M., Le Suavé, R., Lafoy, Y., 1996. Mission ZoNéCo 3 (30 Aout au 20 Septembre 1996), RV  
938 L'Atalante. <https://doi.org/10.17600/96010070>

939 Mitchell, J.K., Holdgate, G.R., Wallace, M.W., Gallagher, S.J., 2007. [Marine geology of the Quaternary Bass Canyon system,  
940 southeast Australia: A cool-water carbonate system.](#) *Mar. Geol.* 237, 71–96.  
941 <https://doi.org/10.1016/j.margeo.2006.10.037>

942 Mitchum, R.M., Vail, P.R., Sangree, J.B., 1977. Seismic stratigraphy and global changes of sea-level, part 6: stratigraphic  
943 interpretation of seismic reflection patterns in depositional sequences, part 6, in: Payton, C.E. (Ed.), *Seismic  
944 Stratigraphy: Applications to Hydrocarbon Exploration*, AAPG Memoir. pp. 117–133.

945 Montaggioni, L.F., Cabioch, G., Thouveny, N., Frank, N., Sato, T., Sémah, A.-M., 2011. Revisiting the Quaternary  
946 development history of the western New Caledonian shelf system: From ramp to barrier reef. *Marine Geology*  
947 280, 57–75. <https://doi.org/10.1016/j.margeo.2010.12.001>

948 Moretti, I., Turcotte, D.L., 1985. A model for erosion, sedimentation, and flexure with application to New Caledonia.  
949 *Journal of Geodynamics* 3, 155–168. [https://doi.org/10.1016/0264-3707\(85\)90026-2](https://doi.org/10.1016/0264-3707(85)90026-2)

Field Code Changed

Formatted: English (United States)

Field Code Changed

Field Code Changed

Field Code Changed

Formatted: English (United States)

Field Code Changed

Formatted: Hyperlink, Font: 11 pt

Field Code Changed

Field Code Changed

- 950 Mortimer, N., Campbell, H., Tulloch, A.J., King, P.R., Stagpoole, V.M., Wood, R.A., Rattenbury, M.S., Sutherland, R., Adams,  
951 C.J., Collot, J., Seton, M., 2017. Zealandia: Earth's Hidden Continent. *The Geological Society of America* 27, 27–35.
- 952 Nebelsick, J.H., Stingl, V., Rasser, M., 2001. Autochthonous facies and allochthonous debris flows compared: Early  
953 oligocene carbonate facies patterns of the Lower Inn Valley (Tyrol, Austria). *Facies* 44, 31.  
954 <https://doi.org/10.1007/BF02668165>
- 955 O'Connell, B., Dorsey, R.J., Hasiotis, S.T., Hood, A.V.S., 2021. Mixed carbonate–siliciclastic tidal sedimentation in the  
956 Miocene to Pliocene Bouse Formation, palaeo-Gulf of California. *Sedimentology* 68, 1028–1068.  
957 <https://doi.org/10.1111/sed.12817>
- 958 Paquette, J.-L., Cluzel, D., 2007. U–Pb zircon dating of post-obduction volcanic-arc granitoids and a granulite-facies  
959 xenolith from New Caledonia. Inference on Southwest Pacific geodynamic models. *International Journal of Earth  
960 Sciences* 96, 613–622. <https://doi.org/10.1007/s00531-006-0127-1>
- 961 Paris, J.P., 1981. Géologie de la Nouvelle-Calédonie, Un essai de synthèse, Mémoire du BRGM, Orléans, France.
- 962 Patriat, M., Collot, J., Etienne, S., Poli, S., Clerc, C., Mortimer, N., Pattier, F., Juan, C., Roest, W.R., VESPA scientific voyage  
963 team, 2018. New Caledonia Obducted Peridotite Nappe: Offshore Extent and Implications for Obduction and  
964 Postobduction Processes. *Tectonics* 37, 1077–1096. <https://doi.org/10.1002/2017TC004722>
- 965 Pautot, G., Lafoy, Y., Dupont, J., Le Suavé, R., 1993. Campagne ZoNéCo 1 (25 juin au 16 juillet 1993), RV L'Atalante.  
966 <https://doi.org/10.17600/93000130>
- 967 Pelletier, B., Butscher, J., Panché, J.-Y., Perrier, J., Maloune, A., 2002. Cartographie au sondeur multifaisceaux des pentes  
968 externes du récif barrière de la Province Nord de la Nouvelle-Calédonie. Campagne Province Nord 1, côte Est de  
969 la passe de Thio à la passe de Balade (24 juillet au 1er août 2002). (No. 48). Rapports de missions, Sciences de la  
970 Terre, Géologie-Géophysique, Centre IRD Nouméa.
- 971 Pelletier, B., Cabioch, G., Chardon, D., Yamano, H., 2006. Lithologie des pentes externes du récif barrière de Nouvelle-  
972 Calédonie. Campagne de dragages « 2005-NC-DR » du N.O. Alis (30 mai – 7 juin 2005). (No. 68). Rapports de  
973 missions, Sciences de la Terre, Géologie Géophysique, Centre IRD de Nouméa.
- 974 Pelletier, B., Juffroy, F., Flamand, B., Perrier, J., 2012. La bathymétrie des marges de la Grande Terre et des îles Loyauté.  
975 Planche 5, in: Bonvallot, J., Gay, J.C., Habert, E. (Eds.), Atlas de La Nouvelle Calédonie. Nouméa : IRD ; Congrès de  
976 la Nouvelle-Calédonie, Marseille (FRA), pp. 33–36.
- 977 Pelletier, B., Perrier, J., Juffroy, F., Flamand, B., Panché, J.-Y., Gallois, F., 2004. Cartographie systématique par sondeur  
978 multifaisceaux des pentes externes du récif barrière de la Grande Terre et des îles Loyauté, Nouvelle-Calédonie.  
979 Assises de la Recherche Française dans le Pacifique, 24-27 août 2004, Nouméa, Nouvelle-Calédonie. Résumés  
980 des communications scientifiques, p.271-272. Poster. Presented at the Assises de la Recherche Française dans le  
981 Pacifique, 24-27 août 2004, Nouméa, Nouvelle-Calédonie.
- 982 Perrier, J., Flamand, B., Juffroy, F., Panché, J.-Y., Le Houarno, H., 2004a. Cartographie au sondeur multifaisceaux de la  
983 zone côtière de la Province Sud. Campagne Province Sud 1, N.O. Alis (2-5 février et 11-20 février 2004). (No. 62).  
984 Rapports de missions, Sciences de la Terre, Géologie-Géophysique, Centre IRD Nouméa.
- 985 Perrier, J., Flamand, B., Robineau, B., Panché, J.-Y., Le Houarno, H., 2004b. Cartographie au sondeur multifaisceaux de la  
986 zone côtière de la Province Sud, Campagne Province Sud 2. N.O. Alis du 23 septembre au 2 octobre 2004. Côte  
987 Ouest: de la passe de Boulari à la passe Koko; Sud: Corne Sud. (No. 63), Rapports de missions, Sciences de la  
988 Terre, Géologie-Géophysique, Centre IRD de Nouméa.
- 989 Perrier, J., Panché, J.-Y., Juffroy, F., Barazer, J.-F., 2005. Cartographie au sondeur multifaisceaux de la zone côtière de la  
990 Province Sud. Campagne Province Sud 4, NO Alis. 21 au 24 septembre 2005. Hauts fonds à l'extrémité sud de la  
991 Grande Terre : Banc 93, Banc Antigonina, Mont 1 (No. 65). Rapports de missions Sciences de la Terre. Géologie  
992 Géophysique, Centre IRD de Nouméa.
- 993 Perrier, J., Pelletier, B., Panché, J.-Y., Barazer, J.-F., Juffroy, F., 2004c. Cartographie au sondeur multifaisceaux de la zone  
994 côtière de la Province Sud. Campagne Province Sud 3, N.O. Alis du 26 novembre au 30 novembre 2004. Côte Sud  
995 Est : de la passe de la Sarcelle à la terminaison sud de l'île des Pins (banc de la Torche). (No. 64). Rapports de  
996 missions, Sciences de la Terre, Géologie-Géophysique, Centre IRD de Nouméa.

Field Code Changed

Field Code Changed

Formatted: English (United States)

997 Puillandre, N., Samadi, S., 2016. Kanacono cruise, RV Alis, <https://doi.org/10.17600/16003900>

998 Purdy, E.G., Gischler, E., 2005. The transient nature of the empty bucket model of reef sedimentation. *Sedimentary Geology* 175, 35–47. <https://doi.org/10.1016/j.sedgeo.2005.01.007>

1000 Rigolot, P., 1989. Origine et évolution du "système" ride de Nouvelle-Calédonie/Norfolk (Sud -Ouest Pacifique) :  
1001 synthèse des données de géologie et de géophysique marine. Etude des marges et bassins associés. UBO, Brest.

1002 Rovere, A., Khanna, P., Bianchi, C.N., Droxler, A.W., Morri, C., Naar, D.F., 2018. Submerged reef terraces in the Maldivian  
1003 Archipelago (Indian Ocean). *Geomorphology* 317, 218–232. <https://doi.org/10.1016/j.geomorph.2018.05.026>

1004 Schlager, W., 1989. Drowning Unconformities on Carbonate Platforms, in: Controls on Carbonate Platforms and Basin  
1005 Development, SEPM SPECIAL PUBLICATION.

1006 Sevin, B., Maurizot, P., Cluzel, D., Tournadour, E., Etienne, S., Folcher, N., Jeanpert, J., Collot, J., Iseppi, M., Meffre, S.,  
1007 Patriat, M., 2020. Chapter 7 Post-obduction evolution of New Caledonia. Geological Society, London, *Memoirs*  
1008 51, 147. <https://doi.org/10.1144/M51-2018-74>

1009 Smith, W.H.F., Sandwell, D.T., 1997. Global Sea Floor Topography from Satellite Altimetry and Ship Depth Soundings.  
1010 *Science* 277, 1956. <https://doi.org/10.1126/science.277.5334.1956>

1011 Sutherland, R., Viskovic, G.P.D., Bache, F., Stagpoole, V.M., Collot, J., Rouillard, P., Hashimoto, T., Hackney, R., Rollet, N.,  
1012 Patriat, M., Roest, W.R., 2012. Compilation of seismic reflection data from the Tasman Frontier region, southwest  
1013 Pacific (GNS Science Report No. 2012/01).

1014 Tcherepanov, E.N., Droxler, A.W., Lapointe, P., [Dickens, G.R.](#), [Bentley, S.J.](#), [Beaufort, L.](#), [Peterson, L.C.](#), [Daniell, J.](#), [Opdyke,](#)  
1015 [B.N.](#), 2008a. Neogene evolution of the mixed carbonate-siliciclastic system in the Gulf of Papua, Papua New  
1016 Guinea. *J. Geophys. Res.* 113, F01S21. <https://doi.org/10.1029/2006JF000684>

1017 [Tcherepanov, E.N.](#), [Droxler, A.W.](#), [Lapointe, P.](#), Mohn, K., ~~20082008b~~. Carbonate seismic stratigraphy of the Gulf of  
1018 Papua mixed depositional system: Neogene stratigraphic signature and eustatic control. *Basin Research* 20,  
1019 185–209. <https://doi.org/10.1111/j.1365-2117.2008.00364.x>

1020 [Tcherepanov, E.N.](#), [Droxler, A.W.](#), [Lapointe, P.](#), [Mohn, K.](#), [Larsen, O.A.](#), 2010. Siliciclastic influx and burial of the Cenozoic  
1021 carbonate system in the Gulf of Papua. *Marine and Petroleum Geology* 27, 533–554.  
1022 <https://doi.org/10.1016/j.marpetgeo.2009.09.002>

1023 Teillet, T., Fournier, F., Borgomano, J., Hong, F., 2020a. Origin of seismic reflections in a carbonate gas field, Lower  
1024 Miocene, offshore Myanmar. *Marine and Petroleum Geology* 113, 104110.  
1025 <https://doi.org/10.1016/j.marpetgeo.2019.104110>

1026 Teillet, T., Fournier, F., Montaggioni, L.F., BouDagher-Fadel, M., Borgomano, J., Braga, J.C., Villeneuve, Q., Hong, F.,  
1027 2020b. Development patterns of an isolated oligo-mesophotic carbonate buildup, early Miocene, Yadana field,  
1028 offshore Myanmar. *Marine and Petroleum Geology* 111, 440–460.  
1029 <https://doi.org/10.1016/j.marpetgeo.2019.08.039>

1030 Terry, J.P., Wotling, G., 2011. Rain-shadow hydrology: Influences on river flows and flood magnitudes across the  
1031 central massif divide of La Grande Terre Island, New Caledonia. *Journal of Hydrology* 404, 77–86.  
1032 <https://doi.org/10.1016/j.jhydrol.2011.04.022>

1033 Toomey, M.R., Woodruff, J.D., Donnelly, J.P., Ashton, A.D., Perron, J.T., 2016. Seismic evidence of glacial-age river  
1034 incision into the Tahaa barrier reef, French Polynesia. *Marine Geology* 380, 284–289.  
1035 <https://doi.org/10.1016/j.margeo.2016.04.008>

1036 Tournadour, E., Fournier, F., Etienne, S., Collot, J., Maurizot, P., Patriat, M., Sevin, B., Morgans, H.E.G., Martin-Garin, B.,  
1037 Braga, J.C., 2020. Seagrass-related carbonate ramp development at the front of a fan delta (Burdigalian, New  
1038 Caledonia): Insights into mixed carbonate-siliciclastic environments. *Marine and Petroleum Geology* 121,  
1039 104581. <https://doi.org/10.1016/j.marpetgeo.2020.104581>

1040 [Wallace, M.W.](#), [Holdgat, G.R.](#), [Daniels, J.](#), [Gallagher, S.J.](#), [Smith, A.](#), 2002. Sonic velocity, submarine canyons, and burial  
1041 diagenesis in Oligocene-Holocene cool-water carbonates, Gippsland Basin, southeast Australia. *AAPG Bull.* 86,  
1042 1593–1607. <https://doi.org/10.1306/61EEDD14-173E-11D7-8645000102C1865D>

Formatted: French (France)

Field Code Changed

Formatted: Hyperlink, Font: 9 pt

Formatted: English (United States)

Field Code Changed

Field Code Changed

Formatted: Hyperlink, Font: 11 pt, French (France)

Field Code Changed

1043 Webster, J.M., Braga, J.C., Humblet, M., Potts, D.C., Iryu, Y., Yokoyama, Y., Fujita, K., Bourillot, R., Esat, T.M., Fallon, S.,  
 1044 Thompson, W.G., Thomas, A.L., Kan, H., McGregor, H.V., Hinestrosa, G., Obrochta, S.P., Lougheed, B.C., 2018.  
 1045 Response of the Great Barrier Reef to sea-level and environmental changes over the past 30,000 years. *Nature*  
 1046 *Geoscience* 11, 426–432. <https://doi.org/10.1038/s41561-018-0127-3>

1047 Weij, R., Reijmer, J.J.G., Eberli, G.P., Swart, P.K., 2019. The limited link between accommodation space, sediment  
 1048 thickness, and inner platform facies distribution (Holocene–Pleistocene, Bahamas). *The Depositional Record* 5,  
 1049 400–420. <https://doi.org/10.1002/dep2.50>

1050 Wilson, J.L., 1967. Cyclic and Reciprocal Sedimentation in Virgilian Strata of Southern New Mexico. *GSA Bulletin* 78,  
 1051 805–818. [https://doi.org/10.1130/0016-7606\(1967\)78\[805-CARSIV\]2.0.CO;2](https://doi.org/10.1130/0016-7606(1967)78[805-CARSIV]2.0.CO;2)

1052 Wilson, P.A., Roberts, H.H., 1995. Density cascading; off-shelf sediment transport, evidence and implications, Bahama  
 1053 Banks. *Journal of Sedimentary Research* 65, 45–56. <https://doi.org/10.1306/D426801D-2B26-11D7-8648000102C1865D>

1055 Wilson, P.A., Roberts, H.H., 1992. Carbonate-periplatform sedimentation by density flows: A mechanism for rapid off-  
 1056 bank and vertical transport of shallow-water fines. *Geology* 20, 713–716. [https://doi.org/10.1130/0091-7613\(1992\)020<0713:CPSBDF>2.3.CO;2](https://doi.org/10.1130/0091-7613(1992)020<0713:CPSBDF>2.3.CO;2)

1058 Yamano, H., Cabioch, G., Pelletier, B., Chevillon, C., Tachikawa, H., Lefèvre, J., Marchesiello, P., 2015. Modern carbonate  
 1059 sedimentary facies on the outer shelf and slope around New Caledonia. *Island Arc* 24, 4–15.  
 1060 <https://doi.org/10.1111/iar.12085>

1061 [Yordanova, E.K., Hohenegger, J., 2007. Studies on settling, traction and entrainment of larger benthic foraminiferal  
 1062 tests: implications for accumulation in shallow marine sediments. \*Sedimentology\* 54, 1273–1306.  
 1063 <https://doi.org/10.1111/j.1365-3091.2007.00881.x>](https://doi.org/10.1111/j.1365-3091.2007.00881.x)

1064 [Yordanova, E.K., Hohenegger, J., 2002. Taphonomy of larger foraminifera: Relationships between living individuals and  
 1065 empty tests on flat reef slopes \(Sesoko Island, Japan\). \*Facies\* 46, 169–203. <https://doi.org/10.1007/BF02668080>](https://doi.org/10.1007/BF02668080)

1066 Zeller, M., Verwer, K., Eberli, G.P., Massaferrro, J.L., Schwarz, E., Spalletti, L., 2015. Depositional controls on mixed  
 1067 carbonate–siliciclastic cycles and sequences on gently inclined shelf profiles. *Sedimentology* 62, 2009–2037.  
 1068 <https://doi.org/10.1111/sed.12215>

1069 Zinke, J., Reijmer, J.J.G., Thomassin, B.A., 2001. Seismic architecture and sediment distribution within the Holocene  
 1070 barrier reef–lagoon complex of Mayotte (Comoro archipelago, SW Indian Ocean). *Palaeogeography,  
 1071 Palaeoclimatology, Palaeoecology* 175, 343–368. [https://doi.org/10.1016/S0031-0182\(01\)00379-0](https://doi.org/10.1016/S0031-0182(01)00379-0)

1072

1073

Field Code Changed

Field Code Changed

Field Code Changed

Field Code Changed

Formatted: English (United States)

Field Code Changed

Formatted: Hyperlink, Font: 11 pt, French (France)

Field Code Changed

1074

## FIGURE AND TABLE CAPTIONS

1075

1076 **Figure 1:** **A.** Regional location map of the study area. **B.** Simplified geological map of Grande  
1077 Terre, New Caledonia (modified after Maurizot and Vendé-Leclerc, 2009) and shaded  
1078 bathymetric map of surrounding offshore areas with the southern extensions of the Peridotite  
1079 Nappe and metamorphic belt (Pines and Félicité ridges, respectively; after Patriat et al., 2018).  
1080 Drill sites of the Quaternary barrier reef (Coudray, 1975; Cabioch et al., 2008; Montaggioni et al.,  
1081 2011) and outcrops of the Lower Miocene mixed carbonate siliciclastic systems of Népoui are  
1082 also indicated (Maurizot et al., 2016 ; Tournadour et al., 2020). **C.** Simplified SW to NE oriented  
1083 geological cross-section of Grande Terre (modified after Lagabrielle et al., 2005 and Collot et al.,  
1084 1987). N: Nouméa ; Pn: Ponérihouen ; Th: Thio ; Yt: Yaté ; IP: Isle of Pines ; T : Banc de la Torche ;  
1085 S : Stylaster seamount ; B : Brachiopod seamount ; A : Antigonie seamount ; C : Crypthelia  
1086 seamount ; M : Munida seamount.

1087 **Figure 2:** Bathymetric map of the eastern margin of Grande Terre, from Poindimié to the Pines  
1088 Ridge with location of the dataset used in this study including seismic profiles AUS-104 (Bitoun  
1089 & Recy, 1982), 206-04 (dashed black lines), NEOMARGES (Chardon, 2006; Chardon et al. 2008,  
1090 black lines), and dredged carbonate samples (yellow circles). T : Banc de la Torche ; S : Stylaster  
1091 seamount ; B : Brachiopod seamount ; A : Antigonie seamount ; C : Crypthelia seamount ; M :  
1092 Munida seamount.

1093 **Figure 3:** **A.** Bathymetric map of the eastern lagoon of Grande Terre from Ponérihouen to Yaté.  
1094 On the outer slope, note the terrace mapped in orange between 300 to 600 m water depths. **B.**  
1095 Bathymetrical profile across the lagoon from the coast of Houailou to the outer barrier reef (see  
1096 location on Figure A) showing three main morphobathymetric zones: 1) a shallow-water coastal  
1097 zone dominated by fine-grained terrigenous sediments; 2) a deeper median lagoon with aligned  
1098 islands and a coast-parallel channel network in front of Cote Oubliée; 3) a barrier reef domain  
1099 cross-cut by passes, dominated by coarse-grained carbonate sedimentation. D: ~~Terrigenous~~ s.

Formatted: Line spacing: Multiple 1.15 li

Formatted: English (United States)

1100 ~~deltas~~Deltas; D\*: Restricted terrigenous deltas; SI: Sandy Islets; PR: Patch Reefs. Red lines are  
1101 positions of seismic profiles. Yellow circles are positions of dredged carbonate samples.

1102 **Figure 4:** Typical bathymetric profiles of the outer slopes of Grande Terre (location on Fig.2)  
1103 highlighting the very steep character of the western margin (dashed green lines; W-01 and W-  
1104 02) contrasting with the more gently inclined eastern margin (solid blue lines; E-01 and E-02).  
1105 The latter illustrate the main morpho-bathymetric domains of the eastern margin slope, which  
1106 can be divided into a low gradient (2-3°) upper slope mostly preserved from erosion, a middle  
1107 slope affected by numerous submarine canyons and a lower slope to to-of-slope region.

1108 ~~Along~~The hatched area shows the elevation difference between the southern and central parts of  
1109 the eastern margin (profile E-01), and E-02, respectively), highlighting that the slope is better  
1110 preserved from retrogressive erosion by slope canyons processes towards the south.

1111 **Figure 5: A.** 3D bathymetrical map of the outer slope in front of Cap Bayes Pass with location of  
1112 dip-oriented seismic profile NM-1. **B.** Seismic profile NM-1 profile with location of quaternary  
1113 terraces (blue arrow, see details in Flamand, 2006), clinoform slope break of U2 prism (green  
1114 arrow) and the bathymetrical scarp associated with the top of U1 seismic unit (red arrow). **C.**  
1115 Interpretation of seismic profile NM-1 highlighting five sub-units inside U2, interpreted as  
1116 parasequences (numbered from 1 to 5). Each parasequence is typified by an alternation of  
1117 lowstand forced regressive wedges (in beige) and aggrading to retrograding shallow-water  
1118 carbonate transgressive sequences (in pink), consistent with the pattern of reciprocal  
1119 sedimentation model.

1120 **Figure 6: A.** 3D bathymetrical map of the outer slope in front of Canala with location of seismic  
1121 profiles NM-4 and NM-9 and dredged carbonate rocks (see Table 3). **B.** Uninterpreted seismic  
1122 profile NM-4. **C.** Interpreted seismic profile NM-4. **D.** Uninterpreted seismic profile NM-9. **E.**  
1123 Interpretation of seismic profile NM-9. Both profiles show U1 seismic unit overlain by  
1124 downlapping U2 seismic unit interpreted as external slope deposits derived from the quaternary  
1125 barrier reef.

Formatted: English (United States)

1126 **Figure 7: A.** 3D bathymetrical map of the outer slope in front of Côte Oubliée with location of  
1127 seismic profiles NM-12B and NM-13 and dredged carbonate rock DR-49 (see [Table 3](#)). **B.**  
1128 Uninterpreted seismic profile NM-12B. **C.** Interpretation of seismic profile NM-12B. **D.**  
1129 Uninterpreted seismic profile NM-13. **E.** Interpretation of seismic profile NM-13. The upper  
1130 slope is characterized by a thick downlapping U1 sedimentary unit incised by numerous gullies  
1131 suggesting significant off-bank transport from the lagoon towards the basin.

1132 **Figure 8: A.** 3D bathymetrical map of the southeastern slope of Grande Terre and Pines Ridge  
1133 with location of AUS-104 and 206-04 seismic profiles. T : Banc de la Torche ; S : Stylaster  
1134 seamount ; B : Brachiopod seamount ; A : Antigonina seamount ; C : Crypthelia seamount ; M :  
1135 Munida seamount. **B.** Seismic profile AUS-14 across the Loyalty Basin bordered by the Loyalty  
1136 and Pines ridges. **C.** Line drawing interpretation of profile AUS-14 showing spectacular normal  
1137 faults affecting the peridotite nappe overlain by post-obduction sedimentary units. This study  
1138 focuses on shallow-water carbonates that cover peridotite horsts of the Pines Ridge and which  
1139 are currently at 300-400 m water depths.

1140 **Figure 9: Bathymetric map (A) and profile (B) of Crypthelia seamount located from 200 to 800**  
1141 **m water depth and marked by N160° oriented faults (f) associated with a channel (Ch) and large**  
1142 **collapses on its southern edge. Bathymetric map of Munida seamount (C) marked by a southern**  
1143 **terrace noted M1, located between 400 to 600 m water depth, and by a relatively flat top above**  
1144 **200 m water depth, noted M2.**

1145 **Figure 10: A.** Seismic profile 206-04 through the Pines Ridge and Munida seamount (see  
1146 location on [Fig.8A](#) and [10C](#)). **B.** Interpretation of profile 206-04 showing the normally faulted  
1147 geometry the Peridotite Nappe and HP-LT Metamorphic complex resulting from post-obduction  
1148 extensional tectonics (Patriat et al., 2018). Associated flat-topped horsts are capped by a shallow  
1149 water carbonate ramp interpreted as being of Mio-Pliocene age based on biostratigraphic  
1150 analysis of DW-4757 and DW-4782-A dredged samples (see [Table 3](#)). **C.** Close-up view on  
1151 seismic profile 206-04 on the Pines Ridge. **D.** Detailed line drawing interpretation of C. showing

1152 3 subunits UP1 to UP3 and an overall asymmetric configuration suggesting a tilt of Pines Ridge  
1153 before and during deposition of the Mio-Pliocene carbonate ramp. The eastern part of UP2  
1154 subunit is characterized by build-up geometries that could be interpreted as aggrading platform.

1155 **Figure 11:** A. DR44 sample, (a.) *Katacycloclypeus martini*, (b.) *Globigerinoides quadrilobatus*. B.  
1156 DR44 sample, (a.) *small rotaliid* in reworked micrite, (b.) *Dentoglobigerina altispira*, (c.)  
1157 *Globorotalia menardii*, (d.) *Globigerinoides conglobatus*, (e.) *Globigerinoides ruber*. C. DR44  
1158 sample, (a.) *Globorotalia plesiotumida*. D. DR45 sample, (a.) *Lepidocyclina sp.*. E. DR46 sample,  
1159 (a.) *Truncorotalia crassaformis*. F. DR47 sample, (a.) *Globoquadrina dehiscens*. G. DR47 sample,  
1160 (a.) *Globorotalia tumida*.

1161 **Figure 12:** A. DR48 sample, (a.) *Alveolinella praequoyi* (b.) *Pulleniatina obliquiloculata*. B. DR49  
1162 sample, (a.) *Alveolinella praequoyi*. C. DR49 sample, (a.) *Globorotalia tumida* D. DR53 sample,  
1163 (a.) *Pulleniatina primalis* E. DW4737-B sample, (a.) *Alanlordia sp.* F. DW4757-A sample, (a.)  
1164 *Planorbulinella solida*. G. DW4770 sample, (a.) *Truncorotalia truncatulinoidea* (d'Orbigny) (b.)  
1165 *Truncorotalia tosaensis* (Takayanagi and Saito).

1166 **Figure 13:** A. Schematic cross-sections showing the geometry and evolution of shallow water  
1167 post-obduction systems on the eastern margin of Grande Terre in the vicinity of Poindimié (1),  
1168 north of Pines Ridges along Banc de la Torche (2), south of Pines Ridge (3), and over Crypthelia  
1169 (4) and (5) Munida seamounts. (location in Fig. 13C). B. Paleogeographical reconstruction and  
1170 spatial distribution of Mio-Pliocene carbonate banks. C. Paleogeographical reconstruction and  
1171 spatial distribution of Quaternary barrier reef of Grande Terre and submerged isolated  
1172 platforms along Pines Ridges and seamounts.

1173 **Table 1:** Characteristics of the seismic acquisition devices.

1174 **Table 2:** List of carbonate rock samples analysed in this study

1175 **Table 3:** Table summarizing microfacies description and interpretation of depositional  
1176 environment, age of *in-situ* components and age of reworked components (identified in red in  
1177 Table 4)  
1178 **Table 4:** List of the component occurrence with identification of reworked elements (red cross).